Dissertation
submitted to the
Combined Faculties for the Natural Sciences and for Mathematics
of the
Ruprecht-Karls-Universität Heidelberg
for the degree of
Doctor of Natural Sciences

Put forward by
Alexander Lehmann
born in: *Berlin*
Oral examination: *May 27, 2020*

Minkowskian Lattice Simulation
for Non-Relativistic Quarks in Classical Fields

Referees:

Assoc.-Prof. Dr. Alexander Rothkopf
Prof. Dr. Thomas Gasenzer

Minkowskische Gittersimulation der Dynamik nicht-relativistischer Quarks unter klassischen Feldern

Die Bindungsdynamik von Quarks in der frühen Zeitentwicklung in Schwerionenkollisionen im Beisein stark-wechselwirkender, hoch-besetzter Felder ist ein inhärenter Nichtgleichgewichtsprozess. Das Verständnis der Existenz, der Zeitskala und des Mechanismus des Bindungsprozesses ist von essentieller Bedeutung für Vorhersagen der Produktion von Hadronen. In dieser Arbeit entwickeln wir eine Methode zur Simulation schwerer Quarks im Hintergrund klassisch-statistisch evolvierter hoch-besetzter Felder. Angelehnt an die Arbeit von Berges et al. [1–3] im Nichtgleichgewicht sowie von Laine et al. [4] im klassisch thermischen Gleichgewicht entwickeln wir eine Simulationsmethode für die Dynamik schwerer Quarks im Hintergrund klassich evolvierter Felder, wie sie außerhalb des Gleichgewichts für die frühe Zeitentwicklung innerhalb des Colour-Glass-Condensate-Bildes gültig ist. Wir reproduzieren bekannte Ergebnisse zur Eichfelddynamik sowohl im klassisch thermischen Gleichgewicht als auch zur frühen Nichtgleichgewichtsphysik. Während wir die schweren Quarks mittels Gitter-NRQCD beschreiben, werden die leichten Quark-Freiheitsgrade aus der Simulation mittels Quenching entfernt. Während wir die Eichfreiheitsgrade mittels eines Leapfrog-Algorithmus evolvieren, wird die Bewegungsgleichung für den schweren Quarkpropagator mittels der Crank-Nicholson-Methode unter Einfluss der Eichfelder integriert. Aus einer so definierten minkowskischen Gittersimulation extrahieren wir Quarkonium-Spektren im Nichtgleichgewicht. Entgegen der aus der euklidischen Gitterfeldtheorie abgeleiteten naiven Erwartung finden wir, dass die Rückkopplung der schweren Quarkfelder auf die Dynamik der Eichfelder von essentieller Bedeutung ist, um Bindungsprozesse zu beschreiben. Dazu präsentieren wir das statische Potenzial im klassich thermischen Gleichgewicht, welches wir aus einer um diese Rückkopplung korrigierten Simulation erhalten. Wir finden im Gegensatz zu Laine et al., dass dieses Potenzial nebst einem Imaginär- nun auch einen Realteil enthält, welcher klare Hinweise auf Debye-Screening gibt.

Minkowskian Lattice Simulation for Non-Relativistic Quarks in Classical Fields

The binding process of quarks in the early time evolution in heavy-ion collisions in the presence of strongly interacting, highly occupied fields is an inherent non-equilibrium phenomenon. Understanding whether such a binding occurs, its time scale and its mechanism is important for predictions of the production of hadrons. Based on the works by Berges et al. [1–3] in the nonequilibrium as well as by Laine et al. [4] in the classical thermal equilibrium, we present a method for the evolution of heavy quark fields in the background of highly occupied gauge fields whose dynamics are obtained from a classical statistical lattice simulation as it is valid within the Colour Glass Condensate framework. We reproduce known results out of as well as in the classical thermal equilibrium. Employing NRQCD for the heavy quark degrees of freedom, we obtain heavy-quarkonium spectra from an in the light fermions quenched Minkowskian lattice simulation. For that we employ a leapfrog-algorithm in the gauge field dynamics, which serves as input for the integration of the heavy-quark propagators which are evolved with the Crank-Nicholson method. We find that the back-coupling of the heavy quarks to the gauge fields is essential for the binding process to occur which is in contrast to the intuition from Euclidean lattice simulations. We present the static potential evaluated in a simulation that was corrected by this back-coupling via the Gauß law. We find in contrast to Laine et al. that this potential obtains a real part which shows clear hints on Debye-screening.

Contents

List of Figures

List of Tables

Chapter 1

Introduction

1.1 Motivation

Starting from Demokrit's atom hypothesis, through Rutherford's atom model derived from scattering of α and β particles at the constituents of gold foils, over Heisenberg's and Schrödinger's formulations of quantum mechanics, the so-far most-satisfying description of the microscopic physics up the TeV-scale is currently given by the standard model of particle physics.

Similar to Rutherford's scattering experiments, but with much higher collision energies, at particle accelerators like BELLE (KEK), BARBAR (SLAC), CLEO (FLAB), BESII+III (BEPC) and LHCb (CERN), a wealth of experiments provides high precision data which serves as tests of the standard model. In contrast to Rutherford's experiments, the scattering in particle collisions, during which new particles are created, is *inelastic*. The fermionic constituents of protons and neutrons, the (u- and d-)quarks, and their heavier siblings like the charm- (c) and bottom- (b) quark, provide important insights into the strong interaction. Heavy quarkonia ($c\bar{c}$ and $b\bar{b}$ bound states) have propelled our understanding of the strong interaction since their first discovery more than 40 years ago at SLAC and BNL, among others by the discovery of the J/ψ-meson and its surprising stability which caused the *November revolution of particle physics*.

The stability of quarkonia like the J/ψ-meson ($c\bar{c}$ with $J^{PC} = 1^{--}$) is explained by the OZI-rule which allows the decay within the strong interaction into three gluons, only, as single gluon decays are rued out due to their non-vanishing colour and two gluon decays due to the symmetry of the corresponding wave function, and thus lead to peak widths of $\Gamma \sim \mathcal{O}(\text{keV})$. Disfavouring decays through the strong interaction, a significant fraction of quarkonia decay into dileptons e^+e^- ($5.971 \pm 0.032\%$) and $\mu^+\mu^-$ ($5.961 \pm 0.033\%$) [5, p. 1505], wherefore these dileptons serve as experimentally well accessible channels for the detection of heavy quarkonia.

Recently reviewed [6] were heavy quarkonia in extreme conditions, i.e. high baryon density and temperature of the surrounding medium. Heavy quark systems have a natural separation of scales $m_Q \gg \Lambda_{\text{QCD}}$ (with $Q = c, b$) between the heavy quark mass and the order of quantum fluctuations in QCD. The physics of heavy quarks is therefore of short-distanced nature and amenable to a non-relativistic treatment, as layed out in section 2.1.4. This non-relativistic behaviour allows a hydrogen-like classification by spin, angular momentum and total spin as ${}^{2S+1}L_J$. The Υ ($b\bar{b}$) and the J/ψ ($c\bar{c}$) are so called S-wave states which are the ground states of these heavy quarkonia. Their binding energies are $E^{\Upsilon}_{\text{bind}} \approx 1.1\,\text{GeV}$ and $E^{\text{J}/\psi}_{\text{bind}} \approx 0.64\,\text{GeV}$ which are obtained by substracting the quark masses from the total energy of the states using the information provided in [5]. These high binding energies set the heavy quarkonium ground states clearly within the coulombic part of the so called *Cornell potential*, a simple potential model which describes the interquark-interaction by a coulombic potential at small and a linear rising one at large distances, allowing it to describe asymptotic freedom as well as confinement – two characteristic qualities of QCD.

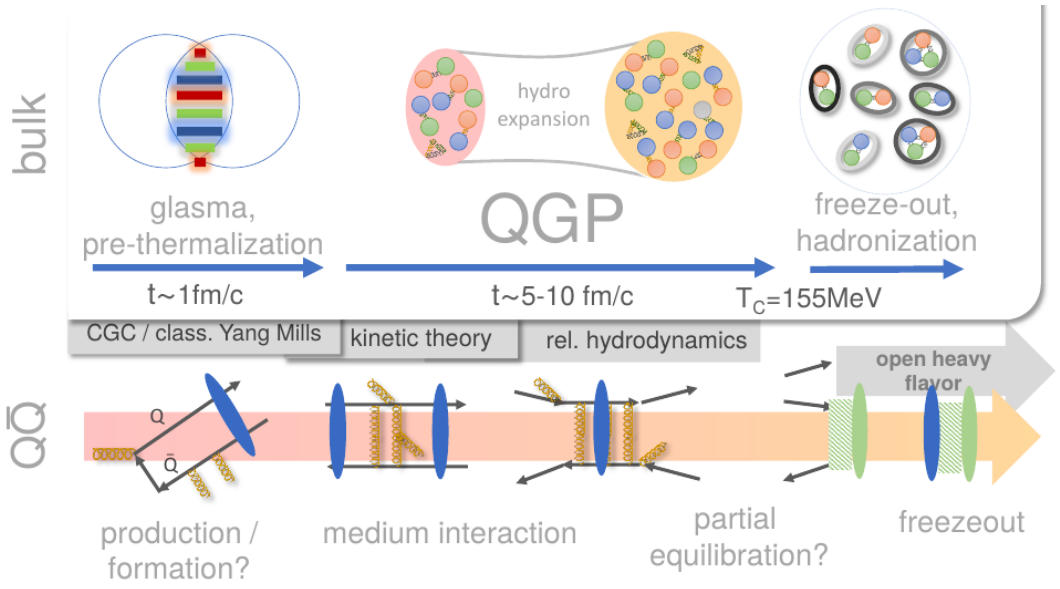

FIGURE 1.1: Sketch of the different stages in a relativistic heavy-ion collision, their dedicated effective theory tools (in grey boxes) and on the bottom the life cycle of a heavy quarkonium created at the initial stage of a relativistic heavy-ion collision. By courtesy of A. Rothkopf [6].

Due to their well-controlled theoretical access, heavy quarkonia provide a direct connection between the microscopic description within QCD on one side and the experiment on the other side.

The study of QCD under extreme conditions in general and heavy quarkonia in particular is motivated by its connection to strongly interacting matter in the early universe [7, pp. 6ff]. Referring to the *big bang*, the relativistic nucleus-nucleus collisions within heavy-ion colliders are called *little bangs*. When accelerating those heavy ions, for example gold (A=197) or lead (A=208), up to ultra-relativistic energies, their nuclei are contracted to pancake-like structures. At center-of-mass energies above 100 GeV, the colliding nuclei tend to pass through one another. Between them, they create matter within a field or environment which is high in energy density and temperature but low in the baryon density. Such conditions are realised at the Relativistic Heavy Ion Collider and the Large Hadron Collider. High baryon densities, on the other hand, are realised at lower energies of a few up to tens of GeV.

In the current picture of the stages within a heavy collision [6], the collision starts with the highly Lorentz contracted nuclei, whose partons form a *colour glass condensate*. When the nuclei collide, those partons are able to interact. This interaction generates a strong coherent colour electric and magnetic field which are referred to as the *glasma*. Those strong fields afterwards create light quarks and gluons. Through energy and momentum exchanges, those gluons and quarks equilibrate locally within ca. 1 fm into the quark gluon plasma (QGP). This plasma expands and thus loses temperature over a time of 5 fm to 10 fm. At the crossover transition temperature $T_C = 155$ MeV the coloured partons combine into colour neutral hadrons in the so-called *chemical freeze out*. This creates a gas of hadrons which reaches through exchanges of energy and momentum the *kinetic freeze out*.

This dynamical picture is, however, not deduced from a single, direct computation based on QCD. While hadron masses in the QGP at vanishing temperature and baryon density are well accessible through lattice QCD simulations, such an approach fails due to the sign problem in a real-time formulation of QCD within the path integral formalism on the lattice. Instead, effective field theory descriptions have been developed which are designed to capture the physics at dedicated stages of the heavy-ion collision. Those descriptions are linked

together at overlapping ranges of validity. In the upper part of fig. 1.1, we show the stages in a heavy-ion collision starting from the glasma and their associated time regimes. In the lower part, the life cycle of a heavy quarkonium in the bulk of gluons and lighter quarks is depicted. In grey boxes, the dedicated effective descriptions are denoted. Starting from a classical statistical simulations of the coloured Yang-Mills fields at the earliest stage, one continues the evolution with kinetic theory tools. The results from the the kinetic theory framework connects to a relativistic hydrodynamics description of the QGP.

It is generally assumed that a heavy $q\bar{q}$-pair forms a bound state before it is situated in the hot medium which constitutes the QGP. Due to the deep binding of the J/ψ and even more so the Υ, it is believed that those states survive deep into the QGP-phase. Depending on the energy density of this medium and the time scales over which it stays within the QGP, the binding between the heavy quark and antiquark gets weakened; one speaks in this context of *melting*. In addition to that, the inverse process, i.e. the regeneration of the bound state, is also possible, if there are enough heavy quark and antiquarks present to chemically push them towards binding [8]. After passing the QGP, the heavy quarkonia evolve as vacuum states and during this evolution decay. In fig. 1.2, we show the dimuon-yield in pp- and PbPb-collisions at $\sqrt{s_{\mathrm{NN}}} = 2.76\,\mathrm{TeV}$ [9]. As the Υ states decay to 6% into dilepton-pairs, the peaks originate from left to right to the decay $\Upsilon(1S)$, $\Upsilon(2S)$ and $\Upsilon(3S)$. Their positions are the masses of the corresponding bound states. The suppression of the excited states $\Upsilon(2S)$ and $\Upsilon(3S)$ in the PbPb-collision opposed to the pp-collision is explained by the presence of the QGP which is created by the multitide of neutrons and protons within the lead ions. The suppression is then understood as the aforementioned (partial) melting of the bound states within this hot environment. This melting, however, does not happen instantaneously. Bottmonium, on the hand, does not equilibrate with the surrounding QGP and thus serves as a viable probe for the full time evolution of its surrounding bulk medium. Charmonium, on the other hand, shows clear signs of kinetic equilibration. This implies that charmonia lose information about their own past evolution and make them suitable probes for the late stages.

In [10], Matsui and Satz present insightful ideas which provide intuition about the production of heavy quarkonium. Two main ideas are discussed: The first one is the aforementioned presence of a quark gluon plasma, which through energy exchanges excites the quarkonium so far until it breaks (melts) and in addition prevents the reformation of quarkonium states. Second, *Debye screening*, which in analogy to an electromagnetic plasma describes the screening by freely moving light charges like of the electric field generated by the heavy quarks which in turn weakens the binding within the $q\bar{q}$-state. The presence of such Debye-screening is well established and will present itself during the investigations presented in chapter 5.

So far, little is known about the formation of quarkonia during the early-time evolution of the glasma. A true understanding from a theoretical point of view, however, demands a calculation based fully on QCD from the early to the late stages of heavy-ion collisions.

The problem lies in the non-perturbative nature of the bound-state formation in the context of QCD which requires a non-perturbative tool able to describe the real-time evolution of the combined system of heavy quark-antiquark pair and bulk matter. This rules out conventional Euclidean lattice simulations due to the sign problem. The time evolution of quantum systems possessing high occupation numbers of the associated fields can be computed within a classical approximation. Through such an approach, vital insights into the dynamics of coloured Yang-Mills fields have been gained through classical statistical lattice simulations. In the context of non-abelian gauge fields, this approach has been used for systems out of equilibrium [1, 2, 11–16] and for heavy quarks in a thermal medium [4, 17, 18]. The production of light fermions in a strong electric field has been discussed [3].

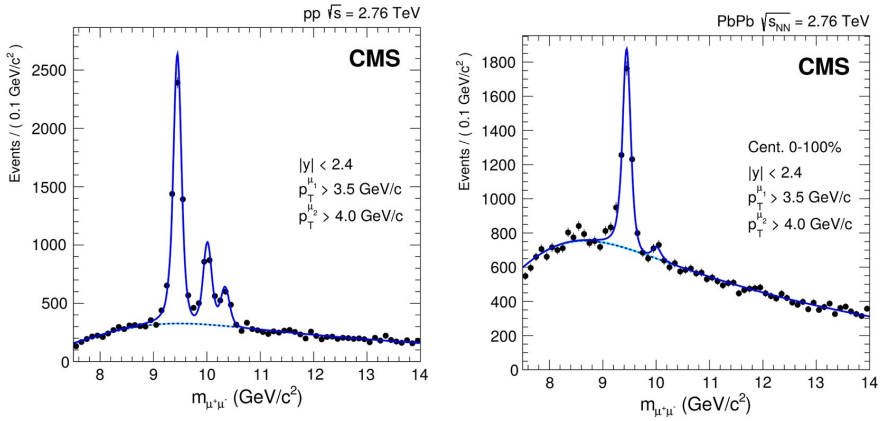

FIGURE 1.2: Dimuon-yield in pp (left) and PbPb (right) collisions at $\sqrt{s_{\mathrm{NN}}} = 2.76\,\mathrm{TeV}$ provided by the CMS-collaboration [9].

The motivation for this work is the development of a theoretical tool, able to grasp the dynamics of heavy quarks in the early-time evolution of the glasma. The strong interaction of heavy quarks has been very successfully described by non-relativistic quantum chromodynamics (NRQCD). For regimes where the production of heavy quarks within the bulk matter is energetically disfavoured, a combination of NRQCD and the classical statistical approach is a promising candidate as a tool to investigate the formation of heavy quarkonium bound states and related questions. The central question in this thesis is therefore to understand how such a combined simulation of NRQCD-quarks within a classically evolving bulk medium has to be setup in order to capture the physics of bound states.

1.2 Outline of this Work

In this thesis, we make use of both the classical approximation for the Yang-Mills fields and non-relativistic QCD for the heavy quarks. Together, they are formulated on as a Minkowskian lattice field theory. This approach is applied to investigate the heavy quarkonium spectrum in the colour singlet and octet channel as well as the static potential.

We now present the outline of this thesis. The chapters start witha short presentation of their objectives and in the main body conclude with a short summary.

The theoretical background for this study is presented in chapter 2. We begin with an introduction to quantum chromodynamics and its non-relativistic formulation. Then, we explain the basics of the Schwinger-Keldysh formalism and how it relates to the classical statistical method. By formulating the classical approach on the lattice, we arrive at the classical statistical simulation method. The heavy fermions, described by NRQCD, are then formulated within the background of the classical fields as a novel Minkowskian lattice NRQCD.

Important technical details regarding the implementation of our evolution scheme are layed out in chapter 3. We start by discussing the parallelisation scheme and continue with details of the Crank-Nicholson and Leapfrog method. We end it by a short notation how we restore Coulomb gauge for gauge-dependent observables and the employed random number generator.

In chapter 4 we study heavy quarkonium in the background of a classically evolving SU(3)-gauge field in the early time regime of the glasma. We start with an important detail of the simultaneous evolution of the quark and antiquark propagators and continue with the definition of the non-equilibrium spectral function within the Wigner-transform of heavy

quarkonium current-current-correlators. This simulation is then tested against known results before we present the colour singlet and octet spectrum within the evolving glasma.

In chapter 5 we extend our discussion of the quark-antiquark-binding to the static quarkonium potential in the pursuit to understand the observations of the preceding chapter. We will consistent results. Then, we generalise the static potential for finite but still heavy quarks and find once more agreement. A study of the static potential in the glasma shows us that our setup shows consistently the absence of heavy quarkonium bound states in all considered physical environments. We then identify the reason for this absence in the missing back-coupling of the quarks onto the Yang-Mills field. We support our hypothesis with a static potential in thermal equilibrium which shows clear hints towards Debye-screening.

The thesis concludes with chapter 6 where we discuss our results and give an outlook to possible future studies.

In the appendices we provide some technical details of our studies.

Chapter 2

Theoretical Background

In this chapter, we introduce the theoretical concepts which form the basis for the subsequent parts of this work. We will focus on the basic concepts which are decoupled from the details of the numerical set-up and specific observables which are discussed in the chapters where they are needed. In section 2.1 we introduce some important details of the notation, basics of Yang-Mills theories and quantum chromodynamics (QCD). We close this section with the by us employed, effective field theory for non-relativistic heavy quarks – NRQCD. We continue with basics of lattice gauge theory and close this section with the introduction of lattice NRQCD. Throughout this work, we evolve the gauge fields classically while their initial conditions are drawn from a statistical ensemble. To justify this approach, we present in section 2.2 basics of non-equilibrium quantum field theory in order to introduce the classical statistical evolution scheme. This sets up the framework to perform the classical statistical real-time simulation of heavy quarks on the lattice.

2.1 Field theories

In this section, we introduce the relativistic and non-relativistic description of quantum chromodynamics. We consider those theories in a minkowskian space-time and make short remarks about the treatment in a longitudinally expanding one.

2.1.1 Coordinates

The metric tensor in a non-expanding Minkwoskian space-time is given by

$$g_{\mu\nu} = \mathrm{diag}\,(+1,-1,-1,-1)\ . \tag{2.1}$$

For the goal of this thesis, it is sufficient to consider this metric. For a description that is more suited in the context of heavy-ion collisions, one should perform a coordinate transformation of the time t and longitudinal spatial coordinate z (on the axis of the colliding heavy ions) to Bjorken coordinates

$$\tau = \sqrt{t^2 - z^2}\,, \quad \eta = \mathrm{atanh}\left(\frac{z}{t}\right)\,, \tag{2.2}$$

with the longitudinal proper time τ, longitudinal proper spatial rapidity η and the transverse coordinates $\vec{x}_\mathrm{T} = (x, y)$. In those coordinates, the metric tensor is given by

$$g_{\mu\nu}^{(\mathrm{expanding})}(\tau) = \mathrm{diag}\left(+1,-1,-1,-1/\tau^2\right)\ . \tag{2.3}$$

Both metrics describe the same physics. The coordinate transformation to Bjorken coordinates only changes the reference frame. The Bjorken variables are superior over the minkowskian ones in the limit of high velocities of the colliding nuclei where approximate boost invariance in the longitudinal spatial direction implies an independence from η.

A non-expanding and homogenous system is characterised by an independence on the spatial coordinates x_i. Such a description is very useful when considering the (classically) thermal system in chapter 5. Bearing in mind that we will draw our conclusion by investigating such a system and moreover are interested in the description of *heavy, non-relativistic quarks*, we are employing the Minkowski coordinates throughout this work.

2.1.2 Notation

Our metric, as mentioned in the previous subsection, is $g_{\mu\nu} = \mathrm{diag}\,(+1,-1,-1,-1)$. The Dirac gamma matrices satisfy

$$\{\gamma^\mu, \gamma^\nu\} = 2\eta^{\mu\nu} \tag{2.4}$$

and are in the Dirac representation

$$\gamma^0 = \begin{pmatrix} +\mathbb{1}_{2\times2} & 0 \\ 0 & -\mathbb{1}_{2\times2} \end{pmatrix}, \quad \gamma^i = \begin{pmatrix} 0 & \sigma^i \\ -\sigma^i & 0 \end{pmatrix}. \tag{2.5}$$

The Pauli matrices σ^i satisfy $\{\sigma^i, \sigma^j\} = 2\delta^{ij}$. We represent them in the eigensystem of the third pauli-matrix, i.e. $\sigma^3 = \mathrm{diag}(+1,-1)$. Furthermore we will use the γ_5-matrix which is given by

$$\gamma_5 = i\gamma^0\gamma^1\gamma^2\gamma^3\,. \tag{2.6}$$

It proves practical to collect the matrices in vectors $\vec{\sigma} = (\sigma^1, \sigma^2, \sigma^3)$ and $\vec{\gamma} = (\gamma^1, \gamma^2, \gamma^3)$.

2.1.3 Basics of Quantum Chromodynamics

Quantum chromodynamics (QCD) consists of gauge part, which itself is a Yang-Mills theory [19], and fermionic part which describes the interaction of the quarks with and via the gauge field. Introductions into it can be found in many textbooks like [20–23]. It is a non-abelian gauge theory coupled to fermions that describes the strong interaction. The fermionic matter fields $\Psi_i^{(f)}(x)$, $\bar{\Psi}_i^{(f)}(x)$ carry the *colour* charges $i \in \{\mathrm{r}, \mathrm{g}, \mathrm{b}\}$. The *flavour* index $f \in \{\mathrm{u}, \mathrm{d}, \mathrm{s}, \mathrm{c}, \mathrm{b}, \mathrm{t}\}$ distinguishes between the different species of *quarks* which are characterised by their masses and electroweak charges $Y_\mathrm{W} = 2(Q - T_3)$ with the electric charge Q and the third component of the isospin T_3. The fermion fields transform in the fundamental representation of the $SU(N_\mathrm{c})$ group ($N_\mathrm{c} = 3$ for QCD), i.e. for a given space-time dependent unitary gauge transformation $G(x) \in SU(3)$ the transformed fermion fields are

$$\Psi_f^{(G)}(x) = G(x) \cdot \Psi(x)\,, \tag{2.7}$$

$$\bar{\Psi}_f^{(G)}(x) = \bar{\Psi}(x) \cdot G^\dagger(x)\,. \tag{2.8}$$

It is important to note that Ψ are $\bar{\Psi}$ are Dirac-spinors. They carry in addition to the flavour f and colour q an additional *spinor* index $\mu \in \{0, ..., 3\}$. If we consider a single flavour f, the spinor Ψ is therefor at a single space-time-point x a vector with $4N_\mathrm{c}$ components.

The bosonic gauge fields A_μ transform under the adjoint representation of the $SU(N_\mathrm{c})$ gauge group

$$A_\mu^{(G)}(x) = G(x)A_\mu(x)G^\dagger(x) - \frac{i}{g}G(x)\partial_\mu G^\dagger(x)\,. \tag{2.9}$$

It can be described as an element of the Lie algebra $\mathfrak{su}(3)$

$$A_\mu(x) = A_\mu(x)^a T^a\,. \tag{2.10}$$

$A^a_\mu(x)$ are real coefficients. The *algebra* index a runs from 1 to $N_c^2 - 1 = 8$. T^a are the generators of the Lie-group which in case of QCD are related to the Gell-Mann matrices λ^a via $T^a = \lambda^a/2$. In this work we use the convention $\mathrm{Tr}\{T^a T^b\} = \delta_{ab}/2$. The commutator of two generators is give by the real and in all indices antisymmetric structure constants f^{abc}

$$[T^a, T^b] = i f^{abc} T^c \,. \tag{2.11}$$

The lagrangian is built such that it is invariant a Lorentz scalar and invariant under local SU(3) gauge transformations. It can be decomposed into a gauge and a matter part

$$\mathcal{L}_{\mathrm{QCD}}[A, \bar{\Psi}, \Psi](x) = \mathcal{L}_{\mathrm{G}}[A](x) + \mathcal{L}_{\mathrm{F}}[A, \bar{\Psi}, \Psi](x) \,. \tag{2.12}$$

The gauge part is given by

$$\mathcal{L}_{\mathrm{G}}[A](x) = -\frac{1}{2}\,\mathrm{Tr}\left\{F_{\mu\nu}(x) F^{\mu\nu}(x)\right\} \tag{2.13}$$

with the field strength tensor

$$F_{\mu\nu}(x) = \frac{i}{g}[D_\mu(x), D_\nu(x)] \tag{2.14}$$

and the covariant derivative

$$D_\mu(x) = \partial_\mu - i A_\mu(x) = \mathbb{1}_{N_c \times N_c}\partial_\mu - i A_\mu(x)^a T^a \,. \tag{2.15}$$

The fermionic part is given by

$$\mathcal{L}_{\mathrm{F}}[A, \bar{\Psi}, \Psi](x) = \bar{\Psi}(x)\left(i\gamma_\mu D^\mu(x) - m\right)\Psi(x) \,. \tag{2.16}$$

The action $S_{\mathrm{QCD}} = \int \mathcal{L}_{\mathrm{QCD}}\,\mathrm{d}^4x$ as well as its gauge S_{G} and fermionic S_{F} parts are invariant under local gauge transformation. The full QCD which contains the gauge bosons and all strongly interacting matter fields is given by

$$\begin{aligned} S_{\mathrm{QCD}} = \int & -\frac{1}{4} F^a_{\mu\nu}(x) F^{\mu\nu,a}(x) \\ & + \sum_{f=u,d,\ldots}^{t} \sum_{i=1}^{N_c} \bar{\Psi}^{(f)}_i(x)\left(\delta_{ij} i\gamma_\mu \partial^\mu + g\gamma_\mu A^{\mu,a} T^a_{ij} - m^{(f)}\delta_{ij}\right)\Psi^{(f)}_i(x)\,\mathrm{d}^4x \,. \end{aligned} \tag{2.17}$$

The fundamental objects of interest in a QFT are correlation functions. To the end of obtaining the quarkonium spectrum, we are left with the task to compute quarkonium current-current correlators of the form [6, pp. 7f] and [24]

$$O_1(^1S_0): \quad \left\langle \hat{\mathcal{O}}(x_2, x_1)\right\rangle = \left\langle \bar{\Psi}(x_2)\gamma_5\Psi(x_2)\left(\bar{\Psi}(x_1)\gamma_5\Psi(x_1)\right)^\dagger\right\rangle , \tag{2.18}$$

$$O_1(^3S_1): \quad \left\langle \hat{\mathcal{O}}(x_2, x_1)\right\rangle = \left\langle \sum_{j=1}^{3} \bar{\Psi}(x_2)\gamma_j\Psi(x_2)\left(\bar{\Psi}(x_1)\gamma_j\Psi(x_1)\right)^\dagger\right\rangle , \tag{2.19}$$

$$O_8(^1S_0): \quad \left\langle \hat{\mathcal{O}}(x_2, x_1)\right\rangle = \left\langle \bar{\Psi}(x_2)T^a\gamma_5\Psi(x_2)\left(\bar{\Psi}(x_1)T^a\gamma_5\Psi(x_1)\right)^\dagger\right\rangle , \tag{2.20}$$

$$O_8(^3S_1): \quad \left\langle \hat{\mathcal{O}}(x_2, x_1)\right\rangle = \left\langle \sum_{j=1}^{3} \bar{\Psi}(x_2)T^a\gamma_j\Psi(x_2)\left(\bar{\Psi}(x_1)T^a\gamma_j\Psi(x_1)\right)^\dagger\right\rangle . \tag{2.21}$$

Due to the large charm and bottom quark mass, a hydrogen-atom-like indexing notation for

the states is adequate. The azimutal momentum is denoted with S ($l = 0$), P ($l = 1$), D ($l = 2$) etc. The principal quantum number is denoted by ^{n}. The spin configuration by $_0$ (singlett) and $_1$ (triplett). The colour state is denoted by O_1 for the singlett and O_8 for the octett.

2.1.4 Non-Relativistic QCD

Non-Relativistic Quantum Chromodynamics (NRQCD) [25] is an effective field theory. For a general introduction into the basic concept behind NRQCD, we refer to [26]. For a broader review we refer to [27]. For a concise introduction to NRQCD with the goal to describe real-time methods, we refer to the recently published review [6].

The interaction of a heavy quark and antiquark in a quarkonium is characterised by several momentum scales. Most important are the mass M of the heavy quark, their typical spatial momentum Mv relative to the meson rest frame and their kinetic energy Mv^2. While the overall rest energy of the quarkonium is set by the heavy quark rest mass M, the momentum Mv sets the quarkoniums size and Mv^2 the energy scale of the splitting between radial and orbital angular-momentum excitations. The aforementioned scales are hierarchically ordered as

$$M \gg Mv \gg Mv^2 \,. \tag{2.22}$$

This hierarchy is fulfilled well for bottomonium and still reasonably well for charmonium, see table 2.1. The typical velocity v decreases with M. Using potential models [28] and later confirmed by lattice calculations, the typical velocity for charm quarks is $v^2 = 0.3$ and for bottom quarks $v^2 = 0.1$. The same would not hold true for lighter quarks. In principle that argument would be even stronger for toponium but due to the short life time of its constituents such considerations are irrelevant for the investigation of bound states in this work. Another

State	v^2 [28]	M [GeV] [5]	Mv [GeV]	Mv^2 [GeV]
Υ	0.1	4.2	1.3	0.42
Ψ	0.3	1.3	0.71	0.39

TABLE 2.1: Hierarchy of scales for quarkonia of bottom and charm quarks

important momentum scale for the dynamics of heavy quarkonium is the one associated with non-perturbative effects by gluons and light quarks – Λ_{QCD}.

This hierarchy of scales can be used to define NRQCD. Our goal is to derive a non-relativistic approximation to the Dirac lagrangian which is valid particularly for heavy quarks at relative velocities which are much smaller than the speed of light in vacuum c_0.

In an effective field theory context, the systematic approach to the QCD Dirac lagrangian is given in an expansion in a dimensionless small parameter which is called a power counting scheme. For NRQCD, this parameter is the relative heavy quark velocity v. At any given order in v, all operators of that order and which have the symmetries of the QCD Dirac lagrangian make up the one of the effective field theory. In order to do that, we need to first identify the relevant degrees of freedom. First insights can be obtained by deriving the lowest order approximation directly from the Dirac lagrangian. To that end, we remove the rest mass from the total energy by the field redefinition

$$\Psi(x) = \mathrm{e}^{-iMc^2t}\tilde{\Psi} \,. \tag{2.23}$$

This modified Dirac-spinor fulfills the Dirac equation

$$\left[i\gamma^\mu D_\mu + Mc(\gamma^0 - \mathbb{1})\right]\tilde{\Psi} = 0, \,. \tag{2.24}$$

Then, one breaks up the Dirac-4-spinor into two 2-spinors

$$\tilde{\Psi} = \begin{pmatrix} \psi \\ \chi \end{pmatrix} \tag{2.25}$$

and insert this into the above Dirac equation which yields

$$\begin{pmatrix} \frac{1}{c} i D_0 & -i\vec{\sigma}\cdot\vec{D} \\ i\vec{\sigma}\cdot\vec{D} & -\frac{1}{c}(2Mc^2 + i D_0) \end{pmatrix} \cdot \begin{pmatrix} \psi \\ \chi \end{pmatrix} = 0\,. \tag{2.26}$$

The solution can be obtained recursively. As ansatz one chooses

$$\chi = \left(2Mc + \frac{1}{c} i D_0\right) i\vec{\sigma}\cdot\vec{D}\psi\,. \tag{2.27}$$

Approximating this to first order in $1/c$, i.e. for a speed of light which is comparativly much larger than any other velocity, yields

$$\chi = \frac{i}{2Mc}\vec{\sigma}\cdot\vec{D}\psi\,. \tag{2.28}$$

Inserting this into the lagrangian yields for the ψ-field

$$\mathcal{L}_\psi(x) = \bar{\psi}(x)\left(i D_0 - \frac{1}{2M}\left(i\vec{D}^2\right) + \frac{g}{2Mc}\vec{\sigma}\cdot\vec{B} + \mathcal{O}\left(c^{-2}\right)\right)\psi(x)\,, \tag{2.29}$$

where $B_i(x) = i\epsilon_{ijk}F^{jk}(x)$ is the *chromo-magnetic field*. This lagrangian is inherently non-relativistic, as one can see in the energy-momentum relation from $\vec{D}^2/(2M)$-term. This approach is systematically performed with the Foldy-Tani-Wouthuysen transformation [29, 30].

We learned from this that in order to formulate a lagrangian for heavy quarks in the context of an effective field theory, one should consider the two separate 2-spinors for the heavy quark and antiquark.This leads to the NRQCD-lagrangian [31, p. 4]

$$\begin{aligned}
\mathcal{L}_{\text{NRQCD}} =& \psi^\dagger\Big[i D_0 + \frac{c_\text{k}}{2M}\vec{D}^2 + \frac{c_\text{F}}{2M}\vec{\sigma}\cdot(g\vec{B}) + \frac{c_\text{D}}{8M^2}\left(\vec{D}\cdot(g\vec{E}) - (g\vec{E})\cdot\vec{D}\right) \\
&+ i\frac{c_\text{S}}{8M^2}\vec{\sigma}\cdot\left(\vec{D}\times(g\vec{E}) - (g\vec{E})\times\vec{D}\right)\Big]\psi \\
&+ \chi^\dagger\Big[i D_0 - \frac{c_\text{k}}{2M}\vec{D}^2 - \frac{c_\text{F}}{2M}\vec{\sigma}\cdot(g\vec{B}) + \frac{c_\text{D}}{8M^2}\left(\vec{D}\cdot(g\vec{E}) - (g\vec{E})\cdot\vec{D}\right) \\
&+ i\frac{c_\text{S}}{8M^2}\vec{\sigma}\cdot\left(\vec{D}\times(g\vec{E}) - (g\vec{E})\times\vec{D}\right)\Big]\chi \\
&+ \mathcal{L}^{(2)}\Big|_{4f} + \mathcal{L}_\text{G} + \mathcal{L}_\text{light} + \mathcal{O}(M^{-3})\,.
\end{aligned} \tag{2.30}$$

The *chromo-electric* $E_i = F_{0i}$ and *chromo-magnetic field* $B_i = i\epsilon_{ijk}F^{jk}$ appear as analoga to the electrodynamical fields in terms as we know them from a hydrogen-atom in an external electric-magnetic field. The gauge ($\mathcal{L}_\text{G}$) and light fermion ($\mathcal{L}_\text{light}$) lagrangians are uneffected by the NRQCD-expansion. Terms at order M^{-2}, which describe the direct interaction of ψ with χ fields, are contained in $\mathcal{L}^{(2)}|_{4f}$ but neglected throughout this work. They become of interest when *matching* NRQCD to QCD [31]. The Wilson coefficients c_k, c_F, c_D and c_S are a-priori complex numbers. They contain all the information from the high energy scales. At tree-level one can set them to 1. Beyond that, one has to perform a procedure which is called *matching*. There, one computes an observable in NRQCD as well as full QCD. That can be done perturbatively [31], if the physical set-up allows so, or using lattice techniques

[32]. Throughout this work we will set them to $c_i \equiv 1$.

The heavy quark and antiquark lagrangians can be transformed into one another via charge conjuagtion, remembering that the quarks transform in the **3** while the antiquarks transform in the $\bar{\mathbf{3}}$ representations of SU(3) [21, pp. 484ff],

$$\psi^{\mathrm{c}} = -i\sigma^2\chi^*, \quad A_\mu^{\mathrm{c}} = -A_\mu^{\mathrm{t}}. \tag{2.31}$$

In QCD, when investing quarkonia, one studies correlation functions of meson operators which are given in eqs. (2.18) to (2.21). When we transit to NRQCD, those mesonic correlators are transformed using the same strategy as presented earlier by using the Foldy-Tani-Wouthuysen transformation. The interpolators for the $O_1(^1S_0)$, $O_1(^3S_1)$, $O_8(^1S_0)$ and $O_8(^3S_1)$ states in NRQCD can be investigated by computing the current-current-correlators [33, p. 24]

$$O_1(^1S_0): \quad \left\langle \hat{\mathcal{O}}(x_2, x_1) \right\rangle = \left\langle \psi^\dagger(x_2)\chi(x_2)\chi^\dagger(x_1)\psi(x_1) \right\rangle , \tag{2.32}$$

$$O_1(^3S_1): \quad \left\langle \hat{\mathcal{O}}(x_2, x_1) \right\rangle = \left\langle \psi^\dagger(x_2)\vec{\sigma}\chi(c_2)\cdot\chi^\dagger(x_1)\vec{\sigma}\psi(x_1) \right\rangle , \tag{2.33}$$

$$O_8(^1S_0): \quad \left\langle \hat{\mathcal{O}}(x_2, x_1) \right\rangle = \left\langle \psi^\dagger(x_2)T^a\chi(x_2)\chi^\dagger(x_1)T^a\psi(x_1) \right\rangle , \tag{2.34}$$

$$O_8(^3S_1): \quad \left\langle \hat{\mathcal{O}}(x_2, x_1) \right\rangle = \left\langle \psi^\dagger(x_2)\vec{\sigma}T^a\chi(x_2)\cdot\chi^\dagger(x_1)\vec{\sigma}T^a\psi(x_1) \right\rangle . \tag{2.35}$$

From these correlators the heavy-quarkonium spectral functions can be computed. In the free case, i.e. $A_\mu \equiv 0$ or $g = 0$, one can compute the spectral functions. In this case, the colour and spin structure becomes irrelevant and only the angular moment discriminates the states. The result for the S-wave at $\vec{p} = 0$ is [34]

$$\rho_{\mathrm{S}}^{\text{free NRQCD}}(\omega, \vec{p} = 0) \sim \int \delta\left(\omega - 2\frac{q^2}{2M}\right)\frac{\mathrm{d}^3q}{(2\pi)^3} \sim \omega^{1/2}\theta(\omega), \tag{2.36}$$

with the step function $\theta(\omega)$. In contrast to a spectral function in QCD, the one in NRQCD obtains non-vanishing values already starting from $\omega = 0$. This lies in the shift by $-2M$ which we performed by removing the rest masses of the quark and antiquark from the total energy. We will make use of this result when we later on discuss the free spectrum on the lattice.

2.2 Non-Equilibrium QFT

The early-time physics that is adressed in parts of this work requires a treatment of the field dynamics out of equilibrium. The theoretical framework is discussed in various works. For the beginners to non-equilibrium quantum field theories, we refer to the theoretical introductions of the phd-theses [14, 15, 18] and the review of heavy quarkonia [6, pp. 6ff]. For an in-depth discussion we recommend the script of J. Berges [35].

This introduction aims at providing the origin of the classical statistical method based on the Schwinger-Keldysh formalism. We therefore present the Schwinger-Keldysh-contour, the arguments that lead to the classical statistical simulation method and its restrictions based on the high-occupancy of the field modes.

2.2.1 The Schwinger-Keldysh-Contour

The Schwinger-Keldysh formalism is best introduced together with the path integral formalism. The path integral is a third approach to quantum mechanics besides the Heisenberg and Schrödinger picture. In this formalism, the fundamental degrees of freedom are gauge

field configurations $A = \{A^a_\mu(x)\}$. Those configurations are weighed by the classical action in the evaluation of n-points functions $\mathcal{O}(x_1, x_2, ..., x_n)$, which are expectation values of functionals $\mathcal{O}(x_1, x_2, ..., x_n; A)$, in the *path integral*

$$\langle \mathcal{O}(x_1, ..., x_n) \rangle = \int \mathcal{O}(x_1, ..., x_n; A) \mathrm{e}^{iS[A]} \, \mathrm{D}[A] \,, \tag{2.37}$$

$$Z = \int \mathrm{e}^{iS[A]} \, \mathrm{D}[A] \,, \tag{2.38}$$

with the integration measure $\mathrm{D}[A]$ is not defined here. We will discuss it and the details of the path integration in the section regarding lattice gauge theory and its formulation on a space-time lattice, where the integration becomes well-defined.

Before we arrive at the path integral, we need to describe the initial state of a quantum mechanical system and its evolution. This can be done with the density operator $\hat{\rho}(t)$. The initial state, which a-priori can be in or out of equilibrium, is described by the density operator $\hat{\rho}(t_0)$. In the Schrödinger picture, its dynamics is governed by the von-Neumann equation

$$\partial_t \hat{\rho}(t) = -i[\hat{H}(t), \hat{\rho}(t)] \,. \tag{2.39}$$

The unitary time-evolution operator

$$\hat{U}(t, t') = \mathrm{T} \exp\left(-i \int_{t'}^{t} \hat{H}(t'') \, \mathrm{d}t'' \right), \tag{2.40}$$

where T denotes time-ordering, allows to formally solve the von-Neumann equation for a any initial density matrix. This solution can then be written as

$$\hat{\rho}(t) = \hat{U}(t, t_0) \hat{\rho}_0 \hat{U}(t_0, t) \,. \tag{2.41}$$

The initial density matrix is normalised to $\mathrm{Tr}\hat{\rho}(t_0) = 1$ which is conserved due to the unitarity of the time evolution. The expectation value of observables at any time can be evaluated with

$$\left\langle \hat{O} \right\rangle_{\hat{\rho}_0}(t) = \mathrm{Tr}\{\hat{\rho}(t)\hat{O}\} \tag{2.42}$$

$$= \mathrm{Tr}\{\hat{\rho}_0 \hat{U}(t_0, t) \hat{O} \hat{U}(t, t_0)\} \,. \tag{2.43}$$

The time evolution operator $U(t, t_0)$ describes the dynamics along the path $t_0 \to t$ whereas $U(t_0, t)$ describes the one back from t to t_0. Therefore, the second line of the above equation can be interpreted as a closed path from t_0 to t and back to t_0 where the initial density matrix was defined. This time path is called the *Schwinger-Keldysh contour* $\mathcal{C}$ [36, 37] and is illustrated in fig. 2.1 where the path from t_0 to t is called $\mathcal{C}^+$ and the one backwards $\mathcal{C}^-$. The shifts in the imaginary part of the time $\pm i\,\mathrm{Im}(t)$ between the contours $\mathcal{C}^\pm$ is to be understood as a limiting procedure $\mathrm{Im}(t) \to 0$. Time ordering in this context is to be understood *along the contour* $\mathcal{C}$. We denote the corresponding time ordering operator with $\mathrm{T}_\mathcal{C}$. Note that any time on $\mathcal{C}^-$ is later than on $\mathcal{C}^+$.

In a nonequilibrium quantum field theory, all information is contained in the nonequilibrium generating functional

$$Z[J, R; \rho_0] = \mathrm{Tr}\left\{ \rho_0 T_\mathcal{C} \exp\left[i \int J^a_\mu(x) A^{\mu,a}(x) \, \mathrm{d}x \right] \right\} \,, \tag{2.44}$$

which is an analogon to the aforementioned quantum mechanical concepts involving the density matrix $\hat{\rho}$. The source terms J^a_μ are needed to construct the 1PI effective action. One

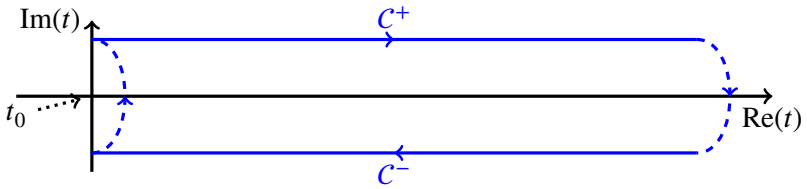

FIGURE 2.1: Illustration of the closed time path in the Schwinger-Keldysh formalism. The paths $\mathcal{C}^{\pm}$ describe the forward and backward propgators. The dashed lines connect are connecting the forward and backward branches and thus complete the contour. They vanish in a $\mathrm{Im}(t) \to 0$-limit.

can go beyond that by including $\frac{1}{2}\int R^{ab}_{\mu\nu}(x,y)A^{\mu,a}(x)A^{\nu,b}(y)\,\mathrm{d}x\,\mathrm{d}y$ in the exponential and derive the *2PI effective action* which is more than what we need in this work. For that we refer to [35, pp. 29-35]. The nonequilibrium correlation functions are expectation values of time-ordered products of Heisenberg field operators $\hat{A}^a_\mu(x)$. Using the generating function we obtain the two-point correlator via

$$\mathrm{Tr}\left\{\rho_0 \mathrm{T}_{\mathcal{C}}\hat{A}^a_\mu(x)\hat{A}^b_\mu(y)\right\} = \left\langle \mathrm{T}_{\mathcal{C}}\hat{A}^a_\mu(x)\hat{A}^b_\nu(y)\right\rangle = \left.\frac{\delta^2 Z[J,\rho]}{i\delta J^a_\mu(x) i\delta J^b_\nu(y)}\right|_{J=0}. \tag{2.45}$$

The trace of the initial density matrix with the time-dependent Heisenberg field operators can be written as a path integral on the closed time path contour as

$$Z[J;\rho] = \int \underbrace{\mathrm{d}A^+_0\,\mathrm{d}A^-_0\left\langle A^+_0\right|\rho_0\left|A^+_0\right\rangle}_{\text{initial conditions}} \int_{A^+_0}^{A^-_0} \underbrace{\mathrm{D}[A]\mathrm{e}^{i\left(S[A]+\int J(x)\phi(x)\mathrm{d}x\right)}}_{\text{quantum dynamics}}. \tag{2.46}$$

We denote the fields at initial time $t = 0$ as $A^-_0 \equiv \{A^a_\mu(0^-,\vec{x})\}$ on the backwards contour $\mathcal{C}^-$ and $A^+_0 \equiv \{A^a_\mu(0^+,\vec{x})\}$ on the forwards contour $\mathcal{C}^+$. For a given pair of initial conditions (A^-_0, A^+_0) the matrix element $\left\langle A^+_0\right|\rho_0\left|A^-_0\right\rangle$ is computed and serves as weight for the inner integration along the whole contour $\mathcal{C}$. That inner integration encodes the quantum dynamics in a path integral with fixed start and endpoint $A^{\pm}_0$. It is similar to the euclidean path integral that one considers a closed time path. But it is in several aspects very different from it:

1. The variable parametrising the contour from 0 to T and back, let us call it λ, is translated to the time t as
$$t(\lambda) = \begin{cases} \lambda & ,\lambda \le T, \\ 2T-\lambda & ,\lambda \ge T\,. \end{cases} \tag{2.47}$$
This implies that a with λ expressed time derivative $\mathrm{d}/\mathrm{d}\lambda$ changes its sign at $\lambda = T$ and thus the action on the backwards branch enters with a relative negative sign compared to the forward one. In euclidean field theory one usually deals with a periodic, imaginary time axis where such a change in sign does not occur.

2. The initial conditions are sampled in an external integral, weighed with the density matrix. In contrast to the euclidean field theory, those stay unchanged in the inner integration (quantum dynamics) as fixed start and endpoints.

There are various correlation functions one can investigate. For the scope this work, of interest are the real-valued statistical and spectral correlation functions

$$F^{ab}_{\mu\nu}(x,y) = \frac{1}{2}\left\langle \{A^a_\mu(x), A^b_\mu(y)\}\right\rangle - A^a_\mu(x)A^b_\mu(y)\,, \tag{2.48}$$

$$\rho^{ab}_{\mu\nu}(x,y) = i\left\langle [A^a_\mu(x), A^b_\mu(y)\}]\right\rangle\,. \tag{2.49}$$

should be mentioned. They are related to the connected 2-point-function

$$G^{ab}_{\mu\nu}(x,y) \equiv \left\langle \mathrm{T}_C A^a_\mu(x)A^b_\mu(y)\right\rangle = F^{ab}_{\mu\nu}(x,y) - \frac{i}{2}\rho^{ab}_{\mu\nu}(x,y)\mathrm{sgn}_C(x_0-y_0)\,. \tag{2.50}$$

The signum function $\mathrm{sgn}_C(x_0-y_0)$ on the contour is $+1$ when x_0 is later on the path than y_0 and -1 when it is earlier. The spectral and statistical function themselves, however, are given by not time-ordered correlation functions. We note, that the statistical function is symmetric while the spectral function is antisymmetric $\rho^{ab}_{\mu\nu}(x,y) = \rho^{ba}_{\nu\mu}(y,x)$.

The classicality condition [38]

$$|F_{ab}(x,y)F_{cd}(z,w)| \gg \frac{3}{4}|\rho_{ab}(x,y)\rho_{cd}(z,w)| \tag{2.51}$$

indicates when the results of a full quantum mechanical evolution of the system and one, where the inner integral is solved with a classical evolution, agree. In the free field theory, one can connect the statistical function to a distribution function $f(t,p)$. The above condition is then fulfilled, whenever this distribution is much bigger than the quantum fluctuations, i.e. $f(t,p) \gg 1/2$.

Similarly, in the thermal theory, the statistical and spectral function are connected via the Kubo-Martin-Schwinger condition [39, 40]

$$F(p) = -i\left(n(p)+\frac{1}{2}\right)\rho(p)\,, \tag{2.52}$$

where $n(\vec{p})$ is the Bose-Einstein distribution function

$$n(p) = 1/\left(\exp\left[p_0/k_\mathrm{B}T\right]-1\right)\,, \tag{2.53}$$

where due to the homogenity of the considered systems as well as time-translation invariance in the thermal scenario, the arguments have been reduced to relative coordinates and momenta, respectively. In this case, the classicality condition is fulfilled for high temperatures.

In temporal gauge $A^a_0(x) \equiv 0$, the statistical function and its second derivative are in terms of the gauge and chromo-electric field given by

$$F^{ab}_{jk}(x,x') = \frac{1}{2}\left\langle \{\hat{A}^a_j(x), \hat{A}^b_k(x')\}\right\rangle\,, \tag{2.54}$$

$$\ddot{F}^{ab}_{jk}(x,x') = \frac{1}{2}\left\langle \{\hat{E}^a_j(x), \hat{E}^b_k(x')\}\right\rangle\,. \tag{2.55}$$

The relative coordinates are the central time $t = (t_2+t_1)/2$ and relative time $s = t_2 - t_1$ as well as the $\vec{x}_0 = (\vec{x}_1+\vec{x}_2)/2$ and $\vec{x} = \vec{x}_2 - \vec{x}_1$. Due to the spatial homogenity, there is no $\vec{x}_0$-dependcy. The t-dependency, however, is out of equilibrium present.

The distribution function, also known as occupation number, is based on the free field theory defined as the geometric mean

$$f(t,p) = \sqrt{F(t,p)\cdot \ddot{F}(t,p)} = \sqrt{\mathcal{O}_{EE}(t,\vec{p})\cdot \mathcal{O}_{AA}(t,\vec{p})}\,, \tag{2.56}$$

where the expectation values in the relative coordinates are given as

$$\mathcal{O}_{AA}(t,s,\vec{x}) = \left\langle A_i^a\left(t+\frac{s}{2},\vec{x}\right) A_i^a\left(t-\frac{s}{2}\right),\vec{x}\right\rangle\,, \tag{2.57}$$

$$\mathcal{O}_{EE}(t,s,\vec{x}) = \left\langle E_i^a\left(t+\frac{s}{2},\vec{x}\right) E_i^a\left(t-\frac{s}{2}\right),\vec{x}\right\rangle\,. \tag{2.58}$$

After a Fourier transform in $\vec{x}$ and s, one then obtains the building blocks for the distribution function. Such a procedure is necessary, because we are interested in correlators out of equilibrium. The associated transform is called the Wigner transform [41]

$$\mathcal{O}(t,\omega,\vec{p}) = \int_{-\infty}^{+\infty} \mathcal{O}(t,s,\vec{p})\mathrm{e}^{-i\omega s}\,\mathrm{d}s\,. \tag{2.59}$$

2.2.2 Classical Statistical Evolution Scheme

From the Schwinger-Keldysh formalism the classical statistical evolution scheme is derived. In this scheme, the path integral is expressed in an integration over the field and its canonical momentum. Because we are going to perform a quantum-mechanical evolution of the fermion field, derived from the full path integral, we will for the time being suppress fermionic degrees in the notation. To the end of deriving the classical evolution scheme, we express the fields $A^+_{\mu,a}$ and $A^-_{\mu,a}$ along the forward (+) and backward (-) parts of the Schwinger-Keldysh-contour in terms of a *classical field* $A^{(\mathrm{cl})}_{\mu,a}$ and its *fluctuations* $A^{(\mathrm{fl})}_{\mu,a}$ [42]

$$A^+_{\mu,a} = A^{(\mathrm{cl})}_{\mu,a} + \frac{1}{2}A^{(\mathrm{fl})}_{\mu,a}\,,\quad A^-_{\mu,a} = A^{(\mathrm{cl})}_{\mu,a} - \frac{1}{2}A^{(\mathrm{fl})}_{\mu,a}\,. \tag{2.60}$$

In this notation, the difference between the forward and backwards fields is the fluctuation $A^{(\mathrm{fl})}_{\mu}$. As mentioned earlier, the action of the backwards path enters with a relative negative sign due to the change in time direction along the Schwinger-Keldysh contour. Thus, the action in terms of the classical field and its fluctuation is given by

$$S_{\mathrm{QCD}}[A^{(\mathrm{cl})}_{\mu,a}, A^{(\mathrm{fl})}_{\mu,a}] = S_{\mathrm{QCD}}[A^{(\mathrm{cl})}_{\mu,a} + \frac{1}{2}A^{(\mathrm{fl})}_{\mu,a}] - S_{\mathrm{QCD}}[A^{(\mathrm{cl})}_{\mu,a} - \frac{1}{2}A^{(\mathrm{fl})}_{\mu,a}]\,. \tag{2.61}$$

This action is expressed in a functional Taylor series around $A^{\pm}_{\mu,a} = A^{(\mathrm{cl})}_{\mu,a}$ as

$$\begin{aligned} S[A^{(\mathrm{cl})}_{\mu,a}, A^{(\mathrm{fl})}_{\mu,a}] = &\int_x \frac{\delta S[A]}{\delta A_{\mu,a}(x)}\Big|_{A=A^{(\mathrm{cl})}}\cdot A^{(\mathrm{fl})}_{\mu,a}(x) \\ &+ \int_{x,y,z} \frac{\delta^{(3)} S[A]}{\delta A_{\gamma,c}(z)\delta A_{\nu,b}(y)\delta A_{\mu,a}(x)}\Big|_{A=A^{(\mathrm{cl})}}\cdot A^{(\mathrm{fl})}_{\gamma,c}(z)A^{(\mathrm{fl})}_{\nu,b}(y)A^{(\mathrm{fl})}_{\mu,a}(x)\,. \end{aligned} \tag{2.62}$$

The Taylor series contains only odd powers of the fluctation $A^{(\mathrm{fl})}$. It terminates at fourth order because the classical action contains terms up to fourth order in the field, only. Dropping

the second term, we can integrate out the fluctuations:

$$\begin{aligned}\int\int \exp\left[i\int_x \frac{\delta S[A]}{\delta A_{\mu,a}(x)}\Big|_{A=A^{(\mathrm{cl})}}\cdot A^{(\mathrm{fl})}_{\mu,a}(x)\right]\mathrm{D}[A^{(\mathrm{fl})}]\,\mathrm{D}[A^{(\mathrm{cl})}]\\ =\int\delta\left(\frac{\delta S[A]}{\delta A_{\mu,a}(x)}\Big|_{A=A^{(\mathrm{cl})}}\right)\mathrm{D}[A^{(\mathrm{cl})}]\,.\end{aligned} \tag{2.63}$$

The principle of stationary action reappears here as

$$\delta S/\delta A|_{A^{(\mathrm{cl})}}=0\,. \tag{2.64}$$

The term cubic in the fluctuations, which we had dropped, thus encodes the difference between the quantum and the classical field dynamics. For the scope of this work, we will investigate the behaviour of the classical approach and exclude those quantum effects in the gauge field.

From the principle of stationary action the equations of motion follow. We consider them in temporal gauge $A_0\equiv 0$. In the continuum, they are given for the gauge field $A^a_i(x)$ and its canonical momentum $E^a_i(x)$, the chromo-electric field, by

$$D^{ab}_\nu(x)F^{\nu\mu,b}(x)=-j^{a,\mu}(x)\,, \tag{2.65}$$

where $j^a_\mu(x)$ denotes a coloured 4-current. This current is a conserved quantity which follows from an additional derivative

$$D^{ab}_\mu(x)j^{\mu,b}(x)=0\,. \tag{2.66}$$

In case of full QCD, it is given by

$$j^a_\mu(x)=\bar\Psi(x)T^a\gamma_\mu\Psi(x)\,. \tag{2.67}$$

The source-free version of those evolution equations are given by

$$\partial_0 A^a_i(t,\vec x)=E^a_i(t,\vec x)\,, \tag{2.68}$$

$$\partial_0 E^a_i(t,\vec x)=-D^{ab,j}(t,\vec x)F^b_{ji}(t,\vec x)\,. \tag{2.69}$$

In this work we investigate how the evolution of quantum mechanically treated quarks in the presence of classically evolving gauge fields works. To this end, we will first investigate the quark evolution *in the background* of those fields. In the second part of chapter 5 we will investigate the effect of the back-coupling of the quarks to the dynamics of the gauge and chromo-electric field.

In the classical statistical approach, the anticommutators of the Heisenberg field operators reduce to a product of classical fields

$$\mathcal{O}_{EE}(t,p)=\frac{1}{n_\mathrm{g}}\left\langle E^j_a(t,\vec p)P^T_{ij}(\vec p)\left(E^i_a(t,\vec p)\right)^*\right\rangle\,, \tag{2.70}$$

$$\mathcal{O}_{AA}(t,p)=\frac{1}{n_\mathrm{g}}\left\langle A^j_a(t,\vec p)P^T_{ij}(\vec p)\left(A^i_a(t,\vec p)\right)^*\right\rangle\,, \tag{2.71}$$

where $n_\mathrm{g}=N_\mathrm{C}^2-1$ is the number of generators. The transverse projection operator is given in eq. (A.40).

With the occupation number, we are able to charaterise the ensemble at $t=0$. The mode function expansion of the gauge and chromo-electric fields in terms of Heisenberg operators employing temporal and furthermore Coulomb gauge are presented in [3]. Reducing the anticommutators of the Heisenberg operators to simple products of classical fields, we

employ

$$\vec{A}^a(0,\vec{p}) = \sqrt{\frac{f(t=0,p)}{|\vec{p}^{\,\mathrm{C}}|}} \sum_\lambda c_{a,\lambda}(\vec{p})\vec{\epsilon}^{\,\lambda}(\vec{p}), \tag{2.72}$$

$$\vec{E}^a(0,\vec{p}) = \mathrm{i}\sqrt{|\vec{p}^{\,\mathrm{C}}|\, f(t=0,p)} \sum_\lambda c_{a,\lambda}(\vec{p})\vec{\epsilon}^{\,\lambda}(\vec{p}), \tag{2.73}$$

with complex, gaussian random numbers $c_{a,\lambda}(\vec{p})$ fulfilling

$$\left\langle c^*_{a,\lambda}(\vec{p}) \cdot c_{a',\lambda'}(\vec{p}\,')\right\rangle_{\mathrm{cl}} = \delta_{\vec{p},\vec{p}'}\delta_{a,a'}\delta_{\lambda,\lambda'}\,. \tag{2.74}$$

for the initialisation of the fields. In appendix A we present the details of this expansion like the definition of the polarisation vectors ϵ and the difference between the fourier momentum/index p and the eigenvalues p_i^{C} of the momentum operators $\hat{p}_i$.

The initial distribution, describing the glasma state, is given by a box-like function

$$f(t=0,p) = \begin{cases} 1, & \text{if } |\vec{p}| \le Q\,, \\ g^2/2, & \text{if } |\vec{p}| > Q\,, \end{cases} \tag{2.75}$$

where the field modes are occupied up to a saturation scale $Q \approx 1\,\mathrm{GeV}$ [43].

At this point, it is important to adress the validity of the combined theory of NRQCD-fermions and classical gauge fields. Similar to the hierarchy of scales in eq. (2.22), the distribution function $f(t,p)$ has to be big for the simulation to be valid. The first restriction is that the box-like shaped distribution function, in the course of its evolution, must not run into the momentum cut-off. At the same time it also must not describe a system which allows the creation of a heavy quark-antiquark-pair. To this end, we will always put the free quark-antiquark-pair creation threshold $2M$ at the momentum cut-off or even higher. Using the later on presented translation between lattice and physical units and assuming $Q = 1\,\mathrm{GeV}$, this refers to considering quarks which are as heavy or even heavier than charm quarks.

The next step is to formulate the classical statistical method on the lattice. To that end, we present the basics of lattice gauge theory and afterwards the lattice version of the above presented method.

2.2.3 Basics of Lattice Gauge Theory

The lattice formulation is at present the most successful approach to Quantum Chromodynamics. It is characterised by the discretisation of space and usually also time while retaining the gauge-invariance of the underlying quantum field theory. The lattice regularisation $\Lambda = \{x \in \mathbb{N}_{\le N_0} \times \mathbb{N}_{\le N_1} \times \mathbb{N}_{\le N_2} \times \mathbb{N}_{\le N_3}\}$ with lattice spacings a_μ, as proposed by Wilson [44] and Smit [45], can be interpreted as setting UV-regulators $p_\mu^{\max} = \pi/a_\mu$.

Degress of Freedom

The objects that are the lattice analoga of gauge fields in a lattice gauge theory for QCD are usually the so-called *link variables*. They are positioned between adjacent lattice points and are connected to the gauge field via

$$U_{\mu,x} = \exp\left[ig a_\mu A_\mu\left(x + \hat{\mu}\frac{a_\mu}{2}\right)\right] \in SU(3)\,. \tag{2.76}$$

$\hat{\mu}$ denotes a shift into the μ^{th} direction. Oftentimes [23, p. 39] one finds the definition $U_{\mu,x} = \exp\left[iga_\mu A_\mu(x)\right]$. When formulating the lattice version of the NRQCD-action it is beneficial to shift the link variables by a half step against the gauge fields in order to obtain a discretisation error of order $\mathcal{O}(a^2)$. This is consistent with the picture of links that interconnect adjacent lattice sites while the gauge field being a local quantity. The link variables are elements of the Lie group SU(3) whereas the gauge field is one of the Lie algebra $\mathfrak{su}(3)$.

Our notation for lattice variables will be that their position will be denoted by a subscript $..._x$ in contrast to the $...(x)$-notation for the fields in the continuous space-time. Moreover, we wish to remove the coupling from the system. This is achieved by rescaling with g when defining the lattice variables $A_{\mu,x} := gA_\mu(x)$.

The discretization of fermions is performed by the introduction of Grassman variables $\bar{\Psi}^{(f)}_{c,\mu,x}, \Psi^{(f)}_{c,\mu,x}$ which are anti-commuting anticommuting scalars

$$\{\bar{\Psi}^{(f)}_{c,\mu,x}, \bar{\Psi}^{(f')}_{c',\mu',x'}\} = 0, \quad \{\Psi^{(f)}_{c,\mu,x}, \Psi^{(f')}_{c',\mu',x'}\} = 0, \quad \{\bar{\Psi}^{(f)}_{c,\mu,x}, \Psi^{(f')}_{c',\mu',x'}\} = 0\,. \tag{2.77}$$

The lattice formulation of QCD arises naturally in the path integral formalism. A field QCD-configuration consists of the gauge links $U_{\mu,x}$ and the quark fields $\bar{\Psi}_{\mu,c,x}$ and $\Psi_{\mu,c,x}$. It is important to note that both $\bar{\Psi}_{\mu,c,x}$ and $\Psi_{\mu,c,x}$ appear as independent variables. The path integral, formulated in these degrees of freedom, is

$$\langle \mathcal{O}(x_1, ..., x_n)\rangle = \frac{1}{Z}\int \mathcal{O}(x_1, ..., x_n; U, \bar{\Psi}, \Psi) \mathrm{e}^{iS_{\mathrm{QCD}}[U,\bar{\Psi},\Psi]}\, \mathrm{D}[U]\, \mathrm{D}[\bar{\Psi}, \Psi]\,, \tag{2.78}$$

$$Z = \int \mathrm{e}^{iS_{\mathrm{QCD}}[U,\bar{\Psi},\Psi]}\, \mathrm{D}[U]\, \mathrm{D}[\bar{\Psi}, \Psi]\,, \tag{2.79}$$

with the integration measures

$$\mathrm{D}[U] = \prod_{\mu,x} \mathrm{d}U_{\mu,x}\ , \tag{2.80}$$

$$\mathrm{D}[\bar{\Psi}, \Psi] = \prod_{f,\mu,c,x} \mathrm{d}\bar{\Psi}^{(f)}_{\mu,c,x}\, \mathrm{d}\Psi^{(f)}_{\mu,c,x}\ , \tag{2.81}$$

where μ denotes the Dirac and c the colour index.

Gauge Invariance

In a lattice *gauge* theory, the action, observables and other physical quantities are expressed such that they are invariant under unitary gauge transformations

$$U_{\mu,x} \xrightarrow{\Omega} \Omega_x U_{\mu,x} \Omega^\dagger_{x+\hat{\mu}}\,, \tag{2.82}$$

$$\Psi^{(f)}_{\mu,x} \xrightarrow{\Omega} \Omega_x \Psi^{(f)}_{\mu,x}\,, \tag{2.83}$$

$$\bar{\Psi}^{(f)}_{\mu,x} \xrightarrow{\Omega} \bar{\Psi}^{(f)}_{\mu,x} \Omega^\dagger_x\,, \tag{2.84}$$

$$\tag{2.85}$$

where $\Omega_x \in \mathrm{SU}(N_\mathrm{c})$ are special unitary matrices and $\hat{\mu}$ denotes a shift into the μ'th direction.

Wilson Action

A lattice version of the Yang-Mills action is given by the Wilson action [44], whose explicit form [46, p. 19] is

$$\begin{aligned} S_{\mathrm{G}}^{\mathrm{Wilson}}[U] =& \nu \sum_x \Big[\sum_i \frac{1}{\left(a_0 a_i\right)^2} \mathrm{Tr}\left(2 \cdot \mathbb{1} - P_{x,0i} - P_{x,0i}^\dagger\right) \\ & - \frac{1}{2} \sum_{i,j} \frac{1}{\left(a_i a_j\right)^2} \mathrm{Tr}\left(2 \cdot \mathbb{1} - P_{x,ij} - P_{x,ij}^\dagger\right) \Big], \end{aligned} \tag{2.86}$$

where the plaquette is defined as

$$P_{\mu\nu,x} = U_{\mu,x} U_{\nu,x+\hat{\mu}} U_{\mu,x+\hat{\nu}}^\dagger U_{\nu,x}^\dagger \tag{2.87}$$

and the trace ensures its gauge-invariance under local gauge transformations. The volume of a unit cell is $\nu = \prod_\mu a_\mu = a_0 a_1 a_2 a_3$. The Wilson action approximates the Yang-Mills action in the continuum limit $a_\mu \to 0$ as

$$S_{\mathrm{G}}^{\mathrm{Wilson}} = S_{\mathrm{G}}^{\mathrm{YM}} + \mathcal{O}(a_\mu^2)\,. \tag{2.88}$$

The plaquette is a specific variant of a general *Wilson line* which is the product of all the link variables along a contour C on the lattice. Objects made up of traces over closed Wilson lines are invariant under gauge tranformations (2.82).

Path Integral of Grassman Numbers

From the anticommutativity relations in eq. (2.77) of Grassman numbers follow unusual integration rules [23, pp. 106ff], like

$$\int 1 \,\mathrm{d}\eta_i = 0\,, \quad \int \eta_i \,\mathrm{d}\eta_i = 1\,, \quad \mathrm{d}\eta_i \,\mathrm{d}\eta_j = -\,\mathrm{d}\eta_j \,\mathrm{d}eta_i\ . \tag{2.89}$$

When integrating over the Grassman variables in the next section, we will employ the integration rule for gaussian integrals

$$\int \exp\left(\sum_{i,j=1}^{N} \bar{\eta}_i M_{ij} \eta_j\right) \mathrm{d}\eta_N \,\mathrm{d}\bar{\eta}_N \ldots \mathrm{d}\eta_1 \,\mathrm{d}\bar{\eta}_1 = \det[M]\,. \tag{2.90}$$

This leads to Wick's theorem

$$\begin{aligned} \left\langle \eta_{i_1} \bar{\eta}_{j_1} \ldots \eta_{i_n} \bar{\eta}_{j_n} \right\rangle_{\mathrm{F}} &= \frac{1}{Z_{\mathrm{F}}} \int \prod_{k=1}^{N} \mathrm{d}\eta_k \,\mathrm{d}\bar{\eta}_k \,\mathrm{d}\eta_{i_1} \,\mathrm{d}\bar{\eta}_{j_1} \ldots \mathrm{d}\eta_{i_n} \,\mathrm{d}\bar{\eta}_{j_n} \exp\left(\sum_{l,m}^{N} \bar{\eta}_l M_{lm} \eta_m\right) \\ &= (-1)^n \sum_{P(1,2,\ldots,n)} \mathrm{sign}(P) (M^{-1})_{i_1 j_{P_1}} (M^{-1})_{i_2 j_{P_2}} \ldots (M^{-1})_{i_n j_{P_n}}\,. \end{aligned} \tag{2.91}$$

We will need this integration rule when formulating lattice NRQCD.

2.2.4 Classical Statistical Lattice Simulation

By applying the principle of stationary action onto the Wilson action, we can derive the lattice formulation of the classical statistical approach. The degrees of freedom are therefore the link variables and the fermion fields. It is important to note that the variation is performed

only in the link variables because the fermion fields are treated fully quantum mechanically, i.e. their dynamics is not described by a classical evolution scheme.

The variation is best performed with respect to the gauge fields because they are independent real parameters. A single links variation with respect to a gauge field component is given by

$$\frac{\delta}{\delta A^a_{\mu,x}} U_{\nu,y} = i a_\mu \delta_{\mu,\nu} \delta_{x,y} T^a U_{\nu,y} \,. \tag{2.92}$$

Applying this variation to the Wilson action

$$0 = \frac{\delta S_{\mathrm{G}}[U]}{\delta A^a_{\mu,x}} = \sum_{y,\nu<\kappa} \frac{1}{2 a_\nu a_\kappa} \mathrm{Tr} \left(\frac{\delta P_{\nu\kappa,y}[U]}{\delta A^a_{\mu,x}} + \frac{\delta P^\dagger_{\nu\kappa,y}[U]}{\delta A^a_{\mu,x}} \right) . \tag{2.93}$$

leaves us with the task to perform the variation of the individual plaquettes

$$\begin{aligned} \frac{\delta P_{\nu\kappa,y}[U]}{\delta A^a_{\mu,x}} =& i \big[\delta_{\mu\nu} \delta_{xy} T^a P_{\nu\kappa,x} \\ &+ \delta_{\mu\kappa} \delta_{x,y+\hat{\nu}} U_{\nu,x-\hat{\nu}} T^a U_{\mu,x} U^\dagger_{\nu,x-\hat{\nu}+\hat{\mu}} U^\dagger_{\kappa,x-\hat{\nu}} \\ &- \delta_{\mu\nu} \delta_{x,y+\hat{\kappa}} U_{\nu,x-\hat{\kappa}} U_{\kappa,x+\hat{\nu}-\hat{\kappa}} U^\dagger_{\nu,x} T^a U^\dagger_{\kappa,x-\hat{\kappa}} \\ &- \delta_{\mu,\kappa} \delta_{x,y} U_{\nu,x} U_{\kappa,x+\hat{\nu}} U^\dagger_{\nu,x+\hat{\kappa}} U^\dagger_{\kappa,x} T^a \big] \,. \end{aligned} \tag{2.94}$$

There are two distinct cases we have to consider: The variation with respect to spatial components and the one with respect to the temporal gauge field. It is at that point important to note that the temporal gauge is to be applied only after the principle of stationary action.

The variation of the Wilson action with respect to the spatial compoents of the gauge field $A^a_{i,x}$ combined with an overall trace results in the equation of motion

$$\begin{aligned} 2\mathrm{ImTr}(T^a P_{0i,x}) =& 2\mathrm{ImTr}(T^a P_{i,x-\hat{0}} U_{i,x}) \\ &- \sum_{j=1}^{3} \frac{a_0^2}{a_j^2} 2\mathrm{ImTr} \left(P_{ij,x} + U_{i,x} U^\dagger_{j,x-\hat{j}+\hat{i}} U^\dagger_{i,x-\hat{j}} U_{j,x-\hat{j}} \right) . \end{aligned} \tag{2.95}$$

A closer inspection of $\mathrm{ImTr}(T^a P_{0i,x})$ is due to understand why this is an equation of motion: The field strength tensor is connected to the plaquette via $P_{\mu\nu}(x) \approx \exp\big(i a_\mu a_\nu F_{\mu\nu,x}\big) = 1 + i a_\mu a_\nu F_{\mu\nu,x} + \mathcal{O}(a_\mu^2, a_\nu^2)$. It is also connected to the chromo-electric rield via $F_{0i}(x) = E_i(x)$. The coordinate in the $\mathfrak{su}(3)$ Lie algrebra is extracted with

$$E^a_i(x) = 2\mathrm{ReTr}(T^a E_i(x)) \,. \tag{2.96}$$

Defining the lattice discretised chromo-electric field with the same rescaling as the gauge field, i.e. $F_{\mu\nu,x} = g^2 F_{\mu\nu}(x)$, results in

$$E^a_{i,x} = E^a_{i,x-\hat{0}} - \sum_{j=1}^{3} \frac{a_0^2}{a_j^2} 2\mathrm{ImTr} \left(P_{ij,x} + U_{i,x} U^\dagger_{j,x-\hat{j}+\hat{i}} U^\dagger_{i,x-\hat{j}} U_{j,x-\hat{j}} \right) . \tag{2.97}$$

The equation of motion for the gauge links is obtained from the temporal plaquette

$$P_{0i,x} = U_{0,x} U_{i,x+\hat{0}} U^\dagger_{0,x+\hat{i}} U^\dagger_{i,x} \,. \tag{2.98}$$

The left-hand side is indentified with the chromo-electric field $E^a_{i,x} T^a = P_{0i,x}$. The right hand side can be shortened due to the temporal gauge $A_{0,x} \equiv 0 \to U_{0,x} \equiv \mathbb{1}$. We therefore

obtain the equation of motion for the gauge links

$$U_{i,x\hat{0}} = \mathrm{e}^{i a_0 a_i E^a_{i,x} T^a} U_{i,x} \,. \tag{2.99}$$

The variation with respect to the temporal gauge field components $A^a_{0,x}$ results in the Gauß law constraint

$$\gamma[U,E] = \frac{1}{a_0}\sum_{i=1}^{3}\frac{1}{a_i}\mathrm{Im}\left[\mathrm{Tr}T^a\left(E_{i,x} - U^\dagger_{i,x-\hat{i}}E_{i,x-\hat{i}}U_{i,x-\hat{i}}\right)\right] , \tag{2.100}$$

where for physical, i.e. the constraint satisfying, configurations $\gamma[U,E] = 0$ applies.

The equations of motion eqs. (2.97) and (2.99) set up an evolution scheme of the leapfrog form. This can be readily seen from the by $a_0/2$ shifted position of the links against the lattice sites x on which the gauge field but also the chromo-electric is defined. This scheme conserves the energy of the system

$$H[U,E] = a_1 a_2 a_3 \sum_{\vec{x}}\left[\sum_{i=1}^{3}\frac{E^a_{i,x}E^a_{i,x}}{2} + \sum_{i<j}\frac{1}{\left(a_i a_j\right)^2}\mathrm{ReTr}\left(\mathbb{1} - P_{x,ij}\right)\right]. \tag{2.101}$$

2.2.5 Real-Time Lattice NRQCD

In the previous sections we introduced the classical statistical evolution method for the gauge fields on the lattice and non-relativistic QCD for the heavy quarks. In this section we combine both approaches to define NRQCD on a minkowskian lattice.

As we are ultimately interested in the quarkonium spectral function, we need to investigate the retarded heavy quarkonium current-current correlator

$$D(x_2,x_1) = \left\langle [J^\mu(x_2)^\dagger, J_\mu(x_1)]\Theta(t_2-t_1)\right\rangle , \tag{2.102}$$

where $J_\mu(x)$ is the current at the space-time-position x. Its path integral representation is

$$D(x_2,x_1) = \frac{i}{Z}\int [J^\mu(x_2)^\dagger, J_\mu(x_1)]\Theta(t_2-t_1)\mathrm{e}^{iS[A,\psi^\dagger,\psi,\chi^\dagger,\chi]}\,\mathrm{D}[A,\psi^\dagger,\psi,\chi^\dagger,\chi] , \tag{2.103}$$

$$Z = \int \mathrm{e}^{iS[A,\psi^\dagger,\psi,\chi^\dagger,\chi]}\,\mathrm{D}[A,\psi^\dagger,\psi,\chi^\dagger,\chi] . \tag{2.104}$$

As mentioned earlier, we will keep only $\left\langle J_\mu(x_1)J_\mu(x_2)^\dagger\right\rangle$. This is justified in the structure of the surrounding medium: The energy density of the gauge field is not high enough, to contain an additional heavy quark-antiquark-pair ($c\bar{c}$, $b\bar{b}$). This implies that the operation of the meson *destructor* J_μ on the time-dependent fermionic ground-state $|\Omega\rangle$ of the combined system of quarks and gluons has to vanish. We are therefore left with the current-current-correlators as they are given in eqs. (2.32) to (2.35). They are of the form

$$J^\mu(x) = \chi_\alpha(x)^\dagger M^\mu_{\alpha\beta}\psi_\beta(x) . \tag{2.105}$$

Inserting this general current into the path integral (2.103) yields

$$\begin{aligned} D(x_2,x_1) =& \frac{-i}{Z}\int \chi_\delta(x_1)\chi^\dagger_\alpha(x_2)\psi_\beta(x_2)\psi^\dagger_\gamma(x_1)M^\mu_{\alpha\beta}M^*_{\mu,\delta\gamma} \\ & \cdot \mathrm{e}^{iS[A,\psi^\dagger,\psi,\chi^\dagger,\chi]}\,\mathrm{D}[A,\psi^\dagger,\psi,\chi^\dagger,\chi] . \end{aligned} \tag{2.106}$$

We express the bilinear forms, given in the fermionic part of the NRQCD-action,

$$S_F[A,\psi^\dagger,\psi,\chi^\dagger,\chi] = \sum_{x=(x_0,\vec{x})} \left[\mathcal{L}_\psi[x;A,\psi^\dagger,\psi] + \mathcal{L}_\chi[x;A,\chi^\dagger,\chi]\right] , \tag{2.107}$$

in matrix form

$$\mathcal{L}_\psi[x;A,\psi^\dagger,\psi] = \psi^\dagger_\beta(y)\left(\mathcal{A}_\psi\right)^{y,x}_{\beta,\alpha}\psi_\alpha(x)\,, \tag{2.108}$$

$$\mathcal{L}_\chi[x;A,\chi^\dagger,\chi] = \chi^\dagger_\beta(y)\left(\mathcal{A}_\chi\right)^{y,x}_{\beta,\alpha}\chi_\alpha(x)\,. \tag{2.109}$$

The matrices $\mathcal{A}_\psi$ and $\mathcal{A}_\chi$ are the NRQCD-analoga to the Dirac operator for the heavy quark- and antiquarks, respectively. The integration rules for Grassman variables can be found in textbooks like [22, pp. 23-33] and [23, pp. 106-110]. Employing Wick's theorem (2.91), this integration yields

$$\begin{aligned} D(x_2,x_1) =& \frac{-i}{Z_\mathrm{G}}\int \frac{\det\left(\mathcal{A}_\psi\right)\det\left(\mathcal{A}_\chi\right)}{Z_\mathrm{F}} \\ &\cdot \left(\mathcal{A}^{-1}_\chi\right)^{x_1,x_2}_{\delta,\alpha}\left(\mathcal{A}^{-1}_\chi\right)^{x_2,x_1}_{\beta,\gamma} M^\mu_{\alpha,\beta}\,(M^\mu)^*_{\gamma,\delta}\,\mathrm{e}^{iS_\mathrm{G}[A]}\,D[A]\,, \end{aligned} \tag{2.110}$$

where we have split off the fermionic partition function $Z_\mathrm{F} = \int \exp\left(iS_\mathrm{F}\right) D[\psi^\dagger,\psi,\chi^\dagger,\chi]$ from the remaining gauge part. As is usual in lattice gauge theory (cf. [22, p. 107] and [23, pp. 133-135]) containing heavy quarks, we employ the *quenched approximation*. This means that we set

$$\frac{\det\left(A_\psi\right)\det\left(A_\chi\right)}{Z_\mathrm{F}} = 1\,. \tag{2.111}$$

The fermionic determinant corresponds to the sea quark contributions which can be safely neglected for heavy quarks like the charm and bottom [47].

This reduces the path integral (2.110) to

$$D(x_2,x_1) = \frac{-i}{Z_\mathrm{G}}\int \left(A^{-1}_\chi\right)^{x_1,x_2}_{\delta,\alpha}\left(A^{-1}_\chi\right)^{x_2,x_1}_{\beta,\gamma} M^\mu_{\alpha,\beta}\,(M^\mu)^*_{\gamma,\delta}\,\mathrm{e}^{iS_\mathrm{G}[A]}\,D[A]\,. \tag{2.112}$$

The quark- and antiquark-two-point-function are given by the inverse of the Dirac operator

$$\left(G_{\psi/\chi}[A]\right)^{x_2,x_1}_{\beta,\alpha} = \left(A^{-1}_{\psi/\chi}[A]\right)^{x_2,x_1}_{\beta,\alpha}\,. \tag{2.113}$$

Those propagators follow the Schrödinger equations

$$\left(i\,\partial_0 - \hat{H}_{\psi/\chi}[A]\right)\left(G_{\psi/\chi}[A]\right)^{x_2,x_1}_{\beta,\alpha} = \delta_{\alpha\beta}\delta^{(4)}(x_2-x_1)\,, \tag{2.114}$$

with an Hamilton operator that is given by

$$\begin{aligned} \hat{H}_\psi(m,\{c_i\}) =& -\frac{c_\mathrm{k}}{2M}\vec{D}^2 - \frac{c_\mathrm{F}}{2M}\vec{B}\cdot\vec{\sigma} - \frac{c_\mathrm{D}}{8M^2}\left(\vec{D}\cdot\vec{E} - \vec{E}\cdot\vec{D}\right) \\ &- i\frac{c_\mathrm{S}}{8M^2}\vec{\sigma}\cdot\left(\vec{D}\times\vec{E} - \vec{E}\times\vec{D}\right)\,, \end{aligned} \tag{2.115}$$

where the coupling g was absorbed into the definition of $B_i = g^2 i\epsilon_{ijk}F_{jk}$ and $E_i = g^2 F_{0i}$ following the convention in the previous section. The hamiltonian for the antiquarks is given by $\hat{H}_\chi(M) = \hat{H}_\psi(-M)$. This equation is similar to the one we would obtain by directly

applying the principle of stationary action on the classical action and thus derive classical equations of motion for the fermion fields in the form

$$i\,\partial_t \psi(x,t) = \hat{H}_\psi \psi(x), \quad i\,\partial_t \chi(x,t) = \hat{H}_\chi \chi(x)\,. \tag{2.116}$$

The formal solution of the Schrödinger equation is obtained from the time evolution operator

$$\hat{U}(t,t_0) = \mathrm{T}\exp\left[-i\int_{t_0}^{t} H(t')\,\mathrm{d}t'\right]. \tag{2.117}$$

This operator is unitary as long as the hamiltonian is hermitian. This is ensured for real Wilson coefffients. Then, the norm

$$||G(t_2,x_1))|| = \sum_{\vec{x}_2} ||G(x_2,x_1)||_{\text{matrix}} \tag{2.118}$$

of the quark and antiquark propagator have is conserved under the time evolution. As matrix norm for $||G||$ one can use for example the Frobenius norm. The time evolution operator for a small time step is given by

$$T_{\psi/\chi}\left(t \pm a_0, t\right) = \mathrm{e}^{\mp i a_0 \hat{H}_{\psi/\chi}(t)} = \mathbb{1} \mp i a_0 \hat{H}_{\psi/\chi}(t) + \mathcal{O}(a_0^2)\,. \tag{2.119}$$

The forward Euler evolution scheme is defined from

$$G_{\psi/\chi}(t+a_0) = \left(\mathbb{1} - i a_0 \hat{H}_{\psi/\chi}(t)\right) G_{\psi/\chi}(t)\,, \tag{2.120}$$

while the backward Euler evolution scheme is defined from

$$G_{\psi/\chi}(t+a_0) = \left(\mathbb{1} + i a_0 \hat{H}_{\psi/\chi}(t)\right)^{-1} G_{\psi/\chi}(t)\,. \tag{2.121}$$

The problem with those discretisations is that the a-priori unitary time evolution operator becomes a non-unitary operation $\mathbb{1} \mp i a_0 \hat{H}_{\psi/\chi}(t)$. Such a non-unitarity is of non-physical origin opposed to any possible contribution due to non-hermiticities in the effective NRQCD-hamiltonian. In order to properly separate the physical norm-decays from the non-physical numerical artifacts, we employ the Crank-Nicholson scheme. Its is readily derived by employing a Padé approximation for the time evolution operator. To this end, we divide the exponential into two equal products

$$T_{\psi/\chi}\left(t+a_0, t\right) = \mathrm{e}^{-i a_0 \hat{H}_{\psi/\chi}(t)} = \mathrm{e}^{-i\frac{a_0}{2}\hat{H}_{\psi/\chi}(t)} \mathrm{e}^{-i\frac{a_0}{2}\hat{H}_{\psi/\chi}(t)}\,, \tag{2.122}$$

then invert the left term

$$T_{\psi/\chi}\left(t+a_0, t\right) = \left(\mathrm{e}^{+i\frac{a_0}{2}\hat{H}_{\psi/\chi}(t)}\right)^{-1} \mathrm{e}^{-i\frac{a_0}{2}\hat{H}_{\psi/\chi}(t)}\,, \tag{2.123}$$

and approximate the exponentials similarly to above as

$$T_{\psi/\chi}\left(t+a_0, t\right) = \left(1 + i\frac{a_0}{2}\hat{H}_{\psi/\chi}(t)\right)^{-1} \cdot \left(1 - i\frac{a_0}{2}\hat{H}_{\psi/\chi}(t)\right) + \mathcal{O}(a_0^2)\,. \tag{2.124}$$

This version of the time evolution operator, however, has the advantage that it is unitary. This is clear by considering applying this operator on its hermitian conjugate. To this end, we denote the Hamiltonian's dependence on the Wilson coefficients as $\hat{H}^{[c_i]}_{\psi/\chi}$ and remark that

$$\left(\hat{H}^{[c_i]}_{\psi/\chi}\right)^\dagger = \hat{H}^{[c_i^*]}_{\psi/\chi}\,. \tag{2.125}$$

Inserting this into the product of the discretised time evolution operator yields

$$\begin{aligned}
&\left(1+i\frac{a_0}{2}\hat{H}^{[c_i]}_{\psi/\chi}(t)\right)^{-1}\cdot\left(1-i\frac{a_0}{2}\hat{H}^{[c_i]}_{\psi/\chi}(t)\right)\\
&\qquad\cdot\left[\left(1+i\frac{a_0}{2}\hat{H}^{[c_i]}_{\psi/\chi}(t)\right)^{-1}\cdot\left(1-i\frac{a_0}{2}\hat{H}^{[c_i]}_{\psi/\chi}(t)\right)\right]^{\dagger}\\
=&\left(1+i\frac{a_0}{2}\hat{H}^{[c_i]}_{\psi/\chi}(t)\right)^{-1}\cdot\left(1-i\frac{a_0}{2}\hat{H}^{[c_i]}_{\psi/\chi}(t)\right)\\
&\qquad\cdot\left(1-i\frac{a_0}{2}\hat{H}^{[c_i^*]}_{\psi/\chi}(t)\right)\cdot\left(1+i\frac{a_0}{2}\hat{H}^{[c_i^*]}_{\psi/\chi}(t)\right)^{-1}.
\end{aligned}\tag{2.126}$$

The intermediate product commutes, if the two hamiltonians do so, i.e.

$$\left[\hat{H}^{[c_i]}_{\psi/\chi},\hat{H}^{[c_i^*]}_{\psi/\chi},\right]=0\,,\tag{2.127}$$

which is always fulfilled for purely real Wilson coefficients. This allows to bring the forward and backward Euler steps together with their inverses

$$\begin{aligned}
&\left(1+i\frac{a_0}{2}\hat{H}^{[c_i]}_{\psi/\chi}(t)\right)^{-1}\cdot\left(1+i\frac{a_0}{2}\hat{H}^{[c_i]}_{\psi/\chi}(t)\right)\\
&\cdot\left(1-i\frac{a_0}{2}\hat{H}^{[c_i]}_{\psi/\chi}(t)\right)\cdot\left(1-i\frac{a_0}{2}\hat{H}^{[c_i]}_{\psi/\chi}(t)\right)^{-1}=\mathbb{1}\,.
\end{aligned}\tag{2.128}$$

Through a von-Neumann stability analysis, one finds that this method is unconditionally stable.

The propagator configurations $G_{\psi/\chi}(t)$ are evolved through discretised time evolution operator. We thus obtain the Crank-Nicholson scheme for the propagators. It is second order in a_0, unconditionally stable and retains the norm conservation – as long as the hamiltonians dictate it through, e.g., by real Wilson coefficients implied hermiticity.

For each on a space-time-lattice defined gauge configuration U we can perform the time evolution of the propagators according to the above presented evolution scheme. Then, we define the observable

$$D(x_2,x_1)=\langle D(x_2,x_1;U)\rangle_{\mathrm{G}}\,,\tag{2.129}$$

$$D(x_2,x_1;U)=\left\langle J^{\dagger}_{\mu}(x_2)J^{\mu}(x_1)\right\rangle_{\mathrm{F}}=i\left(G_{\chi}[U]\right)^{x_1,x_2}_{\delta,\alpha}\left(G_{\psi}[U]\right)^{x_2,x_1}_{\beta,\gamma}\left(M^{\mu}\right)^{*}_{\gamma,\delta}\,.\tag{2.130}$$

The indices G and F denote the integration over the gauge and fermionic degrees of freedom. While the fermionic integration is performed analytically, the one for the gauge fields is going to be performed numerically within the classical statistical approach. This is where we treat the heavy quarks quantum mechanically while leaving the gauge fields for the classical statstical method.

Formally, only spatially discretizing the field while keeping the temporal axis continuous, one obtains a hamiltonian lattice gauge theory as it was proposed by Kogut and Susskind [48]. Starting from the formulation of the classical statistical evolution scheme for the gauge fields, one can formulate an hamiltonian gauge theory for these as well by discretising only the spatial directions. From this hamiltonian lattice gauge theory we readily see, that the total energy $H[U,E]$ in the gauge fields and the norm of the quark- and antiquark-propagator (for real Wilson coefficients) have to be conserved. For the numerical solution of those initial value problems, we have to discretise the temporal direction but still aim at conserving those quantities. The leapfrog algorithm conserves the total energy in order $\mathcal{O}(a_0^2)$. Employing the

Crank-Nicholson method for the evolution of the propagators conserves the total norm *exactly* up to numerical rounding errors. The deails of those algorithm will be presented in chapter 3.

Fully discretizing the fields on the lattice, we describe a field configuration by the spatial gauge links $U_{i,x}$, chromo-electric field $E^a_{i,x}$ and heavy quark and antiquark propagators $G_{\psi/\chi}(x_2, x_1)$. The physical theory is invariant under a local gauge transformation Ω

$$\psi_x \to \Omega_x \psi_x\,, \quad \psi_x^\dagger \to \psi_x \Omega_x^\dagger\,, \tag{2.131}$$

$$\chi_x \to \Omega_x \chi_x\,, \quad \chi_x^\dagger \to \chi_x \Omega_x^\dagger\,, \tag{2.132}$$

$$U_{i,x} \to \Omega_x U_{i,x} \Omega^\dagger_{x+\hat{i}}\,, \tag{2.133}$$

$$E_{i,x} \to \Omega_x E_{i,x} \Omega^\dagger_{i,x}\,. \tag{2.134}$$

The lattice NRQCD lagrangian shall have the following three properties:

1. Converges to the continuum NRQCD lagrangian in order $\mathcal{O}(a_\mu^2)$,
2. is gauge invariant,
3. leads to an hermitian hamiltonian.

The covariant derivative is given by

$$i\,D_i \psi(x) = \frac{i}{2a_i}\left(U_{i,x}\psi_{x+\hat{i}} - U^\dagger_{i,x-\hat{i}}\psi_{x-\hat{i}}\right) + \mathcal{O}(a_i^2)\,. \tag{2.135}$$

The second derivative in the kinetic term is given by

$$D_i^2 \psi(x) = \frac{1}{a^2}\left(U_{i,x}\psi_{x+\hat{i}} + U^\dagger_{i,x-\hat{i}}\psi_{x-\hat{i}} - 2\psi_x\right) + \mathcal{O}(a_i^2)\,. \tag{2.136}$$

The Darwin term is given by

$$\left(D_i E_i - E_i D_i\right)\psi(x) = \frac{1}{2a_i}\left(U_{i,x}E_{i,x+\hat{i}}U^\dagger_{i,x} - U^\dagger_{i,x-\hat{i}}E_{i,x-\hat{i}}U_{i,x-\hat{i}}\right)\psi_x + \mathcal{O}(a_i^2)\,. \tag{2.137}$$

The Seaguall term has to be written as

$$\vec{\sigma}\cdot\left(\vec{D}\times\vec{E} - \vec{E}\times\vec{D}\right)\psi(x) = \epsilon_{ijk}\sigma_i\{D_j, E_k\}\psi(x)\,. \tag{2.138}$$

Its lattice version is defined by the term

$$\begin{aligned}\{D_j, E_k\} =& \frac{1}{2a_j}\big(E_{k,x}U_{j,x}\psi_{x+\hat{j}} - U^\dagger_{j,x-\hat{j}}E_{k,x-\hat{j}}\psi_{x-\hat{j}} \\ &+ U_{j,x}E_{k,x+\hat{j}}\psi_{x+\hat{j}} - E_{k,x}U^\dagger_{j,x-\hat{j}}\psi_{x-\hat{j}}\big) + \mathcal{O}(a_i^2)\,.\end{aligned} \tag{2.139}$$

The spin-orbit-coupling term is translated to

$$B_i\sigma_i\psi(x) = B_{i,x}\sigma_i\psi_x\,. \tag{2.140}$$

The χ-dependend terms are obtained by replacing $\psi \to \chi$. Inserting the above presented

terms into the NRQCD lagrangian, we obtain its lattice counter-part. The lattice NRQCD-hamiltonian following from this lagrangian is in matrix notation

$$\hat{H}_\psi = \sum_i^3 \hat{H}_\psi^{(i)} \tag{2.141}$$

$$\begin{aligned}
\left(\hat{H}_\psi^{(i)}\right)_{x,y} = &+ \delta_{x,y} \cdot \Big(\frac{c_\mathrm{k}}{M a_i^2} \mathbb{1} \\
&- \frac{c_\mathrm{F}}{2M} \sigma_i B_{i,x} \\
&- \frac{c_\mathrm{D}}{16 M^2 a_i} \left(U_{i,x} E_{i,x+\hat{i}} U_{i,x}^\dagger - U_{i,x-\hat{i}}^\dagger E_{i,x-\hat{i}} U_{i,x-\hat{i}} \right) \Big) \\
&+ \delta_{x+\hat{i},y} \cdot \Big(- \frac{c_\mathrm{k}}{2M} U_{i,x} \\
&- i \frac{c_\mathrm{S}}{16 M^2} \epsilon_{ijk} \sigma_k \left(E_{j,x} U_{i,x} + U_{i,x} E_{j,x+\hat{i}} \right) \Big) \\
&+ \delta_{x-\hat{i},y} \cdot \Big(- \frac{c_\mathrm{k}}{2M} U_{i,x-\hat{i}}^\dagger \\
&+ \hat{i} \frac{c_\mathrm{S}}{16 M^2} \epsilon_{ijk} \sigma_k \left(E_{j,x} U_{i,x-\hat{i}}^\dagger + U_{i,x-\hat{i}}^\dagger E_{j,x-\hat{i}} \right) \Big) .
\end{aligned} \tag{2.142}$$

The hamiltonian for the χ-propagator is obtained by inverting the sign of the mass M.

2.2.6 Comparison: Real-Time Lattice NRQCD and Euclidean Lattice QCD

Fermions and the Doubling Problem

The conventional lattice QCD, as we encounter it in euclidean space-times, is plaqued by the well-known *doubling problem* [23, pp. 110ff], where instead of a single one obtains multiple poles in the Dirac operator. For massless fermions, those poles lie at all corners of the Brillouin zone, thus not only at $p = (0,0,0,0)$. This means that in a d-dimensional space-time, there are 2^d degenerate chiral fermions instead of one if one naively discretises the Dirac lagrangian, for example as

$$\mathcal{L}^\mathrm{Dirac} = \bar{\Psi}_x \left(\sum_{\mu=0}^3 i \frac{U_{\mu,x} \psi_{x+\hat{\mu}} - U_{\mu,x-\hat{\mu}}^\dagger \psi_{x-\hat{\mu}}}{2 a_\mu} - m \Psi_x \right) + \mathcal{O}(a_\mu^2) . \tag{2.143}$$

This phenomenon is explained by the Nielsen-Ninomiya-theorem [49, 50]. It states that it is impossible to formulate a lattice action for *chiral* fermions which leads to a hermitian, local and translational invariant hamiltonian. This problem is resolved by breaking one of the presumptions. For example in Wilsons formulation of fermions on the lattice, the chirality is explicitly broken by adding a chirally variant term which shifts the masses of doublers in the continuum limit to infinity.

The main difficulties with the fermion doubling arise in the desire to maintain chiral symmetry – which is important in the limit of vanishing quark mass. The constituents of the bottomonium- and charmonium-like particles, we are describing by the use of NRQCD, cannot have such a problem, however: They are very massive and thus are not to be considered chiral, anyways. This becomes evident by the use of lattice NRQCD wherefor, for the scope of this work, the doubling problem does not pester our simulation.

Setting the Scale

The observables, for example masses, which are evaluated on the lattice, are a-priori given in arbitray *lattice units*. For example masses are given in units of the (temporal) lattice spacing as $a_0 m$ and the action in units of $\hbar$. In order to express them in physical units (like MeV), one needs to identify an observable (like the pion mass) on the lattice with its experimental value (as an input). This determines the lattice spacing ("sets the scale") and thus allows to express all obervables in physical units. Another approach for euclidean lattice field theories at zero temperature was introduced by R. Sommer. We follow its presentention in [23, pp. 63-67] because this approach will give us important insights for the final parts of this thesis. In an euclidean lattice gauge theory ($g_{\mu\nu} \equiv +1$), Sommer's approach [51] is based on the form of the static quark potential $V(R)$. In a pure gauge theory, described by the Wilson action $S_{\mathrm{G}}^{\mathrm{Wilson}}$, it allows to relate the lattice spacing to the coupling g or equivilently the inverse coupling $\beta \sim 1/g^2$. To that end, one computes the euclidean Wilson loop

$$\langle W_C \rangle = \frac{1}{Z} \int \mathrm{D}[U] \mathrm{Tr} \left[\prod_{x \in C} U_x \mathrm{e}^{-S_{\mathrm{G}}^{\mathrm{Wilson,\ euclidean}}} \right] , \tag{2.144}$$

where the contour C goes along the space-time-trajectory of a $q\bar{q}$-pair which is spatically separated by the distance R. For large euclidean temporal separation $x_4 = a_4 n_4$, one can show that the Wilson loop is connected to a static potential via

$$\langle W_C \rangle \propto \mathrm{e}^{-a_4 n_4 V(R)} . \tag{2.145}$$

In the weak coupling limit, this potential shows a coulombic structure while in the strong coupling limit it is linear. A usual ansatz for the static potential is therefore the Cornell potential

$$V(R) = -\frac{a}{R} + bR . \tag{2.146}$$

The a/R term corresponds to the potential induced by one-gluon exchanges between the quark and its antiquark. The bR term is known as the confinement part of the potential and is a result of non-perturbative effects. The Sommer parameter is then defined as a characteristic length scale R_0. Its physical value is $R_0 \approx 0.5\,\mathrm{fm}^{-1}$. For sufficiently heavy quarks, a non-relativistic Schrödinger equation can be formulated, as derived for example from the aforementioned NRQCD-lagrangian. Then one computes the force $F(R) = \mathrm{d}V(R)/\mathrm{d}R$. From comparing to experimental bottomonium and charmonium spectra one finds that

$$F(R_0) R_0^2 = 1.65 . \tag{2.147}$$

Comparing the lattice result with its experimental counterpart, one is able to set the scale. Such a static potential may as well be investigated for other questions within our real-time scheme.

A method, also employed in euclidean (lattice) NRQCD, is the so-called matching procedure. As a first step, one investigates the theory of full QCD and derives from it constraints on the Wilson coefficients. As a second step, for the underlying effective field theory to reproduce QCD below a cut-off energy scale E_{EFT}, the Wilson coefficients are tuned such that selected correlators in QCD and (lattice) NRQCD agree ("match").

In the combination of classical statistical simulation for the gauge fields and the quantum mechanical, lattice NRQCD description of the heavy quarks, we can set the scale with the saturation scale Q which in lattice units is given by $q = a_3 Q$. Inverting this relation, the spatial lattice spacing is given by

$$a_3 = q \cdot Q^{-1} , \tag{2.148}$$

where the saturation scale is of order $Q^{-1} = 1\,\mathrm{GeV}^{-1}$ [43]. In the same manner, the bare quark M is matched with

$$m_\mathrm{q} = M \cdot Q\,. \tag{2.149}$$

Thermodynamic and Continuum Limit

The results obtained from a lattice simulation need to be extrapolated to vanishing lattice spacings in order to recover the results from the a-priori in the continuous space-time defined physical theory. There are two different limits which need to be discussed and are somewhat intertwined: The *continuum limit* $a_\mu \to 0$ and the *thermodynamic limit* $N_\mu \to \infty$ [23, p. 69]. In a realistic simulation, the path integral is evaluated for decreasing lattice spacing and increasing number of lattice sites such that the volume is kept constant. In that context, one investigates the a_μ-dependence of the results which often is referred to as *scaling analysis*. The results obtained for several such fixed physical volumina can then be extrapolated to an infinite volume.

In the earlier presented real-time lattice NRQCD, the order of the limits is given by the definition as an hamiltonian lattice field theory where the temporal direction is continuous and the spatial ones discretised. The limit $a_0 \to 0$ has thus to be performed *before* the $a_i \to 0$-limit. Although NRQCD captures the physics of heavy quarks inside heavy hadrons, the resulting field theory is non-renormalisable [52, p. 8ff]. On the lattice at a finite spacing, however, no divergences appear. Nevertheless, setting the Wilson coefficients to $c_i = 1$ is only correct at tree level. Including quantum effects, the have to be renormalised. As input, calculations of some physical observables in the full relativistic QCD have to serve. Such calculations are usually done in perturbation theory (perturbative matching).

Markov Chain and Ensemble Averages

In an euclidean lattice simulation, a configuration contains the degrees of freedom on a space-time lattice. Employing a Monte-Carlo simulation, for example via the Metropolis algorithm, a Markov chain is generated along an artifical computer time by altering the preceeding configuration in sn update step. After an initial thermalisation, one is able to compute ensemble averages as the mean of the observables along the Markov chain of length N

$$\left\langle \hat{O} \right\rangle = \frac{1}{N} \sum_i^N O_i\,, \tag{2.150}$$

while taking into account the autocorrelation along the chain.

In an ensemble average, one computes expectation values as averages over independently initialised field configurations. The coincidence of the average along the Markov-chain and the ensemble average within the euclidean approach was justified in the temporal translation invariance within the physical context, there a thermalised QGP. This allowed the approach with an euclidean path integral and its evaluation with a Monte Carlo simulation. The classical statistical lattice simulation evolves only spatial degrees of freedom along a real-time axis. Each update step is therefore directed along the computer time. Out of equilibrium, we have to ressort to the more general ensemble average. Through an average over these independently evolved configurations at a time t, one obtains associated expectation values $\langle O(t) \rangle$ and their standard deviations.

Chapter 3

Numerical Implementation and Technical Details

In this chapter we provide details of the numerical implementation. We start with the Leapfrog and Crank-Nicholson method, continue with the distribution of the lattice points over the MPI-processes. We explain how we solve the linear system, arising in the Crank-Nicholson method, and how technical issues when combining the different MPI-process-distributions in PETSc and FFTW have been resolved.

3.1 Parallelisation Scheme

The work load for the inversion of the linear system is so big that it had to be distributed over up to a thousand single processes in order to finish the computation in an acceptable amount of time. There exist several parallelisation schemes. Among those, the usual ones are OpenMP and MPI. These two differ fundamentally in their concept.

OpenMP is a way to perform computations on shared memory devices where the parallelism occurs such that every parallel *thread* sees all of the data. An example is the sum of two arrays $A_{ij} + B_{ij} = C_{ij}$ where each summation can be performed by the threads independently.

MPI is a way to perform computations on distributed memory devices where the parallelism occurs such that every parallel *process* is working on its own memory space, i.e. in principle isolated from the other processes. It is via communication routines, which explicitly have to be called, that necessary data is transferred between the processes.

In principle one can combine the two into a hybrid method in the hope of minimising the amount of communication. Our first approach was via such a setup for the simulation for the gauge fields. During the attempt to employ such a programming model for the evolution of the quark propagator, we had to realise that such a programming model is not well supported for the inversion of linear systems by parallel Krylov subspace iterative solvers. We therefore switched to a pure MPI-parallelised simulation which also proved to be less error prone due to the simpler programming model.

The workload was distributed by the spatial lattice sites. In order to keep the distribution as simple as possible, we allow only for 2,4,8,16,32,...,1024,... processes, i.e. powers of 2. By doing so, we can consider a lattice of size $N_1 \times N_2 \times N_3$, and then repeatedly cut each dimension in half, starting by the biggest by 2 divisible extension. This way the lattice was distributed in evenly sized partitions over the processes. Due to nearest neighbour interaction terms, like in the fermion evolution in eqs. (2.135) to (2.137) and (2.139) and the staples in the chromo-electric field evolution in eq. (2.97), we had to include *ghost regions* around those partitions. Those additional regions included the needed lattice sites for the nearest-neighbours terms. After each update step of the links, chromo-electric field or propagators,

the values of the corresponding arrays within the ghost regions were updated through communication steps between the process which governed the corresponding partition and the one which had the ghost points.

3.1.1 Compatibility of PETSc and FFT-Implementation

PETSc uses a different distribution of the system matrix among the processes. In PETSc the whole matrix is flattened, i.e. no submatrix structure is retained. Moreover, we used a different indexing for the spatial lattice points. The partitioning itself, however, was the same as ours. The small problem was therefore easily solved by a translation function between PETSc's and our indexing without additional need for communication steps at this point.

A more complex issue was that MKL's and also FFTW's implementation of the fast Fourier transform (FFT) are distributing the to be Fourier-transformed array completely different than PETSc. Instead of dividing the array into small, equally sized partitions, the lattice is cut into slices along the third dimension. Those are then distributed over only a part of the processes. Because the FFT was not the costliest part of the simulation, we did not aim at optimising this step by somehow making all processes participate in this numerical evaluation of the FFT. We therefore aimed solely providing a working interface between PETSc and FFT. This was solved by defining two additional MPI-flags for the fast Fourier transform, where into the first we collected all processes which are going to work on the FFT and into the second only the idle processes. Then, the data was redistributed between all processes such that the working processes could do the FFT. After performing this computation, the transformed data was back-distributed among the processes.

3.2 Crank-Nicholson Method

The Crank-Nicholson method requires the inversion of a linear system of the form

$$\underbrace{\left(\mathbb{1} + i\frac{a_0}{2}\hat{H}(t)\right)\cdot G\left(t+a_0\right)}_{A\cdot\vec{x}} = \underbrace{\left(\mathbb{1} - i\frac{a_0}{2}\hat{H}(t)\right)\cdot G\left(t\right)}_{\vec{b}}, \tag{3.1}$$

where the (spatial) matrix and vector elements themselves are 6×6-submatrices in colour and spin. The resulting matrix is spare and huge, for example on a 64^3-lattice already of order $10^6\times 10^6$. Therefore, a Krylov subspace iterative method is appropriate to solve the linear system. We used version 3.12 of the PETSc library [53] for this work where this algorithm is included, implemented as a set of purely MPI-parallelised routines.

The Crank-Nicholson method can be viewed as the combination of an explicit and an implicit Euler step. The explicit Euler is here the matrix multiplication

$$G\left(t+\frac{a_0}{2}\right) = \left(\mathbb{1} - i\frac{a_0}{2}\hat{H}(t)\right)\cdot G\left(t\right), \tag{3.2}$$

while the implicit Euler step is the subsequent solution of the linear system

$$\left(\mathbb{1} + i\frac{a_0}{2}\hat{H}(t)\right)\cdot G\left(t+a_0\right) = G\left(t+\frac{a_0}{2}\right). \tag{3.3}$$

The algorithm therefore works as follows:

1. Explicit Euler step according to eq. (3.2),
2. communication of the propagators in the ghost regions,

3. use of the previous result as input for the right hand side in the linear system of eq. (3.3),
4. communication of the propagators in the ghost regions,
5. repeat until desired time is reached.

3.3 Leapfrog Method

We employ the Leap frog method for the evolution of the links and their conjugate momenta, the chromo-electric field. It conserves the energy $H[U, E]$ up to order a_0^2. The algorithm works as follows:

1. Update of the chromo-electric field $E^a_{i,x}$ according to eq. (2.97),
2. update of the links $U_{i,x}$ according to eq. (2.99),
3. communication of links and chromo-electric field in ghost regions,
4. repeat until desired time is reached.

We would like to remark that point that the communication of the chromo-electric field in the ghost region was necessary only because those values were needed for the update of the quark and antiquark propagators. Otherwise, in a pure gauge simulation, only the link variables would have to be communicated.

3.4 Gauge Fixing

The initial gauge and chromo-electric field at $t = 0$ are constructed as Coulomb gauged. Over the course of the evolution with the Leapfrog algorithm this gauge condition is not preserved. The observables $\langle AA \rangle$ and $\langle EE \rangle$, which are needed to monitor the validity of the gauge simulation, are gauge dependent, however. They are defined in Coulomb gauge. To satisfy this gauge condition, we employed the Fourier accelerated conjugate gradient gauge fixing algorithm as presented in [54].

3.5 Random Number Generator

The initialisation of the gauge and chromo-electric field requires random numbers whose real and imaginary part are each normally distributed real random numbers. The Box-Müller-transform [55] allows to generate those from uniformly random numbers. For two given real, normally distributed random numbers $r, s \in [0, 1]$, two complex, normally distributed, independent random numbers z_1, z_2 are obtained via

$$z_1 = \sqrt{-2\log(r)}\cos(2\pi s)\,, \quad z_2 = \sqrt{-2\log(r)}\sin(2\pi s)\,. \tag{3.4}$$

They satisfy

$$\langle z_i \rangle = 0\,, \quad \left\langle z_i z_j \right\rangle = \delta_{ij}\,. \tag{3.5}$$

We employ F. James Fortran-implementation [56] of M. Lüscher's RANLUX algorithm [57] to generate the statistically independent chains of uniformly distributed random numbers r and s. Employing a discrete approximation of chaotic dynamical systems it generates those random numbers with a high quality by improving on the Marsaglia-Zaman algorithm [58] by picking out elements of the original sequence at time intervals greater than the correlation time.

Chapter 4

Real-Time Heavy Quarkonium Spectral Function

As outlined in the Introduction, the central question of this chapter is whether we can find heavy quarkonium bound states at early times ($1\,\mathrm{fm}/c_0$ to $2\,\mathrm{fm}/c_0$). To this end, we will solve the from Lattice-NRQCD derived Schrödinger equation for the quark- and antiquark-propagator that is evolved in the background of classically evolved gauge fields. Using those, we compute heavy quarkonium current-current-correlators and extract their spectra.

We will address some details of the setup in section 4.1 and introduce the definition of the non-equilibrium heavy quarkonium spectral function and qualitative differences between real- and imaginary-time correlators in section 4.2. In section 4.3 we discuss our tests of the setup against analytical results. In section 4.4 we present the fully interacting colour singlet and octet heavy quarkonium spectral functions and will point out that this setup does not show indications on bound states of a heavy $q\bar{q}$-pair.

4.1 Simultaneous Quark- and Antiquark-Evolution

The heavy quarkonium correlator $D(x_2, x_1)$ is built from the forward quark-propagator $\left(G_\psi\right)^{x_2,x_1}_{\substack{c_2,c_1\\s_2,s_1}}$ and the backwards antiquark-propagator $\left(G_\chi\right)^{x_1,x_2}_{\substack{c_1,c_2\\s_1,s_2}}$. In principle, this would require to initialise the quark propagator at $t = t_1$ as a delta function $\delta(\vec{x} - \vec{x}_1)$ and evolve it to t_2 and do the complete opposite with the antiquark-propagator, i.e. initialising it as a delta function $\delta(\vec{x} - \vec{x}_2)$ at $t = t_2$ and evolving it backwards in time. One way to do this would be to safe the whole history of gauge configurations $\{U(t), E(t)\}$ and performing this evolution. Another way would be to evolve the gauge fields first forward together with the quark-propagator and then backwards together with antiquark-propagator. In scenarios, like the free case, where the correlator is independent from the central time $t = (t_1 + t_2)/2$, one would obtain an additional problem: Even though one can avoid the computationally demanding Wigner transform, one would obtain a quadratic dependence of the computational cost on the number of temporal integration steps. This originates in the necessity to either save at least one of the two propagators complete evolution history, which requires too much memory space, or compute it for each pair (t_2, t_1) again, which would impose an additional (to the Wigner-transform, see section 4.2) quadratic scaling in the number of evolution steps.

A better solution is to use a symmetry of the Schrödinger-like Dirac-operators $\mathcal{A}_\psi$ and $\mathcal{A}_\chi$ appearing in eqs. (2.108) and (2.109) and use their properties to reformulate the backward antiquark-propagator into a forward antiquark-propagator. To this end, we shall have a

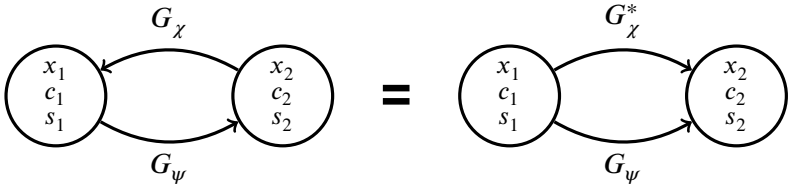

FIGURE 4.1: Sketch of the symmetry in the quark- and antiquark-propagators and their connection to the heavy quarkonium correlator. Left: Correlator constructed from the forward and backward propagators. Right: The same correlator but constructed from both forward propagators where the antiquark-propagator is hermitian conjugated in colour and spin.

closer look at them: Following from the NRQCD-lagrangian, their explicit forms are

$$\begin{aligned}\left(A_\psi\right)_{\substack{x_2,x_1\\c_2,c_1\\s_2,s_1}} =&\Big(i D_0 + \frac{c_\mathrm{k}}{2M}\vec{D}^2 + \frac{c_\mathrm{F}}{2M}\vec{\sigma}\cdot(g\vec{B}) + \frac{c_\mathrm{D}}{8M^2}\left(\vec{D}\cdot(g\vec{E}) - (g\vec{E})\cdot\vec{D}\right)\\ &+ i\frac{c_\mathrm{S}}{8M^2}\vec{\sigma}\cdot\left(\vec{D}\times(g\vec{E}) - (g\vec{E})\times\vec{D}\right)\Big)_{\substack{x_2,x_1\\c_2,c_1\\s_2,s_1}},\end{aligned} \tag{4.1}$$

$$\begin{aligned}\left(A_\chi\right)_{\substack{x_2,x_1\\c_2,c_1\\s_2,s_1}} =&\Big(i D_0 - \frac{c_\mathrm{k}}{2M}\vec{D}^2 - \frac{c_\mathrm{F}}{2M}\vec{\sigma}\cdot(g\vec{B}) + \frac{c_\mathrm{D}}{8M^2}\left(\vec{D}\cdot(g\vec{E}) - (g\vec{E})\cdot\vec{D}\right)\\ &+ i\frac{c_\mathrm{S}}{8M^2}\vec{\sigma}\cdot\left(\vec{D}\times(g\vec{E}) - (g\vec{E})\times\vec{D}\right)\Big)_{\substack{x_2,x_1\\c_2,c_1\\s_2,s_1}}.\end{aligned} \tag{4.2}$$

In lattice QCD, the γ_5-hermiticity of the lattice Dirac-operator is used to reformulate the antiquark-propagator as $\gamma_5 G_\chi \gamma_5^\dagger$. In NRQCD, the γ_5-hermiticity reduces to a simple hermiticity, i.e. $A_{\psi/\chi} = A_{\psi/\chi}^{\dagger\mathrm{full}}$ – in all colour, spin as well as space-time indices. Because the propagators are the inverse of their corresponding Schrödinger-like Dirac-operators, they inherit this property. We use this to write

$$\left(G_\psi\right)_{\substack{x_1,x_2\\c_1,c_2\\s_1,s_2}} = \left(G_\psi^{\dagger\mathrm{full}}\right)_{\substack{x_1,x_2\\c_1,c_2\\s_1,s_2}} = \left(G_\psi^*\right)_{\substack{x_2,x_1\\c_2,c_1\\s_2,s_1}}, \tag{4.3}$$

where we performed the transposition in order to change the indices and are thus left with a complex conjugation. The evolution of the hermitian conjugated antiquark-propagator is governed by

$$\partial_{t_2}\left(G_\chi^*\right)_{\substack{x_2,x_1\\c_2,c_1\\s_2,s_1}} = +i\hat{H}_\chi^*(t,M,\{c_i\})\cdot G_\chi^*(t,\vec{x})_{\substack{x_2,x_1\\c_2,c_1\\s_2,s_1}} \tag{4.4}$$

$$= -i\hat{H}_\chi(t,-M,\{c_i^*\})\cdot G_\chi^*(t,\vec{x})_{\substack{x_2,x_1\\c_2,c_1\\s_2,s_1}}. \tag{4.5}$$

This reformulation is schematically depicted in fig. 4.1 where the interchange of the colour-, spin- and space-time-indices results in a complex conjugation of the antiquark-propagator.

4.2 Definition of the Non-Equilibrium Spectral Function

The spectral functions are extracted from a system out of equilibrium. It therefore has to be extracted from a Wigner-transform [41]

$$\rho(\omega, t, \vec{p}) = \mathrm{Im} \int_{-\infty}^{+\infty} D\left(t + \frac{s}{2}, t - \frac{s}{2}, \vec{p}\right) \mathrm{e}^{-i\omega s} \, \mathrm{d}s \ , \tag{4.6}$$

where $D(t_2, t_1)$ is the current-current-correlator introduced in the previous section. The temporal variable t is called the *central time* whereas s is called the *relative time*. The coordinates t_1 and t_2 are the time at creation and annihilation of the $q\bar{q}$-pair. This translates into an initialisation of a quark-antiquark-pair at $t = t_1$ which then is evolved to $t = t_2$. The time point $t = 0$ is defined as the moment when the gluon distribution function $n(p, t)$ is initialised as the step function from eq. (2.75) until the saturation scale Q.

In this work, we concentrate on the $\vec{p} = \vec{0}$-spectrum because the additional kinetic energy is not expected to support in binding processes. To this end, we sum over all spatial positions in order to perform the corresponding spatial Fourier transform to the momentum space.

Because the correlator contains a step function $\Theta(s)$ (see eq. (2.102)), the negative time range is cut out of the integration and thus the integration reduces to

$$\rho(\omega, t) = \mathrm{Im} \int_{0}^{+\infty} D\left(t + \frac{s}{2}, t - \frac{s}{2}\right) \mathrm{e}^{-i\omega s} \, \mathrm{d}s \ . \tag{4.7}$$

Out of numerical necessity, we cut the above integral at the relative time s_{max}. This connects to the frequency-resolution $\delta_\omega = 2\pi / s_{\mathrm{max}}$. This reduces the above integral to

$$\rho(\omega, t) = \mathrm{Im} \int_{0}^{+s_{\mathrm{max}}} D\left(t + \frac{s}{2}, t - \frac{s}{2}\right) \mathrm{e}^{-i\omega s} \, \mathrm{d}s \ . \tag{4.8}$$

The evolution is performed with a finite step size of a_0. The step size in s is double as big, i.e. $\Delta_s = 2a_0$, because of the the fixed (t_2, t_1)-grid which requires a step back and two steps forward in order to arrive at the next value in s along the s-axis. Thus, relative times are given by $s = i_s \Delta_s$ with $s_{\mathrm{max}} = N_s \Delta_s$. This connects to the UV-frequency cut-off $\omega_{\mathrm{max}} = \pi / \Delta_s$. The integral therefore reduces to the sum

$$\rho(\omega, t) = \mathrm{Im} \sum_{i_s=0}^{N_s} D\left(t + \frac{i_s \Delta_s}{2}, t - \frac{i_s \Delta_s}{2}\right) \mathrm{e}^{i\omega i_s \Delta_s} \ . \tag{4.9}$$

This sum is what we are going to compute in order to obtain the heavy quarkonium spectral function at various central times t. To this end, we need to measure heavy quarkonium correlator at the times $t_1 = t - s/2$ and $t_2 = t + s/2$. The translation prescription $(t_1, t_2) \leftrightarrow (t, s)$ combined with necessity to reinitialise the quark and antiquark propagators $G_\psi(x)$ and $G_\chi(x)$ as $\delta(x - x_1)$-peaks implies that we need to reinitialise for each pair (t_2, t_1). We illustrate this in fig. 4.2. For a fixed central time t, we need the signal $C(t, s) = D(t + s/2, t - s/2)$ in the interval $s \in [0, s_{\mathrm{max}}]$. The number of evolution steps between t_1 and t_2 grows linearly in s and thus also in N_s. Having to compute N_s points along the s-axis itself implies an overall quadratic rise in the computational cost with the integral upper bound.

The correlator is here a real-time signal. Therefore, its analysis deviates from what one might be used from Euclidean field theories, as we will explain in the next section.

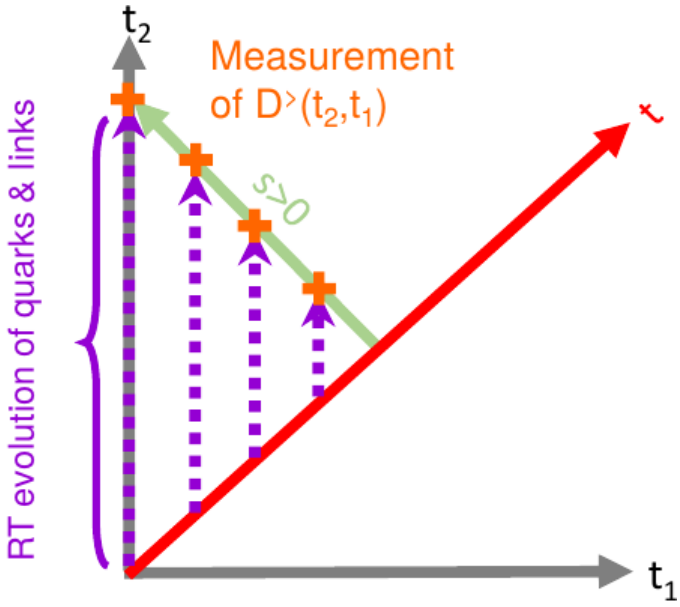

FIGURE 4.2: Sketch for the time evolution in pairs of (t_2, t_1) necessary for the Wigner-transform resulting in a $\mathcal{O}(s^2_{\text{max}})$-scaling of the computational effort.

4.2.1 Difference Between a Real-Time and an Imaginary-Time Correlator

There are several conceptual differences in the analysis of the correlator obtained in imaginary time and ours as a signal in real-time. As a test of the simulation of the heavy quarks as well as for the understanding of those conceptual differences, we consider the free heavy quarkonium correlator. *Free* means in this context that the link variables and chromo-electric-field are set to $U_\mu \equiv \mathbb{1}$ and $E_i \equiv 0$ which suppresses their influence on the heavy quarks dynamics.

Form of a Real-Time Signal

The signal in real-time shows an oscillatory behaviour that arises from the structure of the Schrödinger-equation. It continues a-priori indefinitely in the relative time s. In fig. 4.3 the real and imaginary part of the free heavy quarkonium correlator are shown for a temporal spacing of $a_t/a_s = 0.1$, the lattice sizes $\Lambda = 16^3$ and $\Lambda = 32^3$ and the quark mass $a_s M_Q = \pi/2$. We observe an oscillatory behaviour on top of damping for both lattice sizes. As will be discussed in later in this chapter, the damping originates from a diffusion process. The oscillations, however, are what really sets the real-time correlator apart from its Euclidean counter-part.

Processing of a Real-Time Signal

On the Euclidean lattice the circumference of the periodic imaginary time extension plays a different role than the real-time axis on the minkowskian lattice. The length of the imaginary time axis corresponds to an inverse temperature as $L_\tau \propto 1/T$. When for example changing the temporal lattice spacing a_τ one therefore has to adjust the number of temporal lattice points accordingly to leave the extension $L_\tau = a_\tau \cdot N_\tau$ unchanged if one aims at describing the physics at the same temperature. In the real-time simulation as presented here the situation is fundamentally different: We consider a Hamiltonian lattice field theory where the time axis is a-priori *continuous* and *indefinitely long*. When considering a specific implementation of the classical statistical approach we choose out of practical necessity to

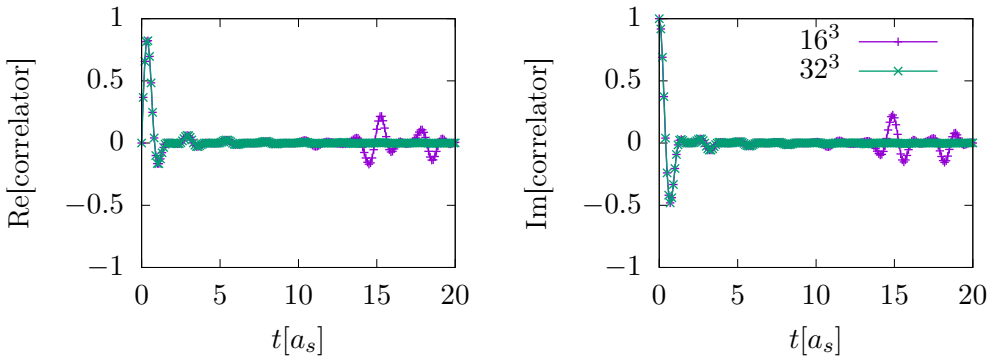

FIGURE 4.3: Real and imaginary part of the free real-time quarkonium correlator on a 16^3 and a 32^3 lattice for $a_s M = \pi/2$. It shows clear recurrence after $s \approx 15\, a_s$.

consider a finite window $[-s_{\max}, +s_{\max}]$ of size $L_t = 2s_{\max}$ and then divide it into N_t numerical update steps, each of size a_t. The step size defines the UV-cut-off $\omega_{\max} = \pi/a_t$. The inverse size of the window defines the frequency resolution $\delta_\omega = \pi/s_{\max}$.

The artificial cropping at an arbitrary time point of the signal leads to *ringing* in the Fourier transform which is a part of the Wigner transform (4.6). Let us consider the signal $D(s) = \sin(\omega_0 s)$ and restrict it to the interval $[s_1, s_2]$, thus defining the restricted signal

$$D_{\text{restr.}}(s, s_1, s_2) = \Theta(s - s_1)\Theta(s - s_2)D(s)\,, \tag{4.10}$$

where $\Theta(s)$ is the step function. In the fast Fourier transform the restricted signal is continued periodically. Only when restricting the signal to a window with a size which is an integer multiple of 2π, one would reproduce the δ-peaks at $\omega = \pm\omega_0$. For any other window the strength of the ringing depends among others on the size of the jump $|D(s_2) - D(s_1)|$ in the periodically continued signal.

If we consider a general signal, which consists of a full, a-priori unknown frequency spectrum, such a cropping cannot be avoided – but its effects on the other hand can be suppressed. The method one usually employs is called *windowing*. First we have to accept that we actually multiplied the signal $D(s)$ with the window function $w_{\text{restr.}}(s) = \Theta(s - s_1)\Theta(s - s_2)$. But then we might very well instead choose a window function which has more desirable properties, for example retaining the positions of the spectral peaks while suppressing the ringing. This is achieved by performing *Hann smoothing* by using instead the *Hann function*. For a periodically symmetric signal it has the form

$$w_{\text{Hann}}(s, s_2, s_1) = \Theta(s - s_1)\Theta(s - s_2)\sin^2\left(\pi\frac{s - s_1}{s_2 - s_1}\right)\,, \tag{4.11}$$

and thus spans over the whole interval of measurement. Only around $s = s_{1/2}$ the signals shape is damped – which leads to broadening of the spectral peaks but no shift in their position. The form of the Hann function for a signal that starts at $s_1 = 0$ is given by

$$w_{\text{Hann}}(s, s_{\max}) = \Theta(s)\Theta(s - s_{\text{cut}})\cos^2\left(\pi\frac{s}{s_{\max}}\right)\,. \tag{4.12}$$

The latter form will be employed throughout this work because the correlator includes a step-function $\theta(s)$, already, which restricted the integral to positive relative times.

Finite Size Effects

The kind of finite size effect we will discuss here are the ones arising for $s \gg \min(L_1, L_2, L_3)$. The principal behind other finite size effects were discussed in the theoretical introduction and are not further investigated throughout this work.

When the temporal separation between creation and annihilation of the quark-antiquark-pair becomes much bigger than any of the spatial extensions L_i, then *recurrence* will be appear. Recurrence refers to the phenomenon in dynamical systems that the state will eventually get close to the initial state (for continuous systems) or the exact initial state (for discrete systems). In our case, it is the diffusion which at first let's the state evolve away from its original condition. Due to the finite volume, however, the diffusing probability amplitudes $G_{\psi/\chi}$ eventually get close to their initial δ-peak like form. This recurrence is the real-time finite-volume-effect and leads to an additional peak structure in the spectrum when evolving the system *for too long*, i.e. such that the wave front of the propagators surpasses the spatial extensions N_i.

In fig. 4.3 the real and imaginary part of the free heavy quarkonium correlator on a 16^3 and 32^3 lattice for $a_\mathrm{s} M = \pi/2$ at $a_0 = 0.1 a_\mathrm{s}$ are compared with one another. The two signals agree until around $s \approx 15 a_\mathrm{s}$ when the recurrence shows itself as an increase in the correlator on the smaller lattice.

4.3 Tests Against Known Results

In this section we discuss tests of the fermionic as well as gauge part of the full simulation in order to verify that it works. We compare to known results for the free singlet heavy quarkonium spectrum and monitor the norm conservation of the quark and antiquark propagator. The gauge simulation is compared against known results from past research and checked for validity in the full setup

4.3.1 Free Heavy Quarkonium

A semi-analytical expression for the spectral function of a free heavy quarkonium on an euclidean lattice was derived in [34, appx. A] for the lowest order in unimproved NRQCD. To this end, we consider a lattice with equally sized spatial extents and spacings. The singlet's spectral function is then given by

$$\rho(\omega) \propto \sum_{\vec{p}} \delta(\omega - 2E(\vec{p}))\,, \tag{4.13}$$

where the sum goes over all momenta in the first Brillouin zone. The dispersion relation $E(\vec{p})$ depends on the discretisation scheme which is put into action. In [34, appx. A] the dispersion relation for a forward Euler scheme is presented as

$$a_0 E(\vec{p}) = -\log\left(1 - a_0 \frac{\vec{p}^2}{2M}\right)\,, \tag{4.14}$$

where all spatial lattice spacings $a_\mathrm{s} \equiv a_i$ are equal. The momenta are given by

$$\vec{p}^2 = \frac{4}{a_\mathrm{s}^2} \sum_{i=1}^{3} \sin^2\left(\frac{\tilde{p}_i}{2}\right)\,, \quad \tilde{p}_i = \frac{2\pi n_i}{N_\mathrm{s}}\,, \quad n_i \in \left\{-\frac{N_\mathrm{s}}{2}+1, ..., \frac{N_\mathrm{s}}{2}\right\}\,. \tag{4.15}$$

We, however, employ the Crank-Nicholson scheme. The derivation of the dispersion relation works as follows: We consider the free field solution wherefore the energy and momentum

eigenstates coincide, i.e. $|E\rangle = \left|\vec{p}\right\rangle$. Then, we apply the time translation operator $\hat{T}(t+a_0, t)$ on this state and use that it is an energy eigenstate, i.e.

$$\hat{T}(t + a_0, t)\,|E\rangle = \mathrm{e}^{-i a_0 E(\vec{p})}\,. \tag{4.16}$$

The next step is the one which depends on the integration scheme. We have to insert the representation of the time translation operator in the given integration scheme which for the Crank-Nicholson method is

$$\hat{T}(t + a_0, t) = \left(\mathbb{1} + i\frac{a_0}{2}\hat{H}_{\text{free}}\right)^{-1}\left(\mathbb{1} - i\frac{a_0}{2}\hat{H}_{\text{free}}\right)\,, \tag{4.17}$$

where we have to insert the free Hamiltonian $\hat{H}_{\text{free}} = \hat{\vec{p}}^2/2M$. Applying this expression on the momentum eigenstate $\left|\vec{p}\right\rangle$ gives

$$\begin{aligned}\left(\mathbb{1} + i\frac{a_0}{2}\hat{H}_{\text{free}}\right)^{-1}\left(\mathbb{1} - i\frac{a_0}{2}\hat{H}_{\text{free}}\right)|\vec{p}\rangle = \\ \left(1 + i\frac{a_0}{2}\frac{\vec{p}^2}{2M}\right)^{-1}\left(1 - i\frac{a_0}{2}\frac{\vec{p}^2}{2M}\right)|\vec{p}\rangle\,.\end{aligned} \tag{4.18}$$

Because of $\left|\vec{p}\right\rangle = \left|\vec{E}\right\rangle$ we obtain

$$\mathrm{e}^{-i a_0 E(\vec{p})} = \frac{1 - i a_0 \frac{\vec{p}^2}{4M}}{1 + i a_0 \frac{\vec{p}^2}{4M}}\,. \tag{4.19}$$

Inverting this relation using the arg-function gives the dispersion relation for the Crank-Nicholson method

$$a_0 E(\vec{p}) = -\arg\left(\frac{1 - i a_0 \frac{\vec{p}^2}{4M}}{1 + i a_0 \frac{\vec{p}^2}{4M}}\right)\,. \tag{4.20}$$

The actual possible values of the spatial momenta p_i depend on the spatial discretisation. In appendix A the different eigenvalues for the forward, backward and central difference scheme are presented. The discretisation of the kinetic term in eq. (2.136) as part of the lattice NRQCD lagrangian corresponds to the central difference scheme.

To summarise: The discretisation scheme of the temporal derivative determines the connection between the energy and the spatial momenta, i.e. the dispersion relation. The discretisation scheme of the spatial derivative, on the other hand, determines the possible values of the spatial momenta. Plugging both into eq. (4.13), we obtain

$$\rho(\omega) \propto \sum_{\vec{p}} \delta\left(\omega + \frac{2}{a_0}\arg\left(\frac{1 - i a_0 \frac{\vec{p}^2}{4M}}{1 + i a_0 \frac{\vec{p}^2}{4M}}\right)\right)\,. \tag{4.21}$$

The summation is evaluated numerically and thus serves as a semi-analytic solution, to which we compare our results for the free singlet spectrum. To this end, we divide the ω-axis up to the Fourier transforms UV-cut-off $\omega_{\text{max}} = \pi/\Delta_s$ into equally sized bins of width $\omega_{\text{max}}/N_{\text{t}}$ where N_{t} is the number of time steps in the simulation. Then, the number of momenta which fall into each bin is counted and the whole spectral function normalised such that its Fourier transform satisfies $C(0) = (2\pi)^{-1/2}\int \rho(\omega)\exp(i\omega s)\,\mathrm{d}\omega\,|_{s=0} = 1$.

In fig. 4.4 we compare the semianalytic to the numerical result for the free heavy singlet spectrum on a 64^3-lattice for $a_0/a_{\text{s}} = 0.1$, $s_{\text{max}} = 50 a_{\text{s}}$ and $a_{\text{s}} M = \pi/2$. We normalised the

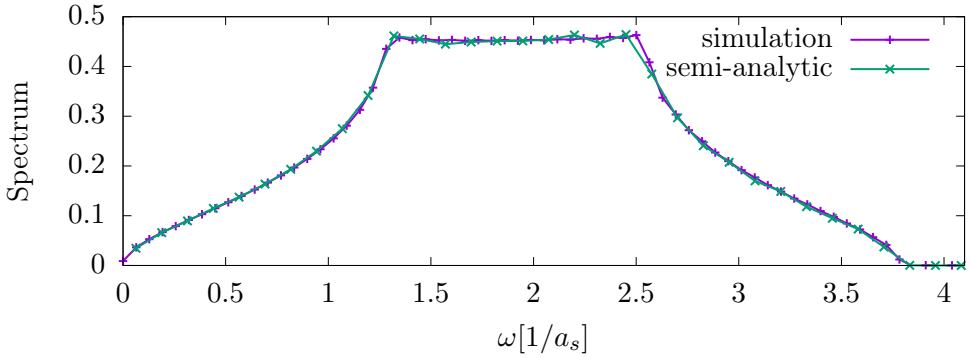

FIGURE 4.4: Semianalytic and free heavy singlet spectrum on a 64^3-lattice for $a_0/a_s = 0.1$, $s_{\max} = 50a_0$ and $a_s M = \pi/2$. The lines shall guide the eye.

correlator such that $D[G = \delta(x - x_0)] = i$. This translates to $1 = \mathrm{Im}D(t = 0) = \int \rho(\omega)\,\mathrm{d}\omega$. The results match well and thus indicate that the NRQCD-part of the simulation works as intended.

The characteristic *cusps* at $a_s\omega \approx 1.25$ and $a_s\omega \approx 2.5$ are finite momentum cut-off artifacts, i.e. relate to the finite lattice spacing. As discussed above, the particular form of the spectrum is given by the dispersion relation in combination with the spectrum of the free lattice momentum operator. Important for the interpretation of the later on presented spectrum in the by NRQCD described interaction in the early-time evolution of the gluon field is the location of the first cusp. Only maximal up to this point we are allowed to draw indications on physical processes. Everything beyond that has to be considered as finite lattice spacing artifacts.

Norm Conservation

As a second test of the fermionic simulation serves the norm conservation. Due to the unitarity of the time translation operator of the Crank-Nicholson scheme, the norm of the quark and the antiquark propagator each are conserved. During the course of the free but also the later on showed full NRQCD simulations, the norm

$$||G_{\psi/\chi}(t)|| = \sum_{\vec{x}\in\Lambda} ||G_{\psi/\chi}(t, \vec{x})|| \tag{4.22}$$

was monitored and can confirm that it is indeed conserved up to numerical rounding errors of $\mathcal{O}(10^{-14})$ as long as the Wilson coefficients are real.

4.3.2 Gauge Field Simulation

The classical statistical evolution of the gauge fields is an integral part of the full simulation. In the following we discuss tests against known results from which we draw confidence that this part of the simulation works correctly, as well.

Conservation of the Energy and Gauss Constraint

The energy in eq. (2.101) is a constant of motion. The evolution under the Leapfrog algorithm conserves it to global order $\mathcal{O}(a_0^2)$. In fig. 4.5 we show the relative deviation from its initial value $H(0) := H[U(t = 0), E(t = 0)]$ over time on a 64^3-lattice for $g = 10^{-3}$, $a_s Q = 1$, $f(t = 0, p < Q) = 1$ and $a_0/a_s \in \{0.01, 0.05, 0.1, 0.25, 0.5\}$. The global deviation decreases indeed as a_0^2 as one can see by comparing $a_0/a_s = 10^{-1}$ and $a_0/a_s = 10^{-2}$. We

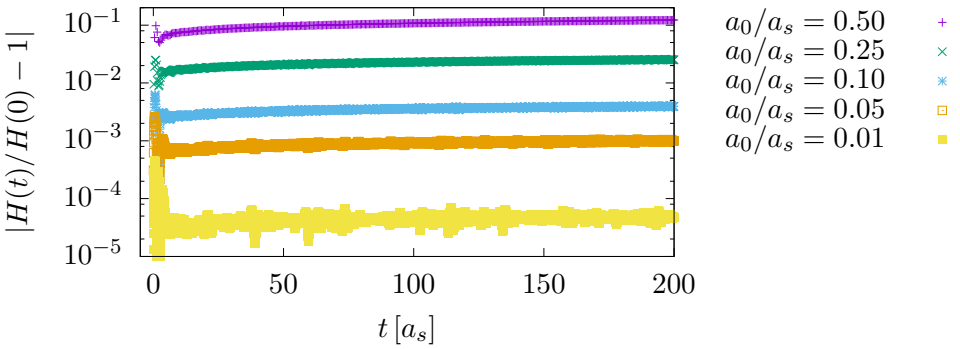

FIGURE 4.5: Relative deviation of the energy from its initial value at $t = 0$ on a 64^3-lattice, $g = 10^{-3}$, $a_s Q = 1$ and $f(t = 0, p < Q) = 1$ for $a_0/a_s \in \{0.01, 0.05, 0.1, 0.25, 0.5\}$.

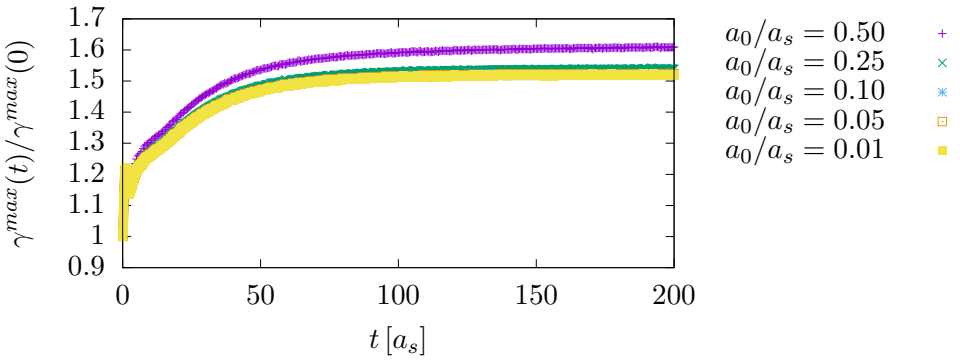

FIGURE 4.6: Deviation from the Gauß constraint relative to its initial value $\gamma^{\max}[U, E; t = 0] = 2.34 \cdot 10^{-11}$ on a 64^3-lattice, $g = 10^{-3}$, $a_s Q = 1$ and $f(t = 0, p < Q) = 1$ for $a_0/a_s \in \{0.01, 0.05, 0.1, 0.25, 0.5\}$.

see that the initial dynamics influence the global error the most, wherefore the error does not increase much past $t = 10a_s$. This initial error could be reduced by employing a much smaller evolution step for the gauge field evolution compared to the one of the quarks. In order to keep the simulation setup as simple as possible, we did not follow this direction in the course of this work.

In contrast to the energy, the Gauß constraint, expressed in eq. (2.100), is to be *conserved exactly up to numerical rounding errors* under the evolution with the Leapfrog algorithm. In fig. 4.6 we show the deviation from the Gauß constraint

$$\gamma^{\max}[U, E] := \max_{\vec{x} \in \Lambda} |\gamma[U, E; \vec{x}]| \tag{4.23}$$

for the same parameters as before relative to its initial value $\gamma^{\max}[U, E]|_{t=0} = 2.34 \cdot 10^{-11}$. We see that over the course of the evolution from $t = 0$ to $t = 200a_s$, the deviation from the Gauß constraint has increased by less than its original value for all step sizes a_0 and thus stays of order 10^{-11}.

Evolution of the Gluon Occupation Number

The gluon distribution function follows a self-similar evolution [16, p. 9f]

$$f(t, |\vec{p}|) = (Qt)^{-4/7} f_s(t, (Qt)^{-1/7} |\vec{p}|)\,, \tag{4.24}$$

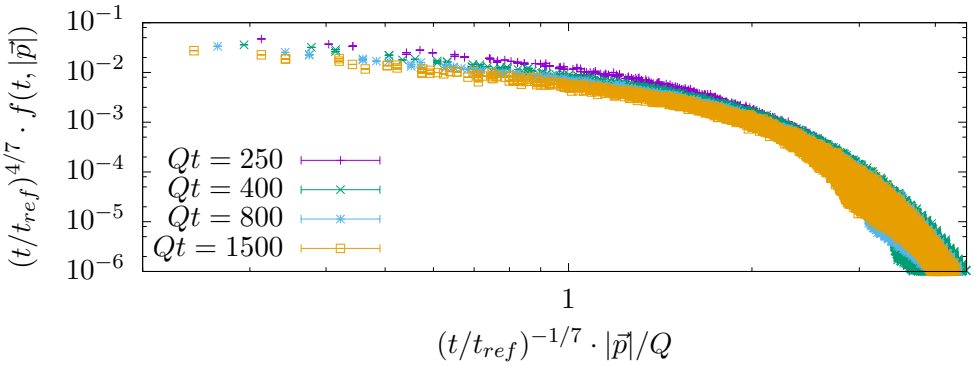

FIGURE 4.7: Rescaled gluon distribution function at times $Qt = 250, 400, 800, 1500$ ($Qt_{\text{ref}} = 1500$) on a 64^3-lattice, $g = 0$, $a_s Q = 0.7$, $f(t = 0, p < Q) = 0.2$ and $a_0/a_s = 0.1$ averaged over 10 independent runs. It shows the same scaling behaviour as in [16, fig. 2].

where f_s is the scaling solution. In order to compare to the results shown in [16, fig. 2], we choose the same parameters except for the lattice size. The scaling behaviour is shown, when the bye eq. (4.24) rescaled gluon distribution functions lay on top of each other. To this end, we show in fig. 4.7 the rescaled distribution function $(Qt)^{4/7} f(t, (Qt)^{-1/7}|\vec{p}|)$, averaged over 10 independent runs on a 64^3-lattice for $a_s Q = 0.2$, $a_t/a_s = 0.1$, $g = 0$, an amplitude $f(t = 0, p < Q) = 0.2$ in the initial box-like distribution for $Qt = 250, 400, 800, 1500$. The data points show agreement for all shown times, especially well for the latest times $Qt = 800$ and $Qt = 1500$ as is to be expected.

The correct evolution of the gluon distribution function in addition to the conservation of the Gauß constraint and the energy lead us to the conclusion that the simulation of the gauge fields is set up correctly.

We are left to monitor the validity of the gauge simulation within the combined framework of the classical statistical approach and lattice NRQCD. In fig. 4.8 we show the non-rescaled gluon distribution function for parameters as we will employ them in the computation of the heavy quarkonium spectrum. The computation is performed on a 64^3 lattice. We set $g = 10^{-3}$, $a_s Q = 1$ and the initial amplitude of the box to $f(t = 0, p < Q) = 1$. The Coulomb gauge condition is fulfilled to 10^{-8}. The ensemble size is 10. While the high momentum tail increases in size, the low momentum region still clearly dominates the distribution function by a 3 magnitudes higher occupation. We conclude that for the evolution of the heavy quarks within the time region $t/a_s \in [0, 100]$, the gauge field dynamics are well controlled and pose no restrictions on the validity of the setup through the classicallity condition (2.51).

4.4 Colour Singlet and Octet

In this section we discuss the heavy quarkonium spectrum in the *background* of a classically evolving glasma. The previous sections provided us with the tools and the confidence to reliably extract heavy quarkonium correlators and their associated spectra.

As discussed in section 2.2.2, we draw the initial configurations from an ensemble that is characterised by a box-like gluon distribution, see eq. (2.75). The simulation is performed on an isotropic, i.e. $a_i \equiv a_s$, 64^3-lattice. The scale is determined by $Q/a_s = 1$. The box-like gluon distribution had an initial amplitude of 1 up to Q. Its quantum fluctuations beyond Q were set to $g = 10^{-3}$ which resulted in a very low occupation of $g^2/2 = 0.5 \cdot 10^{-6}$ wherefore its influence was expectedly negligible. The fermion mass was put to the boundary of the

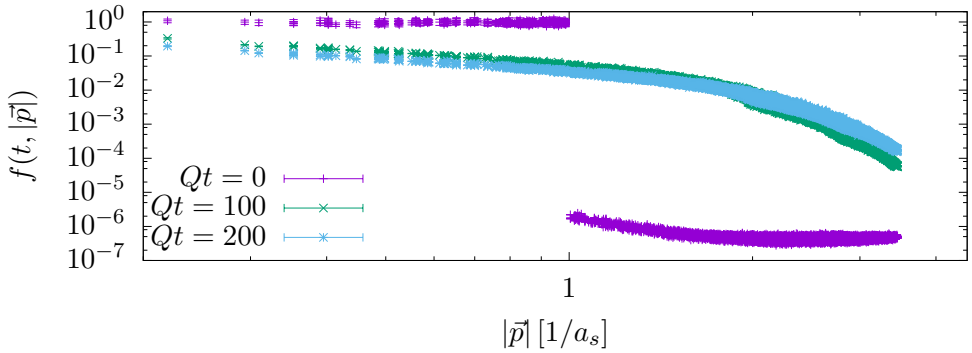

FIGURE 4.8: Gluon distribution function at times $Qt = 0, 100, 200$ on a 64^3-lattice, $g = 10^{-3}$, $a_s Q = 1$, $f(t = 0, p < Q) = 1$ and $a_0/a_s = 0.1$ averaged over 10 independent runs.

Brillouin zone, i.e. $a_s M = \pi/2$. The integration step width was set to $a_0/a_s = 0.1$. The Wilson coefficients were set to their tree-level values $c_i = 1$.

In fig. 4.9 the colour singlet and octet spectrum for $t/a_s = 0, 10, 100$ and the free spectrum are shown. The evolution away from the free spectrum is clearly to be seen but occurs somewhat more drastically between $t = 10a_s$ and $t = 100a_s$. We note that the results were independent from the spin-state wherefore we concentrate on the colour, only. It is very important to be careful when interpreting the change in the shape due to the finite lattice spacing effects which dominate the spectrum past $\omega = \omega^{\text{cusp}} \approx 1.25 a_s^{-1} = 1.25\,\text{GeV}$. We will therefore concentrate on the spectrum in the range $a_s\omega \in [0, 1.25]$. To this end, we show the spectra at $t = 100a_s$ and $t = 0$ (free-like) in fig. 4.10 in the frequency range $\omega \in [0, \omega^{\text{cusp}}]$. We see that the octet and singlet evolve into different directions: While the singlet is enhanced for $\omega \leq \omega^{\text{cusp}}$, the octet is suppressed. That the singlet is favoured over the octet state is not at all surprising as it is generally observed that particles in nature (proton, neutron) are colorless. This enhancement does not, however, indicate the formation of a bound state. For such a conclusion a peak-structure would be necessary which is clearly absent.

4.5 Summary

In this chapter, we have laid out a formalism able to describe heavy quarkonia *in the background* of coloured Yang-Mills fields. Through a study of heavy quarkonium current-current correlators as part of a Wigner transform, we have studied the heavy quarkonium spectral function of the colour singlet and octet channel. We have found that those channels lack the presence peaks and therefore have to conclude that in the presented setup there are no indications to the formation of heavy quarkonium bound states in the background of the classically evolving glasma. This result is very surprising because any kind of bound state was expected to form. The absence of bound states, however, was in agreement with studies from Laine et al. [4] which presented a vanishing real part in the binding potential between static quarks in the context of a classical simulation in thermal equilibrium. In the next Chapter we will reproduce their results and then find reason for the lack of bound states in our previous simulations.

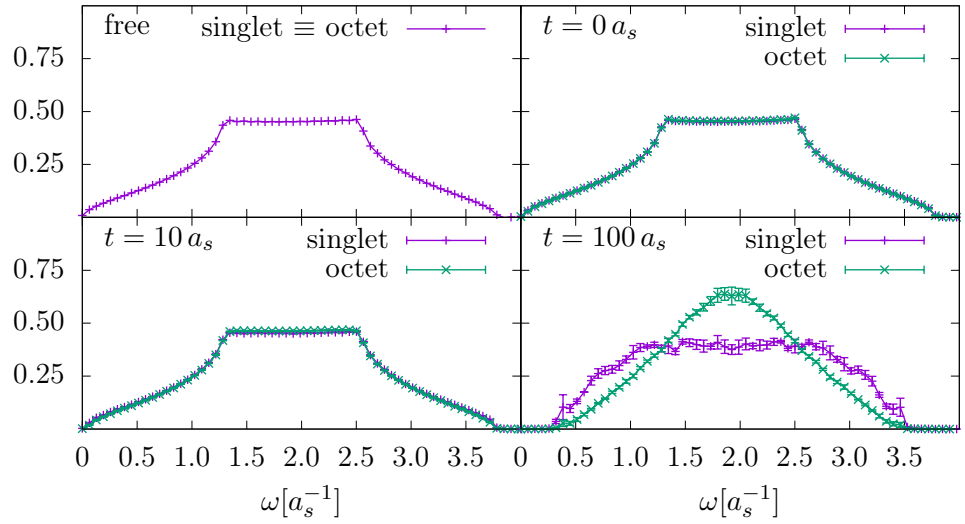

FIGURE 4.9: Time evolution of singlet and octet spectrum on a 64^3-lattice at central times $t/a_s = 0, 10, 100$ for $a_s Q = 1$ and for comparison the free spectrum for $a_0/a_s = 0.1$ and $a_s M = \pi/2$.

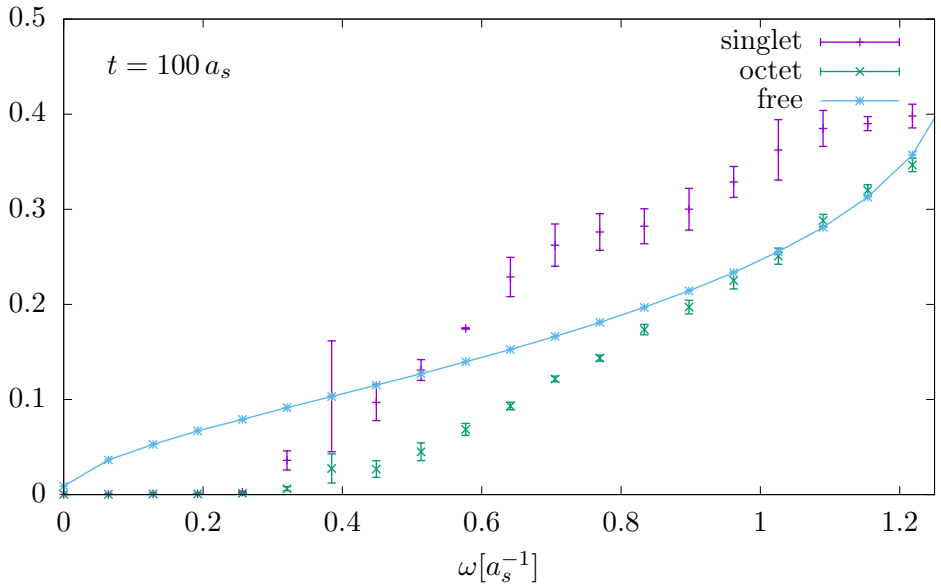

FIGURE 4.10: Free and interacting singlet and octet spectrum in $\omega \in [0, \omega^{\text{cusp}}$ at $t = 100 a_s$ on a 64^3-lattice for $a_s Q = 1$, $a_0/a_s = 0.1$ and $a_s M = \pi/2$. The line of the free spectrum shall solely guide the eye.

Chapter 5

Heavy Quarkonium Potential

In this chapter we extend our view on the heavy quarkonium potential which describes the binding of quarks in an external coloured field. We start with the static quarkonium potential in the classical thermal equilibrium in section 5.1 and compare to known results. As we have found in the previous chapter, we will encounter also here an absence of binding. In order to rule out that this originates in the infiniteness of the mass, i.e. the static limit, we consider a generalisation of the Wilson loop for a finite but still heavy mass in section 5.2. We continue by considering the static potential in the non-equilibrium, i.e. glasma, in section 5.3. We will find that also at early times the potential shows no indication of binding and thus arrive at a complete picture. The aforementioned problem in the puzzling absence of binding is then resolved through the correct simulation set-up in section 5.4 along with first results for the real-time static quarkonium potential in the classical thermal equilibrium.

5.1 Static Potential in the Classical Thermal Equilibrium

The Euclidean Wilson loop, as can be found in textbooks like [22, pp. 95-118] and [23, pp. 54-65], is a well known observable that is used to define a static potential between a pair of an infinitely heavy quark and antiquark. It follows a Schrödinger-like equation in the imaginary time τ

$$\partial_\tau \langle W(R,\tau)\rangle^{(\mathrm{E})} = -V(R,\tau)\,\langle W(R,\tau)\rangle^{(\mathrm{E})}\,, \tag{5.1}$$

where $V(R,\tau)$ is a function that converges to the static potential $V(R)$ at a separation distance of the quarks R. In zero-temperature physics one can define the static potential via a limiting procedure in the temporal extension L_τ

$$V(R) = \lim_{\tau\to\infty} V(R,\tau) = -\lim_{L_\tau\to\infty} \frac{\ln\langle W(R,L_\tau)\rangle^{(\mathrm{E})}}{L_\tau}\,. \tag{5.2}$$

The imaginary time extent corresponds to an inverse temperature $T \sim 1/L_\tau$. Therefore, the zero-temperature-limit prevents us from using this procedure in the thermal scenario at $T \neq 0$ which we are actually interested in.

First results of an alternative approach for a thermal field theory on a minkowskian space-time lattice was presented in [4]. The authors extracted the Wilson loop $\langle W(R,t)\rangle^{(\mathrm{M})}$ and investigated the long-time behaviour of

$$V(R) = \lim_{t\to\infty} \frac{i\,\partial_W(R,t)}{W(R,t)}\,. \tag{5.3}$$

A connection between the Euclidean and Minkowskian Wilson loop is provided by the spectral decomposition [59, 60]

$$\langle W(R,\tau)\rangle^{(\mathrm{E})} = \int_0^{+\infty} \rho_W(\omega, R)\mathrm{e}^{-\omega\tau}\,\mathrm{d}\omega\ , \tag{5.4}$$

$$\langle W(R,t)\rangle^{(\mathrm{M})} = \int_{-\infty}^{+\infty} \rho_W(\omega, R)\mathrm{e}^{i\omega t}\,\mathrm{d}\omega\ . \tag{5.5}$$

The Laplace transform in eq. (5.4) is characteristic for spectral decompositions in imaginary time. Its inversion, however, is difficult [61]. This problem is non-existent in the Minkowskian space-time where the relationship between the Wilson loop and the spectral function is given by a Fourier transform. This Fourier transform can reliably be inverted even for noisy data with

$$\rho_W(\omega, R) = \frac{1}{2\pi}\int_{-\infty}^{+\infty} \langle W(R,t)\rangle^{(\mathrm{M})}\,\mathrm{e}^{-i\omega t}\,\mathrm{d}t\ . \tag{5.6}$$

In the Minkowskian space-time, the potential can be defined as

$$V(R) = \lim_{s\to\infty} \frac{\int i\omega\rho(\omega, R)\mathrm{e}^{i\omega s}\,\mathrm{d}\omega}{\int \rho(\omega, R)\mathrm{e}^{i\omega s}\,\mathrm{d}\omega}\,, \tag{5.7}$$

where the spectrum $\rho(\omega, R)$ controls which physical situation is considered, i.e. a non-equilibrium versus a thermal one.

We are interested in the extraction of the static potential from a Minkowskian lattice simulation. Therefore we will have a closer look at eq. (5.7). If a well defined lowest lying peak in the Wilson loops spectral function exists, then it will dominate the late physics. The authors of [60] start the discussion from the general spectrum of the Wilson loop. In order to relate the spectrum with the time-dependent potential, they discuss the general Schrödinger-like equation for the Wilson loop

$$i\,\partial_t \langle W(R,t)\rangle^{(\mathrm{M})} = V(R,t)\,\langle W(R,t)\rangle^{(\mathrm{M})}\ . \tag{5.8}$$

The time-dependence is described by

$$V(R,t) = V(R) + \phi(R,t)\,, \tag{5.9}$$

containing an offset ϕ that vanishes after a characteristic time $t_{Q\bar{Q}}$. It shall be understood as the time to form a bound state in the presence of the static potential $V(R)$. A formal solution for eq. (5.8) is given by

$$\begin{aligned}&\langle W(R,t)\rangle^{(\mathrm{M})} = \\ &\exp\left[-i\left(t\mathrm{Re}[V(R)] + \mathrm{Re}[\sigma(R,t)] - t|\mathrm{Im}[V(R)]| + \mathrm{Im}[\sigma(R,t)]\right)\right]\ .\end{aligned} \tag{5.10}$$

The function $\sigma = \int_0^t \phi(R,t)\,\mathrm{d}t$ is the integral over the time-dependent part of the potential. Its asymptotic value is $\sigma_\infty(R) = \sigma(R, t=\infty) = \int_0^\infty \phi(R,t)\,\mathrm{d}t$. With the use of that formal

solution they relate the static potential with the spectral function.

$$\begin{aligned}\rho_W(R,\omega) =& \frac{1}{2\pi}\int_{-\infty}^{+\infty} \exp\Big[i\cdot t\,(\omega - \mathrm{Re}[V(R)]) - i\mathrm{Re}[\sigma(R,|t|)]\mathrm{sign}(t) \\ & - |t|\cdot|\mathrm{Im}[V(R)]| + \mathrm{Im}[\sigma(R,|t|)]\Big]\,.\end{aligned} \tag{5.11}$$

The late time physics, described by the real part of the potential, corresponds to the lowest lying peak in the spectrum. The background contributions come from the time-dependence of $\phi(R,t)$. In order to extract the dominant lowest lying peak structure, they expand the above expression in $x = (\mathrm{Re}[V(R)] - \omega)$ and thus obtain

$$\begin{aligned}\rho_W(R,\omega) =& \frac{\mathrm{e}^{\mathrm{Im}[\sigma_\infty(R)]}}{\pi}\cdot \\ & \frac{|\mathrm{Im}[V(R)]|\cos\big(\mathrm{Re}[\sigma_\infty(R)]\big) - (\mathrm{Re}[V(R)]-\omega)\sin\big(\mathrm{Re}[\sigma_\infty(R)]\big)}{(\mathrm{Im}[V(R)])^2 + (\mathrm{Re}[V(R)]-\omega)^2} \\ & + c_0(R) + c_1(R)(\mathrm{Re}[V(R)]-\omega) + c_2(R)(\mathrm{Re}[V(R)]-\omega)^2 + \dots\,.\end{aligned} \tag{5.12}$$

We will follow first a similar path as it was done by Laine et al. by computing the potential via eq. (5.3). Therefore, we employ the classical statistical scheme also here wherefore the initial states have to be drawn from a statistical ensemble, here namely a classical canonical ensemble described by the density matrix

$$\rho = \exp\{-\beta H[U,E]\} \tag{5.13}$$

with the Hamiltonian given in eq. (2.101). A procedure to generate a thermal ensemble was introduced in [62] and explained in detail in the following. What we cannot do is to directly construct a configuration $\{U,E\}$ that is thermal in the sense of being drawn from an ensemble distributed according to

$$P[U,E] \propto \exp\{-\beta H[U,E]\}\,. \tag{5.14}$$

The problem lies in the intricate definition of the magnetic part of the hamiltonian through Wilson loops. The idea to solve this issue is to exploit the fact that the hamiltonian is quadratic in the algebraic components of the chromo-electric field. Instead of directly constructing the gauge links and E-field that is thermal we can draw the electric field and then heat up the gauge links, thus coupling the gauge links through the electric field to the thermal bath. The initialisation procedure is:

1. Initialising the gauge links as $U_\mu(x) \equiv 1_{N_\mathrm{C}\times N_\mathrm{C}}$.
2. The algebraic components of the chromo-electric field are normally distributed random variables according to

$$P[E] \propto \exp\big\{-\beta H_{\mathrm{el.}}[E]\big\}\,. \tag{5.15}$$

Their defining statistical properties are

$$\langle E_j^a(x)\rangle = 0, \quad \langle E_j^a E_k^b\rangle = \sigma^2\delta_{ab}\delta_{jk}, \quad \sigma = 1/\sqrt{\prod_{i=1}^{3} a_i\beta}\,. \tag{5.16}$$

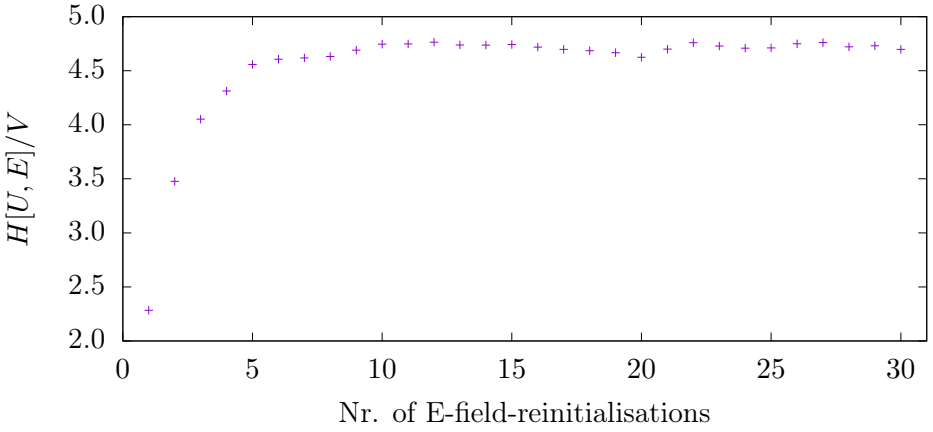

FIGURE 5.1: Thermalisation in the energy saved in the gauge and chromo-electric field over equilibration steps on a $V = 12^3$-lattice for $\beta = 7/3$, $N_{\text{eq.steps}} = 1000$, $R = 1a_s$, $a_t = 0.1a_s$.

3. The configuration $\{U, E\}$ consisting of the gauge field U and the normally distributed E-field is a-priori unphysical in the sense that it does not obey the Gauss law $\gamma[U, E] = 0$. As prescribed by [63, p. 10] one can cure that problem by projecting the chromo-electric field according to

$$\begin{aligned} E_k^{a\prime}(\vec{x}) =& 2\,\mathrm{Tr}\left\{T^a[\kappa\left(U_k(\vec{x})\gamma(\vec{x})U_k^\dagger(\vec{x})\gamma(\vec{x}+\hat{k})-\gamma(\vec{x})\right)\right. \\ &\left. - E_k^a(\vec{x})T^a]\right\} \end{aligned} \tag{5.17}$$

   onto the physical Hilbert space of Gauss law obeying configurations. We found the same value $\kappa = 0.12$ as in [63, p. 10] to stably converge at the considered values for β and thus enforce the Gauss constraint.

4. The chromo-electric field is evolved forward by $a_t/2$ via a naive forward Euler step in order to be able to start the Leapfrog algorithm.

5. The configuration $\{U, E\}$ is evolved according to the Hamiltonian dynamics described in section 2.2.4 to equilibrate both the gauge as well as electric field. After $N_{\text{eq.steps}} = 1000$ of these equilibration steps the E-field was discarded and redrawn, thus going back to step 2. This cycle was repeated for $N_{\text{cycle}} = 15...30$ steps in order to thermalise the gauge links against the thermal bath.

The random numbers are drawn as described in section 3.5.

The thermalisation of the configuration $\{U, E\}$ is shown in fig. 5.1. We present the value of the energy after each cycle of the above described initialisation procedure. The configuration thermalises against the thermal bath clearly after $\sim 10..15$ reinitialisations of the E-field.

In fig. 5.2 we show the real part of the temporal Wilson loop for $\beta = 7/3$ on a 12^3-lattice for $a_t = 0.1a_s$ at $R \in \{1a_s, ..., 6a_s\}$. The potential was defined via the temporal Wilson loops long-time behaviour. Therefore we will concentrate on the late-time-tail. We can see clearly that there are no oscillations but a clear exponential decay in time. This indicates that the potential, as defined in eq. (5.3), will have an imaginary part only. In addition to that, the plot clearly shows that this suppression becomes stronger with the separation distance of the static quarks. That indicates that the imaginary part of the potential grows with the distance R.

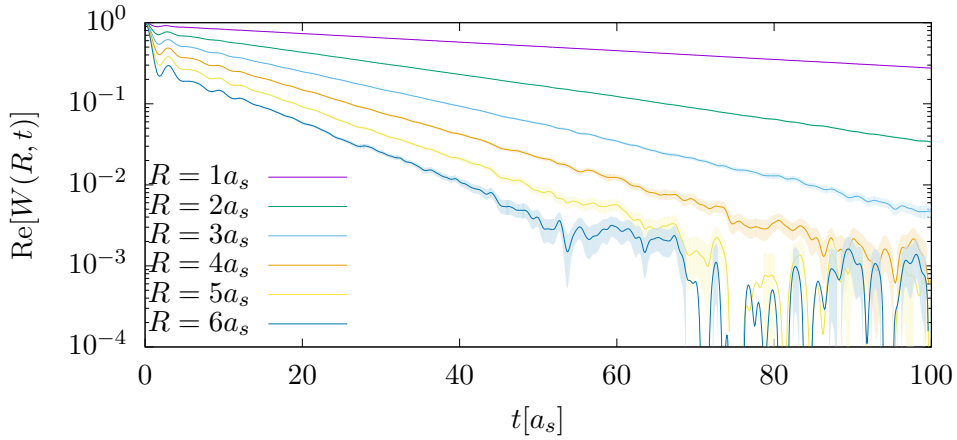

FIGURE 5.2: Real part of the Wilson loop for $\beta = 7/3$ on a 12^3-lattice for $a_t = 0.1a_s$. The lighter coloured bands are the 1σ confidence intervals. The not-shown imaginary part is compatible with 0.

In fig. 5.3 we show the corresponding values for the real and imaginary part of $i\partial_t W(R,t)/W(R,t)$. The imaginary part has a finite value while retaining strong oscillations which grow over time. The real part shows a similar behaviour in its oscillation around zero. We see that the energy looses its time dependence at late times, only, and also that it becomes ill-behaved at the latest times due to insufficient statistics. Therefore, we compute the late-time limit in eq. (5.3) as an by the standard deviation geometrically weighted mean over a finite window of time points. The boundaries of the windows can be found in table 5.1. In fig. 5.4 we show the resulting mean values for the imaginary and real part of the potential. We find that the real part indeed stays zero for all distances. We also find that the imaginary part grows with increasing separation distance R. This observation matches the results of [4].

5.1.1 Comparison to the Spectral Method

Employing the spectral technique requires the computation of the Wilson loops spectrum. In fig. 5.5 the spectra versus the frequency is shown for the same data as above. In solid lines the fits according to eq. (5.12) are shown. It is clear that the spectral peak resides at $\omega = 0$ which implies that the static potentials real part vanishes at all shown distances. This matches the results from above. In order to show the effect of the windowing we show the static potentials imaginary part in fig. 5.6. The spectral method with and also without employing prior windowing of the Wilson loop is compared to the results from the conventional procedure. We note first that the results without prior windowing match the ones of the limiting procedure. We have to note also that the results at $R = 6a_s$ do not coincide. The problem lies in the difficult extraction of the static potential employing the late-time-limit in eq. (5.3) due to the sharp increase in statistical fluctuations as mentioned earlier. Comparing the results from the windowed signal with the ones of the unmodified Wilson loop, we see a clear positive offset of the data points when employing the windowing. This is due to the broadening of the peaks that is usual for windowing techniques.

Because the spectral method gives the same result as the conventional one where we can safely extract the potential employing both methods and moreover is able to handle the statistical fluctuations at bigger distances more reliable, we will employ it throughout the following parts of this chapter.

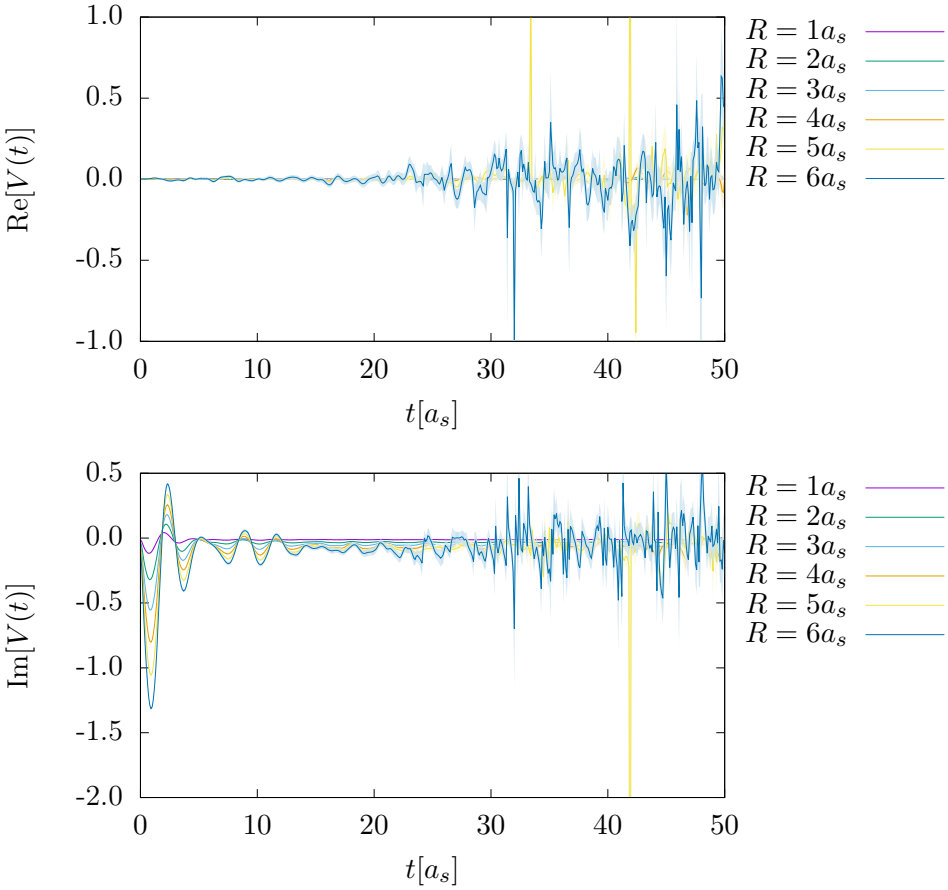

FIGURE 5.3: Real (top) and imaginary part (bottom) of $i\partial_t W(R,t)/W(R,t)$ on a 12^3-lattice for $\beta = 7/3$, $N_{\text{eq.steps}} = 1000$, $a_t = 0.1a_s$. The lighter coloured bands are the 1σ-confidence intervals. The imaginary part converges to a finite, non-zero value while the real part vanishes.

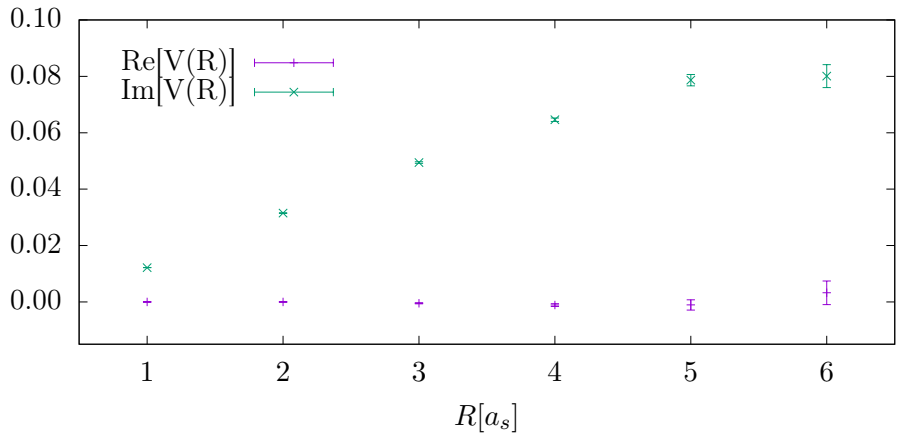

FIGURE 5.4: Real and imaginary part of the static potential on a 12^3-lattice for $\beta = 7/3$, $N_{\text{eq.steps}} = 1000$, $a_t = 0.1a_s$. One can clearly see that its real part is zero for all distances R while its imaginary part grows with the distance.

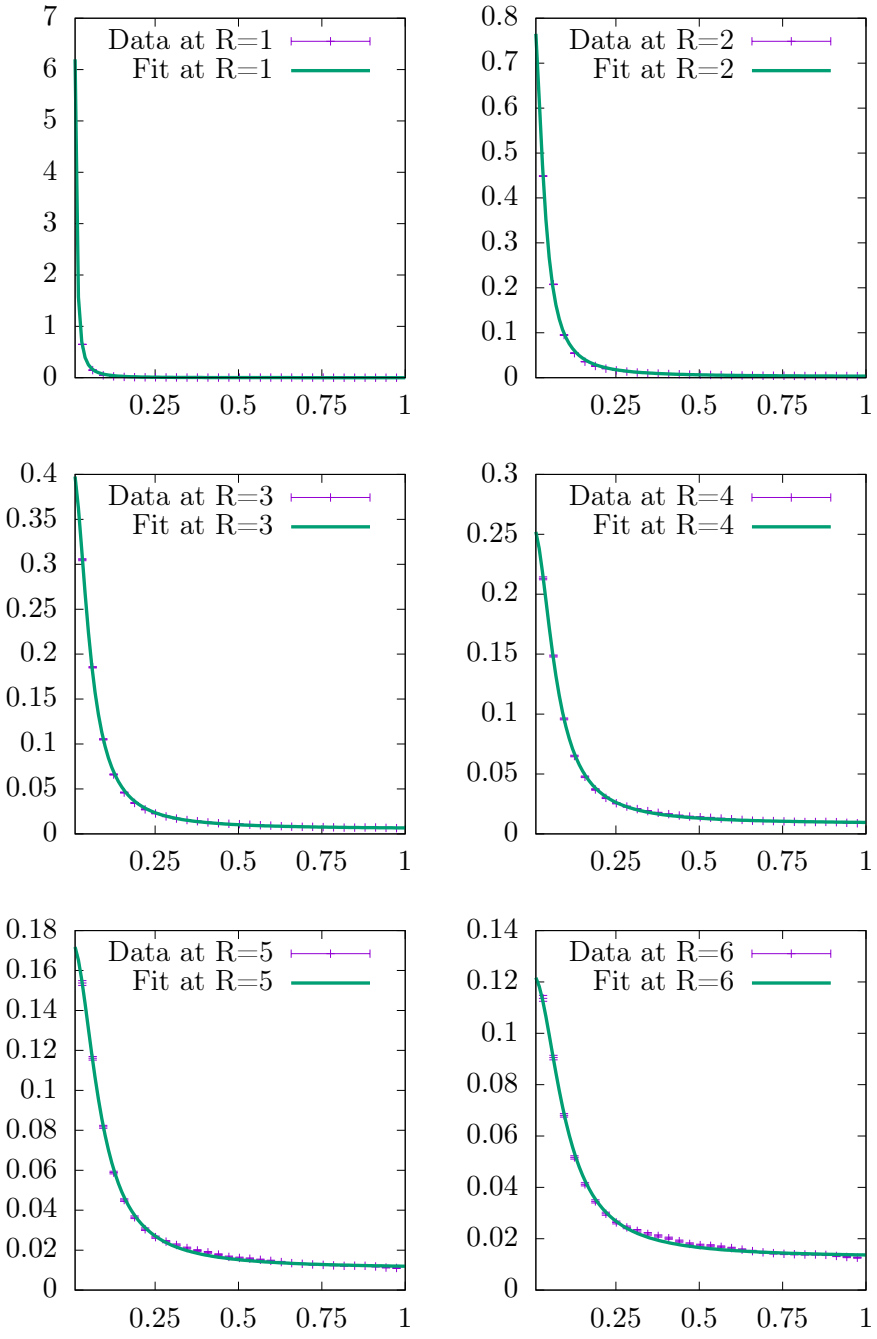

FIGURE 5.5: Spectrum of the Wilson loop and fit employing eq. (5.12) for $V = 12^3$, $\beta = 7/3$, $N_{\text{eq.steps}} = 1000$, $a_t/a_s = 0.1$. The spectrum was obtained using windowing.

$R\,[a_s]$	$t^{\text{fit}}_{\text{min}}\,[a_s]$	$t^{\text{fit}}_{\text{max}}\,[a_s]$
1	10	50
2	10	50
3	15	40
4	15	40
5	20	30
6	20	30

TABLE 5.1: Lower and upper boundaries for the temporal extension in the computation of the real and imaginary part of the potential with eq. (5.3)

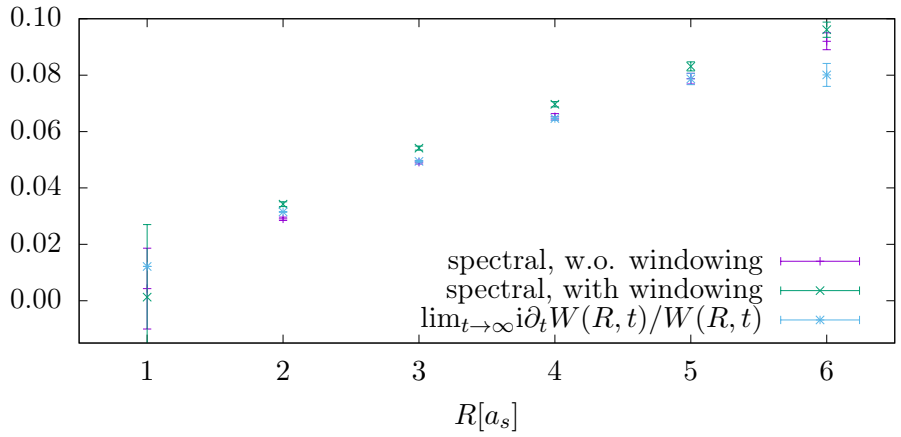

FIGURE 5.6: Comparison of the imaginary part of the static potential employing the spectral method (with and without windowing) with the conventional procedure through a late-time limit.

5.2 Generalised Heavy Quarkonium Potential

In the previous section we found that the static quarkonium potential lacks a real part. We will now investigate whether this observation stems from the static limit. It is motivated by the notion that besides the covariant derivative D_0 all interaction terms in the NRQCD-action vanish for $M \to \infty$. As a viable generalisation of the Wilson loop to a finite quark mass, we are looking for these four properties:

1. Spin- and colour-singlet,
2. gauge-invariance,
3. conventional Wilson loop for $M \to \infty$,
4. propagation of a free quark-antiquark-pair in the weak-coupling limit $g \to 0$.

The generalisation, which we suggest, is

$$\begin{aligned} W_{\text{h}} \propto \text{Tr}\big[& G_\psi\left((\vec{x},t) \to (\vec{x},0); U\right) \cdot U\left((\vec{x},t) \to (\vec{y},t)\right) \\ & \cdot G_\chi\left((\vec{y},0) \to (\vec{y},t); U\right) \cdot U\left((\vec{y},0) \to (\vec{x},0)\right)\big]\,. \end{aligned} \tag{5.18}$$

It is related to the conventional Wilson loop by replacing its temporal Wilson lines by the quark- and antiquark-propagator, respectively. A diagram, which depicts the generalised Wilson loop, is presented in fig. 5.4.

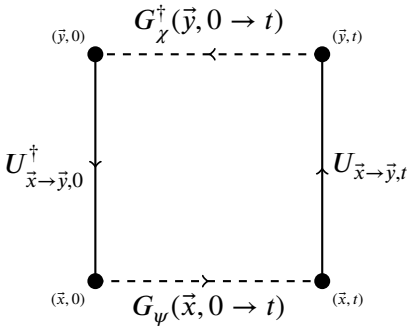

FIGURE 5.7: Sketch of the for finitely heavy quarks generalised Wilson loop.

The gauge-invariance is ensured through the transformation properties of the gauge links in eq. (2.82) and heavy quark and anti quark fields in eqs. (2.83) and (2.84) as well as the cyclicity of the trace-operation.

In the static limit, the Schrödinger equation (2.114) reduces to the temporal covariant derivative D_0 which then translates into $\exp\left(-i \int_0^t A(t')\,\mathrm{d}t'\right) = U(0 \to t)$. Thus, we recover the two temporal Wilson lines $U((\vec{x}, 0) \to (\vec{x}, t))$ and $U((\vec{y}, t) \to (\vec{y}, 0))$ of the conventional Wilson loop.

In the weak coupling limit, the Schrödinger equation looses its $A_\mu(x)$-dependence and thus reduces to free diffusion $i\partial_t G = -\Delta/(2M)G$. Therefore, the colour structure of the propagator becomes diagonal and the gauge-field becomes constant in time. This implies that the spatial Wilson lines 0 and t are hermitian conjugates. Then, due to the diagonal colour structure of the propagator, they cancel each other. What remains is the free diffusion.

It is in principle possible to perform a volume average over the initial quark-antiquark-positions. This would require the evolution of the at different positions reinitialised propagators through the same history of gauge configurations which would leave us with an additional source for correlation. Because the initialisation of the gauge configuration and its evolution is comparably cheap, the generation of a completely new, statistically independence gauge configuration is overall faster and less memory-demanding.

The expectation value of the generalised Wilson loop, shown in fig. 5.8, was evaluated on a 12^3-lattice for $a_t/a_s = 0.1$, $a_s M = 5\pi$ and $\beta = 7/3$. As before we see an exponential decay which increases with the separation distance. The oscillations in the real part of the Wilson loop persist and are of the same frequency independent of R. In fig. 5.9 the corresponding spectrum of the generalised Wilson loop is shifted away from $\omega = 0$ to a finite value. Even though this observation looks promising, this shift does not originate from an emerging real part. What we extract is the energy which describes the Wilson loop in a Schrödinger-equation. Because we are considering a finite mass, the diffusion term does not vanish in contrast to the static case. This implies that the kinetic energy, leading to diffusion, is a part of the total energy $E = p^2/2M + \mathrm{Re}[V(R)]$. The black, dashed line shows the spectrum of the generalised Wilson loop in the free case, i.e. g=0 or $U \equiv \mathbb{1}$. It peaks at the same energy as the other spectra. In the free case $(E)_{\text{free}} = p^2/2M$ must hold. Even for $g \neq 0$ the diffusion due to $\Delta/2M$ is not influenced by the gauge field, wherefore the kinetic energy should be unchanged. From that we conclude that the generalised Wilson loops energy consists solely of the kinetic part and thus lacks the emergence of a finite real part in its heavy-quarkonium potential.

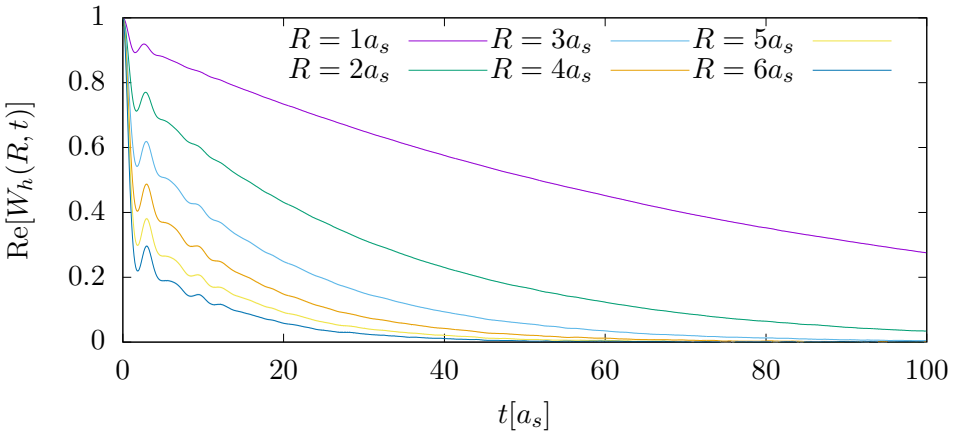

FIGURE 5.8: Real part of the generalised Wilson loop for $V = 12^3$, $\beta = 7/3$, $R/a_s \in \{1, ..., 6\}$, $a_t/a_s = 0.1$. The imaginary part is compatible with zero.

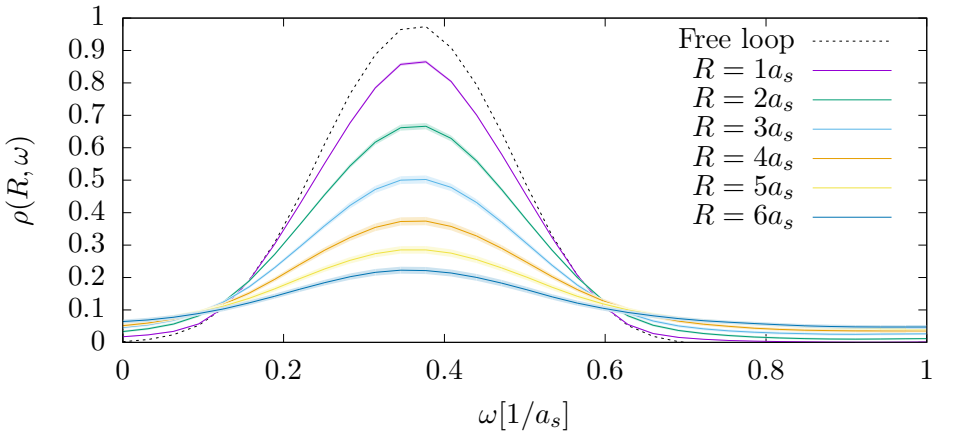

FIGURE 5.9: Spectrum of the generalised Wilson loop for $V = 12^3$, $\beta = 7/3$, $R/a_s \in \{1, ..., 6\}$, $a_t/a_s = 0.1$.

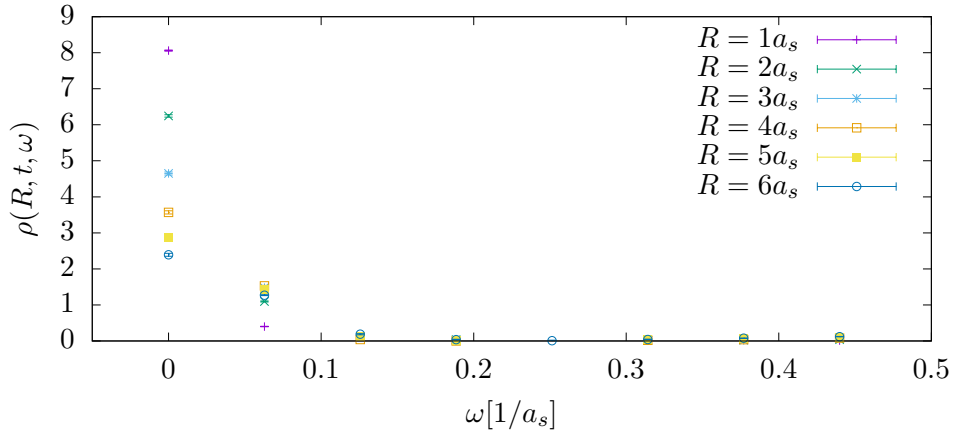

FIGURE 5.10: Non-equilibrium spectrum of the Wilson loop for $V = 12^3$, $g = 0.001$, $n = 1$, $Q_s = 1a_s^{-1}$, $R/a_s \in \{1, ..., 6\}$, $a_t/a_s = 0.1$ at $t = 100a_s$.

5.3 Static Potential in the Non-Equilibrium

In this section we investigate the emergence of a static potential in the early time-evolution of the glasma as presented in section 4.4. This way we will find an explanation for the absence of bound states in the heavy quarkonium spectra.

In contrast to the previous definition of the Wilson loops spectrum via a Fourier transform, we have to use the Wigner-transform [41]

$$\rho_W(R,t,\omega) = \int_{-\infty}^{+\infty} W\left(R, t_2 = t + \frac{s}{2}, t_1 = t - \frac{s}{2}\right) \mathrm{e}^{-i\omega s}\, \mathrm{d}s \ , \tag{5.19}$$

similar to the extraction of the quarkonium spectrum in eq. (4.6).

In fig. 5.10 we show the Wilson loops spectrum at $t = 100a_S$ on a 12^3-lattice for $g = 0.001$, $n_0 = 1$, $Q = 1a_s^{-1}$ and $a_t = 0.1a_s$. It is evident that for all distances it peaks at $\omega = 0$ – as we have found earlier in the classical equilibrium in section 5.1. We performed the same calculation for $t/a_s = 0, 1, 10$ and found the same result. The conclusion is that no binding is visible in the static potential even in the non-equilibrium set-up. That observation matches the absence of bound states in section 4.4. We arrive at a consistent picture where in the current-setup we have found no evidence that binding processes emerge in the evolution of the glasma at early as well as late times. We investigated the quarkonium spectrum as well as the static and to finite masses generalised potential. In the next section we will identify the missing detail.

5.4 Static Potential in Equilibrium with Back-Coupling

The absence of binding can be explained by the missing back-reaction of the quarks to the gauge field. In order to get a rough understanding, imagine a static electric charge and the corresponding electric field as shown schematically on the right hand side of fig. 5.11. The field lines start in the positive and end in the negative charge, thus encoding information about the presence of the charges into the electric field itself. This back-coupling is given by the source-term ρ in the electrostatic Gauss law $\nabla \cdot \vec{E} = \rho(x)$. A neglection of the charge distribution implies a source-free situation in which the electric field is a globally random oriented constant, as shown in the sketch on the left hand side of fig. 5.11. Until now we have

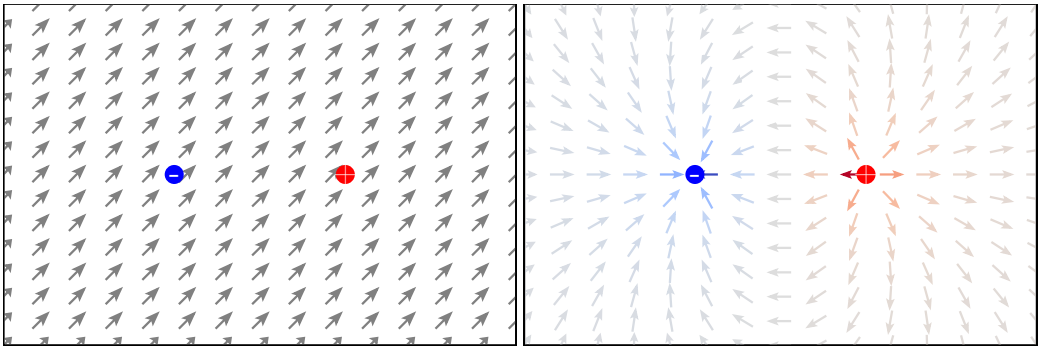

FIGURE 5.11: Field of an electric dipole.
L.: Neglecting Gauss' law leads to an arbitrarily oriented constant field.
R.: Respecting Gauss' law leads to field lines which follow the known pattern.

drawn the initial field configurations from a Hilbert space where the source-free Gauss law was satisfied. As we will understand soon, this is wrong in the classical statistical approach.

To understand at which point those sources enter or, actually, *do not drop* from the to-be computed observable, we will analyse the discussion of the conventional Wilson loop in [22, pp. 96–108]. We will point out what has to be changed and thus define a correct method for computing the static potential when employing the classical statistical approach.

First insights we gain from considering a particle of mass m in a potential $V(x)$ in one space dimension. Its transition amplitude is described by

$$G(x',t;x,0) = \left\langle x' \right| \mathrm{e}^{-iHt} \left| x \right\rangle \,, \tag{5.20}$$

where $H = p^2/(2m) + V(x)$ is the Hamiltonian. Then, we consider the static limit $m \to \infty$, where the kinetic term drops. Recalling $\langle x' | x \rangle = \delta(x - x')$, we obtain

$$G(x',t;x,0) = \delta(x-x')\mathrm{e}^{-iV(x)t} \,. \tag{5.21}$$

The delta-function is the mathematical formulation of the statement that an infinitely massive particle does not change its position. Considering the corresponding static Schrödinger equation for the Greens function

$$i\frac{\partial}{\partial t}G(x',t;x,0) = V(x')G(x',t;x,0) \tag{5.22}$$

it is only able to change its phase. This phase therefore appears in the solution

$$G(x',t;x,0) = \mathrm{e}^{-iV(x')t}G(x,0;x,0) \,. \tag{5.23}$$

This discussion is now generalised to the case of a gauge field theory. For clarity of the main points, we perform the discussion at the example of an abelian gauge theory. We consider the ground state $|\Omega\rangle$ of a quantum system whose dynamics is described by an action similar to the one in eq. (2.17). Then, we introduce a (heavy) quark (Q) and antiquark ($\bar{Q}$) field through this ground state by considering the gauge invariant state

$$\left| \vec{x}\vec{y};\alpha\beta \right\rangle = \bar{\psi}^{(Q)}_{\alpha}(\vec{x},0)U(\vec{x},0;\vec{y},0)\psi^{(Q)}_{\beta}(\vec{y},0) \left| \Omega \right\rangle \,. \tag{5.24}$$

Its gauge invariance is ensured through the phase

$$U(\vec{x},t;\vec{y},t) = \exp\left(i \int_{\vec{x}}^{\vec{y}} A_i(\vec{z},t)\,\mathrm{d}z \right). \tag{5.25}$$

We are interested in the time-ordered Greens function

$$\begin{aligned} G_{\alpha'\beta',\alpha\beta}(\vec{x}',\vec{y}';\vec{x},\vec{y};t) = \langle\Omega|\, T\left\{\bar{\psi}^{(Q)}_{\beta'}(\vec{y}',t)U(\vec{y}',t;\vec{x}',t)\psi^{(Q)}_{\alpha'}(\vec{x}',t)\right. \\ \left.\cdot\bar{\psi}^{(Q)}_{\beta}(\vec{y},0)U(\vec{y},0;\vec{x},0)\psi^{(Q)}_{\alpha}(\vec{x},0)\right\}|\Omega\rangle\ . \end{aligned} \tag{5.26}$$

The spectral decomposition of the four-point-function

$$G(\vec{x}',t,\vec{x},0) = \sum\!\!\!\!\!\!\int_n \left\langle\vec{x}'\middle|n\right\rangle\left\langle n\middle|\vec{x}\right\rangle \mathrm{e}^{-iE_n t} \tag{5.27}$$

can contain discrete as well as continuous parts, indicated by $\sum\!\!\!\!\!\!\int$. This equation is similar to eq. (5.21).

We are left to connect $G(\vec{x}',t,\vec{x},0)$ with the Wilson loop. For that task, we express the 4-point-function as a path integral

$$\begin{aligned} G_{\alpha'\beta',\alpha\beta} = \int \bar{\psi}^{(Q)}_{\beta'}(\vec{y}',t)U(\vec{y}',t;\vec{x}',t)\psi^{(Q)}_{\alpha'}(\vec{x}',t) \\ \cdot\bar{\psi}^{(Q)}_{\beta}(\vec{y},0)U(\vec{y},0;\vec{x},0)\psi^{(Q)}_{\alpha}(\vec{x},0)\mathrm{e}^{iS}\ D[A,\psi^{(Q)},\bar{\psi}^{(Q)}]\,, \end{aligned} \tag{5.28}$$

where the space-time indices in G where hidden. Since the action is quadratic in the fermion fields $\psi^{(Q)}$ and $\bar{\psi}^{(Q)}$, we can perform the integration over the Grassmann variables:

$$\begin{aligned} G_{\alpha'\beta',\alpha\beta} = -\frac{1}{Z}\int \big[G_{\beta\beta'}(y,y';A)G_{\alpha\alpha'}(x',x;A) \\ - G_{\alpha'\beta'}(x',y';A)G_{\beta\alpha}(y,x;A)\big] \\ \cdot U(\vec{x},0;\vec{y},0)U(\vec{y}',t;\vec{x}',t)\det\left\{K^{(Q)}[x,y,x',y';A]\right\}\mathrm{e}^{iS_{\mathrm{G}}[A]}\ D[A]\,, \end{aligned} \tag{5.29}$$

where the two-point function $G_{\alpha\beta}(x,y;A)$ describes the propagation of a quark in the external field A_μ as we have seen earlier in eq. (2.113), here in the form

$$[i\gamma^\mu(\partial_\mu + ieA_\mu(z)) - M_Q]G(z,z') = \delta^{(4)}(z-z')\,. \tag{5.30}$$

The fermion determinant $\det\left\{K^{(Q)}[A]\right\}$ is computed for the matrix

$$K^{(Q)}_{\alpha\beta}(x,y;A) = [i\gamma^\mu\left(\partial_\mu + ieA_\mu(x)\right) - M_Q]_{\alpha\beta}\delta(x-y)\,. \tag{5.31}$$

Usually, one argues that for $M_Q \to \infty$ this determinant approaches a constant that cancels with the corresponding one in the factor $1/Z$ and hence one can set it to 1. In the classical approach, however, this determinant is of utmost importance: It contains the contributions of the fermions as sources to the (classical) Gauss law and is thus an important part of the action. By dropping it one discards a part of the action *before* the application of the principal of stationary action. It comes down to whether the interchange of the path integration and the static limit holds, i.e. if $\lim_{M_Q\to\infty}\int D[U,...]\mathrm{e}^{iS} = \int D[U,...]\lim_{M_Q\to\infty}\mathrm{e}^{iS}$. We will not perform this interchange, thus keeping the limit outside of the integration. The reason why the Euclidean version allows such an interchange will become clear soon.

We study the behaviour of the two-point function $G(z,z';A)$ for $M_Q \to \infty$. The spatial covariant derivatives in eq. (5.30) drop and only the temporal one survives:

$$[i\gamma^0(\partial_0 + ieA_0(z)) - M_Q]G(z,z';A) = \delta^{(4)}(z-z')\,. \tag{5.32}$$

The solution of this initial value problem is for $M \to \infty$ given by

$$G(z, z'; A) = \mathrm{e}^{ie\int_{z_0}^{z'_0} A_0(\vec{z},t)\mathrm{d}t}\hat{G}(z - z')\,. \tag{5.33}$$

$\hat{G}(z - z')$ satisfies a differential equation which does not involve the gauge field:

$$(i\gamma^0\partial_0 - M_Q)\hat{G}(z - z') = \delta^{(4)}(z - z') \tag{5.34}$$

and that can be solved with the Fourier ansatz

$$\begin{aligned}\hat{G}(z - z') = \delta^{(3)}(\vec{z} - \vec{z}')\big[&\Theta(z_0 - z'_0)\left(\frac{1 + \gamma_0}{2}\right)\mathrm{e}^{-iM_Q(z_0 - z'_0)} \\ &+\Theta(z'_0 - z_0)\left(\frac{1 - \gamma_0}{2}\right)\mathrm{e}^{+iM_Q(z_0 - z'_0)}\big]\,.\end{aligned} \tag{5.35}$$

The phase $\mathrm{e}^{ie\int_{z_0}^{z'_0} A_0(\vec{z},t)\mathrm{d}t}$ in eq. (5.33) is the analogue to e^{-iVt} in eq. (5.23). The spatial Kronecker deltas simply tell us that an infinitely heavy fermion can not propagate in space. Inserting the solution for $G_{\alpha\beta}(x, y)$ into eq. (5.29) one obtains

$$G_{\alpha'\beta',\alpha\beta} = \delta^{(3)}(\vec{x} - \vec{x}')\delta^{(3)}(\vec{y} - \vec{y}')(P_+)_{\alpha'\alpha}(P_-)_{\beta\beta'}\mathrm{e}^{-2iM_Qt}\left\langle \mathrm{e}^{ie\oint A_\mu(z)\mathrm{d}z^\mu}\right\rangle\,, \tag{5.36}$$

where

$$P_\pm = \frac{1}{2}\left(\mathbb{1} \pm \gamma^0\right)\,. \tag{5.37}$$

The integral in the expectation value $\left\langle \mathrm{e}^{ie\oint A_\mu(z)\mathrm{d}z^\mu}\right\rangle$ goes along the contour that is defined by the four corners x, y, x' and y'. That object is what we are used to as the Wilson loop. Recalling that we had to keep the fermion contribution to the action until after the application of the principle of stationary action, we see that the spatial Kronecker deltas influence not only the contour of the Wilson loop but also the action itself, for example through the fermion determinant $\det\left(K^{(Q)}[x, y, x', y'; A]\right)$. This implies a third very crucial difference to the conventional methods: The spatial invariance of the system is gone. In a Monte Carlo simulation in thermal equilibrium, when applying for example the Metropolis algorithm, one performs a pure gauge simulation without any restrictions on the configurations. Due to the invariance one then can average the Wilson loop over the whole lattice configuration. Moreover, one can extract the Wilson loop for different separations R from the same Markov chain. In our classical set-up, however, the configuration is not spatially invariant anymore due to the Gauss constraint. Thus, we have to restrict the evaluation of the observable onto the at t_0 via the Gauss law pre-defined contour, separately for each R.

The reason, why one could discard the fermion determinant in the Euclidean version employing a Monte Carlo simulation, is that the Wilson loop resembles the part of the static fermion action from which the Gauss-constraint follows. Let us consider the Wilson loop in

axial gauge $A_0 = 0$. Then it takes the form

$$\left\langle W(\vec{x}', t; \vec{x}, 0)\right\rangle^{(\mathrm{E})} = \int W(\vec{x}', t; \vec{x}, 0; A)\mathrm{e}^{-S_\mathrm{G}[A]}\, D[A] \tag{5.38}$$

$$= \int \mathrm{e}^{ig\int_0^t A_0(\vec{x}',\tau)\mathrm{d}\tau}\, \mathrm{e}^{ig\int_t^0 A_0(\vec{x},\tau)\mathrm{d}\tau}\, \mathrm{e}^{-S_\mathrm{G}[A]}\, D[A] \tag{5.39}$$

$$= \int \mathrm{e}^{-S_\mathrm{G}[A] - ig\int\left(\delta^{(3)}(\vec{y}-\vec{x}) - \delta^{(3)}(\vec{y}-\vec{x}')\right)A_0(\vec{y},y_0)\mathrm{d}^4 y}\,. \tag{5.40}$$

The term $J_0(\vec{y}, y_0) = \delta^{(3)}(\vec{y} - \vec{x}) - \delta^{(3)}(\vec{y} - \vec{x}')$ is the current of the static quark and thus the only remaining term of the fermion action in the limit of $M_\mathrm{Q} \to \infty$. Through reweighting, i.e. during the evaluation of the observable on each element of the Markov chain, the correct statistical weight is recovered.

In the following we will derive the *full* Gauss law which takes into account the presence of the colour sources. Therefore, we consider the static limit of the NRQCD-action containing the gauge sector and one infinitely heavy quark species

$$S_{\text{NRQCD, static}}[U, \psi, \psi^\dagger, \chi, \bar{\chi}] = S_\mathrm{G}[U] + \lim_{M\to\infty} S_{\text{F,NRQCD}}[U, \psi, \psi^\dagger, \chi, \chi^\dagger] \tag{5.41}$$

$$= S_\mathrm{G}[U] + \sum_{\vec{x},t}\left(\psi^\dagger i D_t \psi + \chi^\dagger i D_t \chi\right)\,. \tag{5.42}$$

In the same fashion as in eq. (2.100) Gauss' law is obtained from the variation of the action with respect to $A^a_{0,x}$ bearing in mind the variation rule in eq. (2.92). We demonstrate this at the example of the $\psi^\dagger i D_{x_0}\psi$-term:

$$\frac{\delta}{\delta A^a_{0,x}}\sum_y \psi(y)^\dagger i D_{y_0}\psi(y) = \frac{\delta}{\delta A^a_{0,x}}\sum_y i\psi^\dagger_y \frac{U_{0,y}\psi_{y+\hat{0}} - U^\dagger_{0,y-\hat{0}}\psi_{y-\hat{0}}}{2a_t} \tag{5.43}$$

$$= \sum_y i^2\psi^\dagger_y \frac{\delta_{x,y}T^a U_{0,y}\psi_{y+\hat{0}} + \delta_{x,y-\hat{0}}U^\dagger_{0,y-\hat{0}}T^a\psi_{y-\hat{0}}}{2a_t} \tag{5.44}$$

$$= -\frac{1}{2a_t}\left[\psi^\dagger_x T^a U_{0,x}\psi_{x+\hat{0}} - \psi_{x+\hat{0}}U^\dagger_{0,x}T^a\psi_x\right]\,. \tag{5.45}$$

The very same expression we obtain for the χ-field. In temporal gauge (TP) $U_{0,x} = \mathbb{1}$ those expression take the form

$$\left(\frac{\delta S_{F,NRQCD}}{\delta A^a_{0,x}}\right)_{TP} = -\frac{\psi^\dagger_x T^a\psi_{x+\hat{0}} - \psi_{x+\hat{0}}T^a\psi_x + \chi^\dagger_x T^a\chi_{x+\hat{0}} - \chi_{x+\hat{0}}T^a\chi_x}{2a_t}\,. \tag{5.46}$$

The infiniteness of the heavy-quark mass disallows diffusion. In the classical field theory of NRQCD, the Schrödinger-equation

$$i\partial_t\psi(x,t) = \hat{H}_\psi\psi(x), \quad i\partial_t\chi(x,t) = \hat{H}_\chi\chi(x)\,. \tag{5.47}$$

is obtained from the principle of stationary action. For the heavy quark fields this implies

$$\psi_{x+\hat{0}} = \mathrm{e}^{i\int_{x_0}^{x_0+a_0} A_0(x)\mathrm{d}x_0}\psi_x, \quad \chi_{x+\hat{0}} = \mathrm{e}^{i\int_{x_0}^{x_0+a_0} A_0(x)\mathrm{d}x_0}\chi_x\,, \tag{5.48}$$

which allows the change of the quark sources' colour. Additionally employing axial gauge gives us temporal constantness of the fermionic fields:

$$\psi^{(\dagger)}_{x+\hat{0}} = \psi^{(\dagger)}_x, \quad \chi^{(\dagger)}_{x+\hat{0}} = \chi^{(\dagger)}_x \,. \tag{5.49}$$

In the quantum mechanical theory, we integrate out the fermions and obtain the Schrödinger equation (2.114) for the quark and antiquark propagator for which the same statement holds true. From this follows that the external charges stay unchanged wherefore we can call them static.

In QCD the gauge bosons themselves carry charge. They allow for rotations in the additional colour-degree of freedom of the heavy quarks. In the static limit $M \to \infty$, however, only rotations due to the temporal gauge field are left. In temporal gauge $A_{0,x} \equiv 0$, these rotations are avoided and thus complete the similarity to the above derived static limit in QED.

$$\left(\frac{\delta S_{F,NRQCD}}{\delta A^a_{0,x}}\right)_{\text{static, TP}} = -\frac{\psi^\dagger_x T^a \psi_x + \chi^\dagger_x T^a \chi_x}{a_t} \,. \tag{5.50}$$

Exercising the same for the anti-particle-term and combining it with the variation of the gauge-sector from eq. (2.100), we obtain the full Gauss law in the presence of static quarks

$$\begin{aligned} \gamma[U,\psi,\psi^\dagger,\chi,\chi^\dagger;x] =& \frac{1}{a_t}\Big[\sum_{i=1}^{3}\frac{1}{a_i}\mathrm{Im}\left[\mathrm{Tr}T^a\left(E_{i,x} - U^\dagger_{i,x-\hat{i}}E_{i,x-\hat{i}}U_{i,x-\hat{i}}\right)\right] \\ &+ \psi^\dagger_x T^a \psi_x + \chi^\dagger_x T^a \chi_x\Big] = 0 \,. \end{aligned} \tag{5.51}$$

We integrate out the fermionic degrees of freedom from the Hilbert space by analytically performing the fermionic path integral. After doing so, we are left with

$$\begin{aligned} \langle\gamma[...;x]\rangle_{\mathrm{F}} =& \frac{1}{a_t}\Big[\sum_{i=1}^{3}\frac{1}{a_i}\mathrm{Im}\left[\mathrm{Tr}T^a\left(E_{i,x} - U^\dagger_{i,x-\hat{i}}E_{i,x-\hat{i}}U_{i,x-\hat{i}}\right)\right] \\ &+ \mathrm{Tr}T^a\left(G_\psi(x) + G_\chi(x)\right)\Big] \end{aligned} \tag{5.52}$$

$$\begin{aligned} =& \frac{1}{a_t}\Big[\sum_{i=1}^{3}\frac{1}{a_i}\mathrm{Im}\left[\mathrm{Tr}T^a\left(E_{i,x} - U^\dagger_{i,x-\hat{i}}E_{i,x-\hat{i}}U_{i,x-\hat{i}}\right)\right] \\ &+ \mathrm{Tr}T^a\rho_{\mathrm{C}}(x)\Big] \,. \end{aligned} \tag{5.53}$$

The colour charge density is given by the 3×3-matrix

$$\rho_{\mathrm{C}}(x) = G_\psi(x) + G_\chi(x) \,. \tag{5.54}$$

If we consider more than a single spin, one has to take the trace over the spin-degrees of freedom to obtain the colour-charge density

$$\rho_{\mathrm{C}}(x) = \mathrm{Tr}_{\mathrm{Spin}}\left[G_\psi(x) + G_\chi(x)\right] \,. \tag{5.55}$$

According to eq. (5.33) a static quark at time z_0 is described by

$$G\left((z_0,\vec{z}\,'),(z_0,\vec{z})\right) = M(\vec{z}) \cdot \delta^{(3)}(\vec{z} - \vec{z}\,') \,, \tag{5.56}$$

with a 3×3-matrix $M(\vec{z}_1)$ which describes its colour. Ordering the colours as (red, green, blue), a single red quark at initial time z_0 would then be described by

$$G_\psi\left((z_0,\vec{z}),(z_0,\vec{z}_\psi)\right) = \mathrm{diag}(+1,0,0)\delta^{(3)}(\vec{z}-\vec{z}_\psi), \quad G_\chi\left((z_0,\vec{z}),(z_0,\vec{z}_\chi)\right) = 0\,. \tag{5.57}$$

In a quarkonium the global charge vanishes. This is expressed by

$$\sum_{\vec{x}} \left(G_\psi(x) + G_\chi(x)\right) = 0. \tag{5.58}$$

A pair of a quark and an anti-quark therefore must have opposing colours. The initial condition for a static quarkonium consisting a red quark and an anti-red anti-quark is therefore

$$\begin{aligned} G_\psi\left((z_0,\vec{z}),(z_0,\vec{z}_\psi)\right) &= \mathrm{diag}(+1,0,0)\delta^{(3)}(\vec{z}-\vec{z}_\psi), \\ G_\chi\left((z_0,\vec{z}),(z_0,\vec{z}_\chi)\right) &= \mathrm{diag}(-1,0,0)\delta^{(3)}(\vec{z}-\vec{z}_\chi)\,. \end{aligned} \tag{5.59}$$

To support the consistency of this formalism, we consider a *white* propagator, i.e. one where all colours are equally likely. This has to culminate in a vanishing fermionic contribution to the Gauss law – and so it does:

$$G_\psi(\vec{x},\vec{x}_\psi) = a\mathbb{1}f(\vec{x},\vec{x}_\psi), \quad G_\chi(\vec{x},\vec{x}_\chi) = b\mathbb{1}g(\vec{x},\vec{x}_\psi) \tag{5.60}$$

$$\Rightarrow \mathrm{Tr}T^a\rho_{\mathrm{C}}(x) = (af(x,x_\psi) + bg(x,x_\chi))\underbrace{\mathrm{Tr}T^a}_{=0} = 0\,. \tag{5.61}$$

The physical Hilbert space is the one that satisfies the condition given in eq. (5.53). This condition can be imposed by using the same projection method as presented earlier in section 5.1 by replacing Gauss' law of the pure gauge theory with the new one in eq. (5.53).

While (Euclidean) quenching is something we are not allowed do in the Minkowskian theory, i.e. we have to keep the fermion determinant, something similar is still possible in the $M_Q \to \infty$-limit: Let us consider the equations of motion of the chromo-electric field. From the continuum QCD-action follows

$$D^{ab}_\mu(x)F^{\mu\nu}_b(x) = -j^\nu_a(x)\,, \tag{5.62}$$

where $j^i_a(x)$ is the colour current and $j^0_a(x)$ is the colour charge density. For $\nu = i \in \{1,2,3\}$ we obtain the evolution equations which contain the spatial current j_i. In the static limit this current vanishes while the charge density $j^0_a(x)$ remains. Thus, only the 0th component, the Gauss law, is influenced by static quarks. Quenching in the Minkowskian case means therefore, to neglect the currents effects on the field dynamics while retaining the constraints due to the Gauss law on the Hilbert space of (physical) field configurations.

We will summarize the differences between the Euclidean and the Minkowskian procedure when computing the static potential using the Wilson loop:

- Selection and weighing of the gauge field configurations

  E: All field configurations contribute, weighed by the gauge action, only.

  M: Gauss constraint on the gauge configuration respecting the gauge as well as the heavy fermion action.

- Spatial invariance

  E: Allows a volume average for each gauge configuration, thus reducing the statistical fluctuations in the observable.

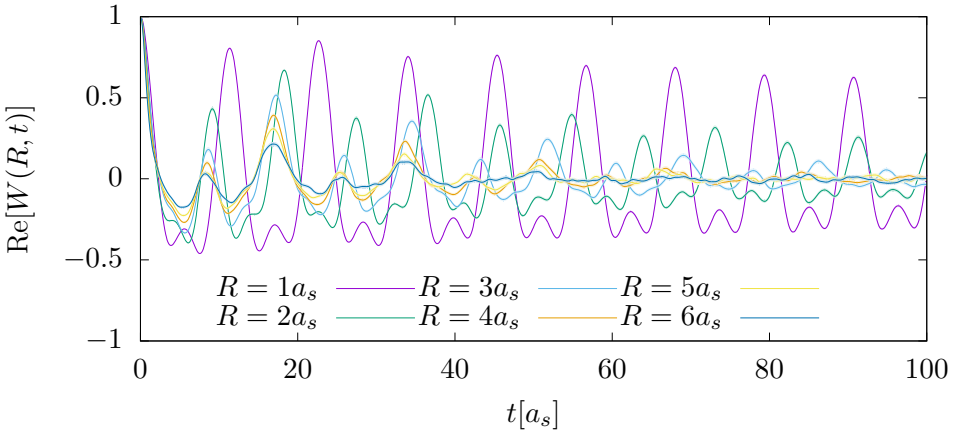

FIGURE 5.12: Real part of the Wilson loop from a the back-coupling of the colour sources onto the gauge field through the Gauss law in eq. (5.51) respecting simulation for $V = 24^3$, $\beta = 8$, $R/a_s \in \{1, ..., 6\}$, $a_t/a_s = 0.1$. The imaginary part is compatible with zero.

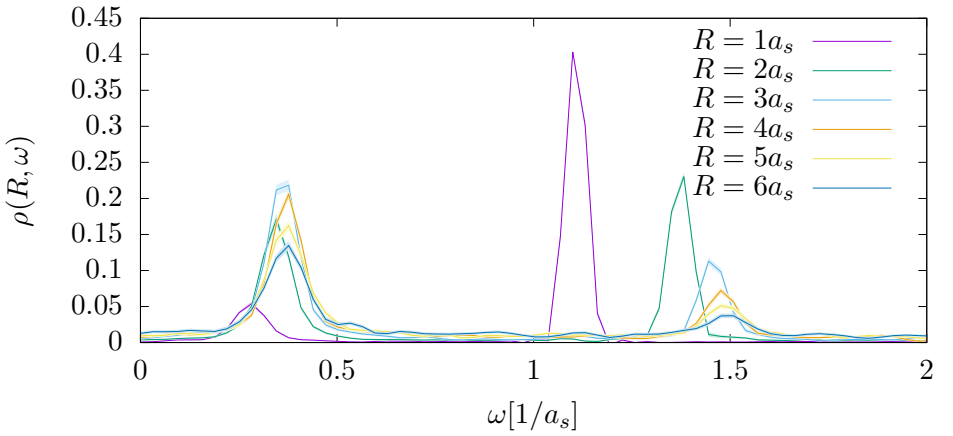

FIGURE 5.13: Spectrum of the Wilson loop for $V = 24^3$, $\beta = 8$, $R/a_s \in \{1, ..., 6\}$, $a_t/a_s = 0.1$.

M: Broken by Gauss' law. We therefore have to compute the Wilson loop for each spatial distance R on separately initialised configurations.

In fig. 5.12 we show the expectation value of the Wilson loop in dependence of the temporal (t) and spatial (R) separation between the point sources on a 24^3-lattice for $\beta = 8$, $R/a_s \in \{1, ..., 6\}$, $a_t/a_s = 0.1$. We see a very clear shift of the lowest lying peaks away from $\omega = 0$ to a finite energies. We can clearly identify an oscillatory behaviour which was absent in the results in fig. 5.2 of the previous, back-reaction-free simulation and implies the presence of a real part in the static potential.

We employ the spectral analysis to extract the real and imaginary part of the static potential. The spectrum is shown in fig. 5.13. The lowest lying peak shifts to higher energies with growing separation distances R. Employing eq. (5.12) we obtain $\mathrm{Re}V(R)$ and $\mathrm{Im}V(R)$. The real part, presented in fig. 5.14, shows a significant dependence on R which follows a $\exp\big(-m_\mathrm{D}R\big)/R$-like behaviour besides an offset. This indicates the presence of Debye screening with a Debye mass m_D in the potential's real part.

Performing this procedure on a 24^3-lattice for $\beta \in \{4, 6, 8\}$ we extracted the real and imaginary part of the static potential. The real part is shown in fig. 5.14. It clearly shows

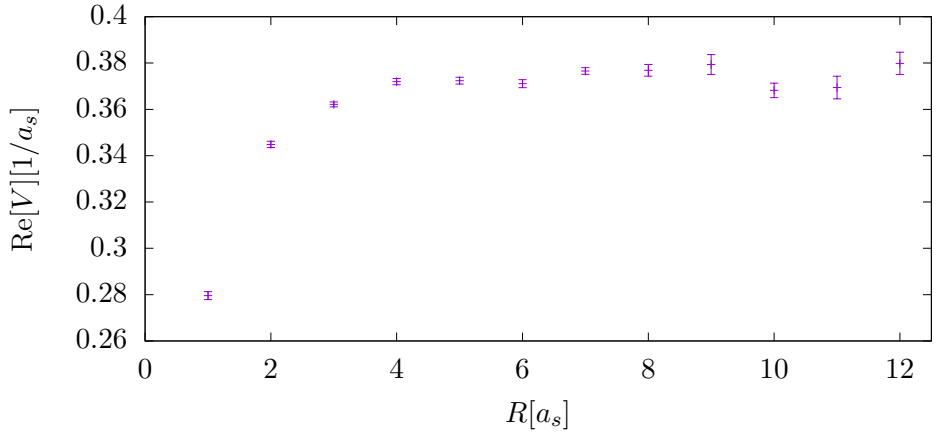

FIGURE 5.14: Real part of the static potential computed while respecting the back-coupling of the colour sources onto the gauge field through the Gauss law in eq. (5.51) for $V = 24^3$, $\beta = 8$, $a_t/a_s = 0.1$.

Debye screening of the $\mathrm{Re}V(R) \propto \exp\left(-m_\mathrm{D} R\right)/R$ with a Debye mass m_D. Fits of this relation were performed with

$$\mathrm{Re}V(R) = -a\frac{\mathrm{e}^{-m_\mathrm{D} R}}{R} + b\,, \tag{5.63}$$

and in solid lines added to the plot. It is clear that those fits agree well with the data. In table 5.2 we present the fit parameters which agree within one standard deviation. This hints to an independence of the potentials real part from the temperature which could be explained by a temperature-independent Debye-mass.

β	$m_\mathrm{D}\ [a_\mathrm{s}^{-1}]$	$a\ [a_\mathrm{s}^{-1}]$	$b\ [a_\mathrm{s}^{-1}]$	χ^2/dof
16	0.68(30)	0.173(39)	0.3701(79)	2.7
24	0.36(16)	0.139(17)	0.3782(53)	2.1
32	0.452(66)	0.151(11)	0.3758(14)	1.9

TABLE 5.2: Fit parameters of the static potential according to eq. (5.63).

In [17] an HTL analysis for the static potential was performed in the continuum. It yielded the result

$$V(R) \propto \frac{1}{(2\pi)^3}\int \left(1-\mathrm{e}^{iq_3 r}\right)\left\{\frac{1}{\vec{q}^2+m_\mathrm{D}^2} - \frac{i\pi m_\mathrm{D}^2}{\beta}\frac{1}{|\vec{q}|(\vec{q}^2+m_\mathrm{D}^2)^2}\right\}\mathrm{d}^3\vec{q} \tag{5.64}$$

$$= -\frac{1}{4\pi}\left[m_\mathrm{D} + \frac{\mathrm{e}^{-m_\mathrm{D} r}}{r}\right] - \frac{i}{4\pi\beta}\phi(m_\mathrm{D} r)\,, \tag{5.65}$$

where m_D is the Debye mass parameter and the dimensionless function $\phi(x)$ is given by

$$\phi(x) = 2\int_0^\infty \frac{z}{(z^2+1)^2}\left[1-\frac{\sin(zx)}{zx}\right]\mathrm{d}z\,, \tag{5.66}$$

with the limiting values $\phi(0) = 0$ and $\phi(\infty) = 1$.

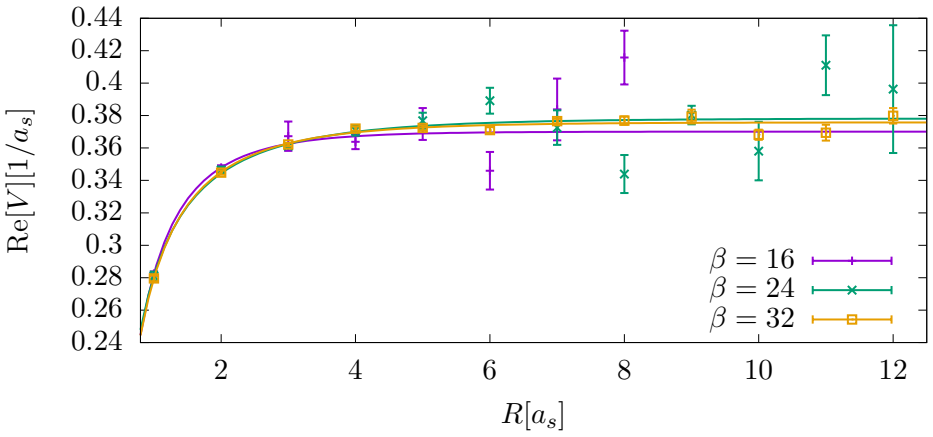

FIGURE 5.15: Real part of the static potential computed while respecting the back-coupling of the colour sources onto the gauge field through the Gauss law in eq. (5.51) for $V = 24^3$, $\beta \in \{4, 6, 8\}$, $a_t/a_s = 0.1$. In addition to the points, the fits with eq. (5.63) with the fits parameters in table 5.2 are added in the same colours as the corresponding simulation data.

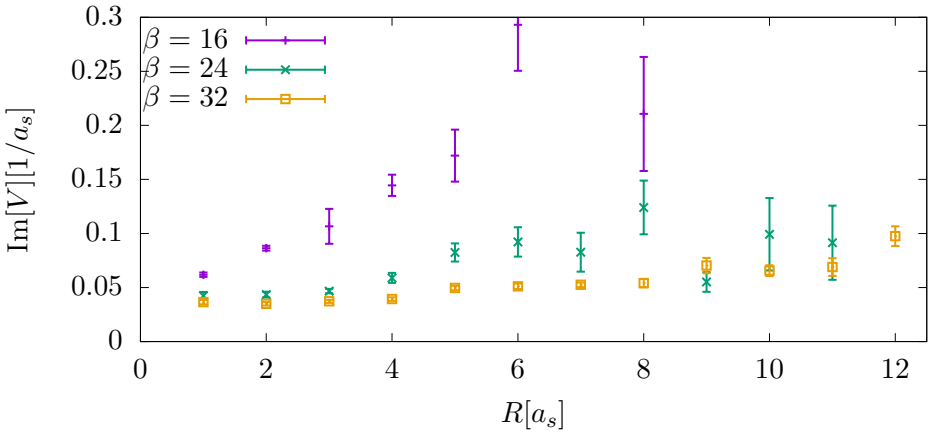

FIGURE 5.16: Imaginary part of the static potential computed while respecting the back-coupling of the colour sources onto the gauge field through the Gauss law in eq. (5.51) for $V = 24^3$, $\beta \in \{4, 6, 8\}$, $a_t/a_s = 0.1$.

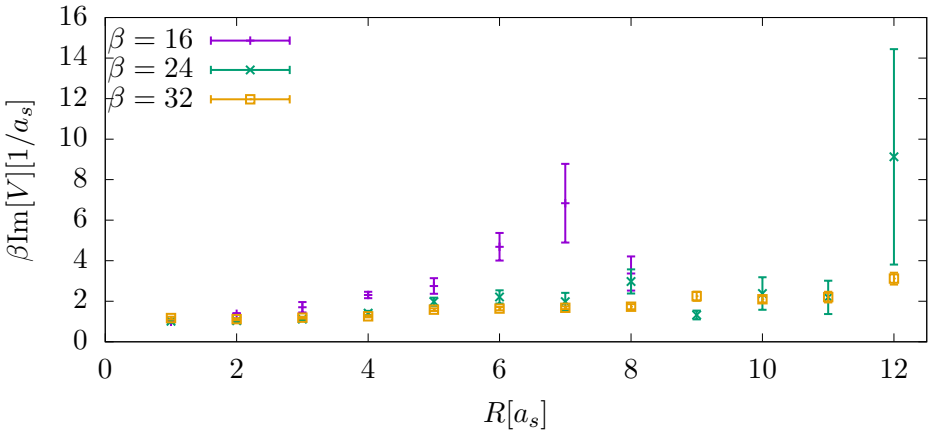

FIGURE 5.17: With β rescaled imaginary part of the static potential computed while respecting the back-coupling of the colour sources onto the gauge field through the Gauss law in eq. (5.51) for $V = 24^3$, $\beta \in \{4, 6, 8\}$, $a_t/a_s = 0.1$.

Let us discuss the limits of the potential and compare to the numerical results: In the limit of $r \to \infty$ the static potential approaches

$$V(\infty) = -\frac{m_{\mathrm{D}}}{4\pi} + \frac{i}{4\pi\beta}\,. \tag{5.67}$$

In the limit of vanishing separation distance the imaginary part vanishes and the real part diverges, i.e.

$$\lim_{r\downarrow 0} \mathrm{Re}[V(R)] = -\infty\,, \tag{5.68}$$

$$\lim_{r\downarrow 0} \mathrm{Im}[V(R)] = 0\,. \tag{5.69}$$

The limit $R \to 0$, however, can only be performed as part of a scaling-analysis during the continuum-limit-extrapolation. These formulas, however, give us a hint that with growing distance the imaginary part rises and that its dependence on β is $\mathrm{Im}V(R) \propto 1/\beta$.

The real part of the static potential is shown in fig. 5.15. Its shape follows the form of a Yukawa-potential with a Debye-mass m_{D} as the HTL-result presented by Laine et al. before employing any classical approximation suggests. We see no significant dependence on $\beta \in [4, 8]$ which indicates a temperature-independent Debye-mass in the HTL-result in eq. (5.65). The presence of a real part is in contrast to what Laine et al. [4, 17] have discussed in the classical limit of the HTL result. It does, however, not contradict their classical simulation because they performed a simulation without the back-reaction of the static quarks through the Gauß-law onto the gauge configuration – as we have done in the earlier parts of this work as well which led to an absence of bound states.

The imaginary part of the potential is shown in fig. 5.16. It rises with the distance as we would naively expect. In fig. 5.17 we show the as $\beta \cdot \mathrm{Im}[V]$ rescaled imaginary part of the potential. It is evident that it follows the from eq. (5.65) predicted $1/\beta$-dependence. It does, however, not vanish at $R = 0$. This is in contrast to our expectation from the HTL-computation in eq. (5.69). This difference might stem from the lattice discretization and the finite volume which translate into an IR- and an UV-cut-off. We did, however, not further investigate the imaginary part.

5.5 Summary

We close this chapter with a brief summary of our results, related studies and possible future directions.

We have studied the non-equilibrium dynamics of static as well for heavy quarks generalised potential which is extracted from the Wilson loop – an observable well known from Euclidean lattice studies. After finding agreement with the results in chapter 4 which indicated an absence of bound states, we concluded that the missing back-coupling of the quarks onto gauge field was causing this unexpected result. We argued that such an investigation does not resemble the physical dynamics correctly already on a qualitative level on the basis of the derivation of the corrected simulation method for the static potential. There, the Gauß law constraint followed as a consequence of the principle of stationary action which in turn stems from the use of the classical statistical approach – regardless of quantum mechanically treated quarks. We found that the fermion determinant, as the translation of the heavy quark action into an effective contribution to the gauge field dynamics, must not be discarded until after the application of the principal of stationary action.

From a by the back-coupling corrected simulation we have obtained a static potential which shows a clear hint on Debye screening. The form of the real part is surprisingly well described by the HTL result present by Laine et al. in [17]. It surprises because the

authors argued that the real part would vanish in the classical limit. Further investigation into the details of the calculation are due in order to find out where this discrepancy in their argumentation and our result stems from.

From the emergence of the static potentials real part, we conclude that the simulation of the heavy quark dynamics in the *classically* evolving glasma requires the quarks back-coupling. Without this back-coupling, the set-up would actually be inconsistent in the sense that one employs the classical equations of motion for the gauge fields but not the full Gauß-law, even though both are implied by the principle of stationary action. The restrictions stemming from the Gauß-law on the physical Hilbert space would be accompanied by coloured current when generalising this setup for finitely heavy quarks.

Chapter 6

Conclusion

In this chapter we summarise our main results and provide a perspective for future research building on our studies of heavy quarks in non-abelian gauge fields out of equilibrium. We also refer to sections 4.5 and 5.5 at the end of the respective chapters.

The central motivation for this work has been to further our understanding of the early-time physics of heavy quarkonia in heavy-ion collisions. This is embedded in the greater effort to develop a full picture of heavy quarkonia in such collision, ranging from the earliest stage (glasma) to the freeze out. The non-perturbative nature of QCD-bound states necessiates a non-perturbative answer. Due to the far-from-equilibrium behaviour of the glasma, conventional lattice QCD were not an appropriate tool to address this question. This necessitated the development of a novel description of heavy quark-antiquark-pairs in the glasma.

This question was approached first with a novel lattice NRQCD-description for the heavy quark evolution in the *background* of classically evolving gauge fields within the classical-statistical framework. Comparing to the in the lattice-community more usual Euclidean lattice gauge theory, we identified conceptual differences between conventional lattice QCD simulations and the combined simulation of heavy quark- and antiquark-propagators in the background of classical fields in a Minkowski space-time. We found an absence of peak-structures in the heavy quarkonium spectral functions of the colour singlet and octet channels. This result was surprising as a-priori we expected to identify the formation of bound states of heavy quark-antiquark-pairs due to a classically to be expected coulombic part in the static heavy-quarkonium potential.

In Chapter 5 we aimed at understanding the absence of bound states. We approached this question by extracting the static quarkonium potential at first also *in the background* of classically evolving gauge fields as it was done by Laine et al. [4] in the classical thermal equilibrium. The portfolio of extraction methods of the static potential from the Wilson loop was extended by the spectral method, given in eq. (5.12), which is based on the work of Burnier and Rothkopf [60]. We found agreement between the two methods but advantages in the reliability of the extraction with the spectral method. We found, consistent with the quarkonium spectra, that the potential has a vanishing real part. In order to rule out that the infiniteness of the quark mass was causing this observation, we generalised the static potential for finitely heavy quarks described by lattice NRQCD and observed that it shows no indication for binding as well. We also ruled out a potential break-down of the classical evolution scheme in the classical thermal equilibrium as the cause for this observation by computing the static potential in the early time evolution of the glasma and finding agreement with the previous observations. We therefore concluded that the setup was missing a fundamental part which lead to a deviation already on the qualitative level.

Revisiting ours and Laine's et al. [4] classical statistical simulation within the classical thermal equilibrium, we identified the missing back-coupling of the heavy quarks through the fermion action onto the Yang-Mills field dynamics as the cause for these observations. This back-coupling is dictated by the principle of stationary action which is an integral part of the classical statistical approach, see eq. (2.64). Employing this principle onto the full

action lead to a Gauß law which took into account the presence of coloured charges. Drawing thermal configurations with an additional projection step onto the physical Hilbert space of this Gauß law, i.e. in the presence of static quarks, have lead to a static potential which shows clear hints to Debye-screening, presented in fig. 5.15.

The investigation of the binding process of heavy quarks and antiquarks in the early-time evolution of the glasma should therefore be revisited. To this end, the classical statistical simulation of the bulk medium has to be modified by the presence of a colour charge density and the classical equations of motion by the colour charge current. The explicit form of this current within our lattice NRQCD approach has still to be derived. From a Wigner transform of NRQCD current-current correlators, the corresponding heavy quarkonium spectral functions are to be extracted. If this procedure proves successful by the emergence of peak-like structures in the spectrum, the results have to be matched to full QCD by tuning the Wilson coefficients.

Despite the present limitations, it is interesting to speculate how the procedure to reach the continuum limit of the above setup would look like. To this end, we start with the situation within the glasma. There, the saturation scale $Q = 1\,\mathrm{GeV}$ provides a physical scale, whose lattice value is $a_\mathrm{s}Q$. As a classical analogy to the (lattice) continuum limit serves the $a_\mathrm{s}Q \to 0$ at constant Q. It is very important, to monitor the gluon distribution in order to ensure that the classicality condition (2.51) is fulfilled. In a quantum mechanical evolution, the distribution function would eventually follow a Bose-Einstein distribution. In the classical setup, however, the gauge fields will inevitably run into the classical thermal equilibrium which is plagued by the Rayleigh-Jeans divergence [12]. Accounting for this limitation, the continuum limit has to be performed while increasing the spatial extents and heavy-quark mass given in lattice units such that the products QN_i and MQ are unchanged. Furthermore, the change in the UV cut-off $\omega_\mathrm{cut} = \pi/a_\mathrm{s}$ necessitates the adjustment (matching) of the Wilson coefficients during this procedure. Since the presented quarkonium spectral functions did not possess the correct qualitative behaviour, we did not follow this scheme so far.

The classical statistical approach hinges on the decoupling of IR modes from the non-classical UV modes. In classical thermal equilibrium, the Rayleigh-Jeans divergence breaks the validity of this decoupling. This divergence has some similarity to the breakdown of NRQCD in the continuum limit. In both, the increase of the UV cut-off couples previously excluded UV degrees of freedom back to the IR modes. In NRQCD, this problem is addressed with the matching procedure. Bödeker, Moore and Rummukainen [64] addressed this question by the addition of auxiliary fields in the context of sphaleron rates of Yang-Mills theories at weak coupling. A similar approach might prove fruitful also in the extrapolation of a system of NRQCD fermions coupled to a classically evolving thermal SU(3) gauge field to the continuuum.

Further questions and opportunities, building on top of our results, are:

- The investigation of the heavy-quarkonium dynamics and its spectrum in the glasma. To this end, the back-coupling of the heavy quarks has to be taken into account. The results are relevant for the further evolution through the stages of the heavy-ion collision and therefore to methods employing kinetic-theory approaches like in [65].

- The behaviour of the generalised Wilson loop and the heavy-quarkonium potential might be revisited by taking into account the back-coupling. Such a study could be of relevance for methods based on potential NRQCD.

- Following the previous point, the study of the static potential in the glasma might give insights into the quarkonium formation process and its time scale. Furthermore, it can serve as a consistency check for the extraction of the heavy-quarkonium spectrum as so far little is known about it far from equilibrium.

- The intricate continuum limit of the combined NRQCD and classical statistical lattice setup is a very important part in the comparison to experimental data. The above described ideas to approach this question within the glasma on the one side and the classical thermal equilibrium on the other side are strongly recommended to be investigated further.

Appendix A

Defining the Initial State

A.1 Definition of Momentum

A.1.1 Fourier Momentum

For a given 3-dimensional lattice with extensions $L_k = a_k N_k$, spacings a_k and points $\{1, ..., N_k\}$ the k^{th} component of the Fourier momentum is given by

$$p_{j,k} = \frac{2\pi j}{a_k N_k} = \frac{2\pi j}{L_k}. \tag{A.1}$$

The spacing between the points in momentum space decreases with growing lattice extension L_k. An increase in the extensions results therefore in an increase of the momentum-resolution.

A.1.2 Forward, Backward and Central Derivative

The forward, backward and central derivative are given by

$$\partial_k^{\mathrm{F}} f(\vec{x}) := \frac{f(\vec{x}+\hat{k}) - f(\vec{x})}{a_k} = \partial_k f(\vec{x}) + \mathcal{O}(a_k^2), \tag{A.2}$$

$$\partial_k^{\mathrm{B}} f(\vec{x}) := \frac{f(\vec{x}) - f(\vec{x}-\hat{k})}{a_k} = \partial_k f(\vec{x}) + \mathcal{O}(a_k^2), \tag{A.3}$$

$$\partial_k^{\mathrm{C}} f(\vec{x}) := \frac{f(\vec{x}+\hat{k}) - f(\vec{x}-\hat{k})}{2a_k} = \partial_k f(\vec{x}) + \mathcal{O}(a_k^3). \tag{A.4}$$

All of the three definitions are approximations to the partial derivative $\partial_k f(\vec{x})$. The first two definitions in eqs. (A.2) and (A.3) approximate the derivative up to a local error which is of second order in the corresponding lattice spacing. The central derivative, however, is already of third order.

There is another difference in the three definitions: The backward and forward derivative are neither skew-hermitian nor hermitian. The central difference, however, is skew-hermitian. Let us write down the lattice equivalent of the momentum operators

$$\hat{p}_k^{\mathrm{F}} := -\mathrm{i} \cdot \partial_k^{\mathrm{F}}, \tag{A.5}$$

$$\hat{p}_k^{\mathrm{B}} := -\mathrm{i} \cdot \partial_k^{\mathrm{B}}, \tag{A.6}$$

$$\hat{p}_k^{\mathrm{C}} := -\mathrm{i} \cdot \partial_k^{\mathrm{C}}. \tag{A.7}$$

Their matrix elements are given by

$$\left(\hat{p}_k^{\mathrm{F}}\right)_{m,n} = \frac{-\mathrm{i}}{a_k}\left(\delta_{m+1,n} - \delta_{m,n}\right), \tag{A.8}$$

$$\left(\hat{p}_k^{\mathrm{B}}\right)_{m,n} = \frac{-\mathrm{i}}{a_k}\left(\delta_{m,n} - \delta_{m-1,n}\right), \tag{A.9}$$

$$\left(\hat{p}_k^{\mathrm{C}}\right)_{m,n} = \frac{-\mathrm{i}}{2a_k}\left(\delta_{m+1,n} - \delta_{m-1,n}\right). \tag{A.10}$$

Due to the symmetry properties of the lattice derivatives, only the central difference has purely real eigenvalues:

$$p_{j,k}^{\mathrm{F}} = \frac{2\sin\left(\frac{\pi j}{N_k}\right)}{a_k} e^{+\mathrm{i}\frac{\pi j}{N_k}} = \frac{2\sin\left(\frac{a_k p_{j,k}}{2}\right)}{a_k} e^{+\mathrm{i}\frac{a_k p_{j,k}}{2}}, \tag{A.11}$$

$$p_{j,k}^{\mathrm{B}} = \frac{2\sin\left(\frac{\pi j}{N_k}\right)}{a_k} e^{-\mathrm{i}\frac{\pi j}{N_k}} = \frac{2\sin\left(\frac{a_k p_{j,k}}{2}\right)}{a_k} e^{-\mathrm{i}\frac{a_k p_{j,k}}{2}}, \tag{A.12}$$

$$p_{j,k}^{\mathrm{C}} = \frac{\sin\left(\frac{2\pi j}{N_k}\right)}{a_k} = \frac{\sin\left(a_k p_{j,k}\right)}{a_k}. \tag{A.13}$$

The eigenvalues can be obtained via a discrete Fourier transformation. The Fourier transform matrix of size $N \times N$ is given by

$$\mathcal{F}_{m,n} = \frac{e^{-\mathrm{i}\cdot 2\pi\frac{m\cdot n}{N}}}{\sqrt{N}}. \tag{A.14}$$

The calculation is very similar for all three momentum operators from eqs. (A.8) to (A.10). Let us look at the central difference momentum operator:

$$\left(\mathcal{F}\cdot\hat{p}_k^{\mathrm{C}}\cdot\mathcal{F}^{\dagger}\right)_{m,n} = \sum_{b,c=1}^{N_k} \frac{e^{-\mathrm{i}\cdot 2\pi\frac{m\cdot b}{N_k}}}{\sqrt{N_k}} \cdot \frac{\delta_{b+1,c} - \delta_{b-1,c}}{\mathrm{i}2a_k} \cdot \frac{e^{+\mathrm{i}\cdot 2\pi\frac{c\cdot n}{N_k}}}{\sqrt{N_k}} \tag{A.15}$$

$$= \frac{1}{a_k}\cdot\frac{1}{N_k}\sum_{b=1}^{N_k} e^{-\mathrm{i}\cdot 2\pi\frac{m\cdot b}{N_k}} \cdot \frac{1}{2\mathrm{i}}\left(e^{\mathrm{i}2\pi\frac{(b+1)\cdot n}{N_k}} - e^{\mathrm{i}2\pi\frac{(b-1)\cdot n}{N_k}}\right) \tag{A.16}$$

$$= \frac{1}{a_k}\underbrace{\frac{1}{N_k}\sum_{b=1}^{N_k} e^{-\mathrm{i}\cdot 2\pi\frac{b\cdot(m-n)}{N_k}}}_{=\delta_{m,n}} \cdot \underbrace{\frac{1}{2\mathrm{i}}\left(e^{+\mathrm{i}\cdot 2\pi\frac{n}{N_k}} - e^{-\mathrm{i}\cdot 2\pi\frac{n}{N_k}}\right)}_{=\sin\left(\frac{2\pi n}{N_k}\right)} \tag{A.17}$$

$$= \frac{\sin\left(\frac{2\pi n}{N_k}\right)}{a_k}\delta_{m,n}. \tag{A.18}$$

Because gluons are massless particles, their hamiltonian in momentum space is given by

$$\hat{H} = \hat{\vec{p}}^2. \tag{A.19}$$

Noting that $\hat{p}^{\mathrm{F}} = \left(\hat{p}^{\mathrm{B}}\right)^{\dagger}$, we can use a combination of forward and backward derivative to construct a hermitian lattice expression for $\hat{\vec{p}}^2$:

$$\hat{H}^{\mathrm{FB}} = \hat{p}^{\mathrm{F}} \cdot \hat{p}^{\mathrm{B}} = \hat{H} + \mathcal{O}\left(a_1^2, \ldots, a_d^2\right) . \tag{A.20}$$

The eigenvalues in momentum space are then given by

$$E^{\mathrm{FB}}\left(\vec{p}\right) = \vec{p}^{\mathrm{F}}\left(\vec{p}\right) \cdot \vec{p}^{\mathrm{B}}\left(\vec{p}\right) = \sum_{k=1}^{d} \left(\frac{2 \sin\left(\frac{a_k p_k}{2}\right)}{a_k} \right)^2 = \vec{p}^2 + \mathcal{O}\left(a_1^2, \ldots, a_d^2\right) . \tag{A.21}$$

Using the central difference we arrive at

$$E^{\mathrm{C}}\left(\vec{p}\right) = \left(\vec{p}^{\mathrm{C}}\right)^2 = \sum_{k=1}^{d} \left(\frac{\sin\left(a_k p_k\right)}{a_k} \right)^2 . \tag{A.22}$$

One important differene between the asymmetric difference operators in eqs. (A.5) and (A.6) and the symmetric, central difference operator in eq. (A.7) is that for $p_k \in [0, 2\pi/a_k]$ the former ones run only once through all momenta, the latter one, however, hits each momentum twice due to the additional factor of 2 inside the sine.

A.2 Definition of the Distribution Function

In [16, p. 4] several definitions for the gluon distribution function are presented:

$$f_{EE}(t,p) := \frac{1}{n_g |\Lambda|} \mathcal{P}^T_{ij}(\vec{p}) \frac{\left\langle E^j_a(t,\vec{p}) \left(E^i_a(t,\vec{p})\right)^* \right\rangle_{\mathrm{cl}}}{\sqrt{m_{\mathrm{HTL}^2} + p^2}}, \tag{A.23}$$

$$f_{AA}(t,p) := \frac{\sqrt{m_{\mathrm{HTL}^2} + p^2}}{n_g |\Lambda|} \mathcal{P}^T_{ij}(\vec{p}) \left\langle A^j_a(t,\vec{p}) \left(A^i_a(t,\vec{p})\right)^* \right\rangle_{\mathrm{cl}}, \tag{A.24}$$

$$f_{\dot{E}\dot{E}}(t,p) := \frac{1}{n_g |\Lambda|} \mathcal{P}^T_{ij}(\vec{p}) \frac{\left\langle \partial_t E^j_a(t,\vec{p}) \left(\partial_t E^i_a(t,\vec{p})\right)^* \right\rangle_{\mathrm{cl}}}{\left(m_{\mathrm{HTL}^2} + p^2\right)^{(3/2)}} . \tag{A.25}$$

We choose the rescaled geometric mean of the definitions in eqs. (A.23) and (A.24)

$$f(t,p) := |\Lambda| \cdot \sqrt{f_{EE}(t,p) \cdot f_{AA}(t,p)}, \tag{A.26}$$

$$= \sqrt{\frac{\left\langle E^j_a(t,\vec{p}) P^T_{ij}(\vec{p}) \left(E^i_a(t,\vec{p})\right)^* \right\rangle_{\mathrm{cl}}}{n_g} \cdot \frac{\left\langle A^k_b(t,\vec{p}) P^T_{kl}(\vec{p}) \left(A^l_b(t,\vec{p})\right)^* \right\rangle_{\mathrm{cl}}}{n_g}} \tag{A.27}$$

$$= \sqrt{\mathcal{O}_{EE}(t,p) \cdot \mathcal{O}_{AA}(t,p)}, \tag{A.28}$$

$$\mathcal{O}_{EE}(t,p) := \frac{1}{n_g} \left\langle E^j_a(t,\vec{p}) P^T_{ij}(\vec{p}) \left(E^i_a(t,\vec{p})\right)^* \right\rangle_{\mathrm{cl}} , \tag{A.29}$$

$$\mathcal{O}_{AA}(t,p) := \frac{1}{n_g} \left\langle A^j_a(t,\vec{p}) P^T_{ij}(\vec{p}) \left(A^i_a(t,\vec{p})\right)^* \right\rangle_{\mathrm{cl}} . \tag{A.30}$$

A.3 Construction of an Ensemble of Initial Gauge Configurations

A.3.1 Kasper and Hebenstreits choice

The gauge and chromo-electric fields fulfill in Coulomb gauge the transversality condition [3, p. 14]

$$\sum_j \tilde{p}_j E_{j,\vec{q}} = 0 = \sum_j \tilde{p}_j A_{j,\vec{q}}, \tag{A.31}$$

$$\tilde{p}_j = \frac{2}{a_j} e^{-\mathrm{i}\pi q_j/N_j} \sin\left(\frac{\pi q_j}{N_j}\right), \tag{A.32}$$

$$|\tilde{p}| = \sqrt{|\tilde{p}_1|^2 + |\tilde{p}_2|^2 + |\tilde{p}_3|^2}, \tag{A.33}$$

$$q_j \in \left\{-\frac{N}{2}, \dots, +\frac{N}{2} - 1\right\} \tag{A.34}$$

The transversality condition is fufilled by the polarisation vectors which are given in [3, p. 15].

For $q_1 \neq 0$ they are given by:

$$\epsilon^{(1)}_{\vec{q}} = \frac{1}{\sqrt{|\tilde{p}_1|^2 + |\tilde{p}_2|^2}} \begin{pmatrix} -\tilde{p}_2 \\ +\tilde{p}_1 \\ 0 \end{pmatrix}, \tag{A.35}$$

$$\epsilon^{(2)}_{\vec{q}} = \frac{1}{|\tilde{p}|\sqrt{|\tilde{p}_1|^2 + |\tilde{p}_2|^2}} \begin{pmatrix} \tilde{p}_1^* \tilde{p}_3 \\ \tilde{p}_2^* \tilde{p}_3 \\ -|\tilde{p}_1|^2 - |\tilde{p}_2|^2 \end{pmatrix}. \tag{A.36}$$

For $q_1 = 0$ they are given by:

$$\epsilon^{(1)}_{\vec{q}} = \frac{1}{\sqrt{|\tilde{p}_2|^2 + |\tilde{p}_3|^2}} \begin{pmatrix} 0 \\ +\tilde{p}_3 \\ -\tilde{p}_2 \end{pmatrix}, \tag{A.37}$$

$$\epsilon^{(2)}_{\vec{q}} = \begin{pmatrix} 1 \\ 0 \\ 0 \end{pmatrix}. \tag{A.38}$$

In [3, p. 15] it is claimed that those polarisation vectors fulfill

$$\mathcal{P}_{ij}(\vec{q}) = \frac{1}{2} \sum_\lambda \epsilon^{(\lambda)}_{i,\vec{q}} \left(\epsilon^{(\lambda)}_{j,\vec{q}}\right)^* = \frac{1}{2}\delta_{ij} - \frac{1}{2}\frac{\tilde{p}_i \tilde{p}_j^*}{|\tilde{p}|^2}. \tag{A.39}$$

This is *wrong*. The *correct* expression is it's complex conjugate

$$\mathcal{P}_{ij}(\vec{q}) = \frac{1}{2}\delta_{ij} - \frac{1}{2}\frac{\tilde{p}_i^* \tilde{p}_j}{|\tilde{p}|^2}. \tag{A.40}$$

A.3.2 Polarisation Vectors for the Central Difference Momentum Operator

Let us follow Kasper and Hebenstreit [3, p. 15].

For $p_1 \neq 0$ they are given by:

$$\epsilon_{\vec{p}}^{(1)} = \frac{1}{\sqrt{\left(p_1^{\mathrm{C}}\right)^2 + \left(p_2^{\mathrm{C}}\right)^2}} \begin{pmatrix} -p_2^{\mathrm{C}} \\ +p_1^{\mathrm{C}} \\ 0 \end{pmatrix}, \tag{A.41}$$

$$\epsilon_{\vec{p}}^{(2)} = \frac{1}{\sqrt{|\vec{p}^{\mathrm{C}}| \left[\left(p_1^{\mathrm{C}}\right)^2 + \left(p_2^{\mathrm{C}}\right)^2\right]}} \begin{pmatrix} p_1^{\mathrm{C}} p_3^{\mathrm{C}} \\ p_2^{\mathrm{C}} p_3^{\mathrm{C}} \\ -\left(p_1^{\mathrm{C}}\right)^2 - \left(p_2^{\mathrm{C}}\right)^2 \end{pmatrix}. \tag{A.42}$$

For $p_1 = 0$ they are given by:

$$\epsilon_{\vec{p}}^{(1)} = \frac{1}{\sqrt{\left(p_2^{\mathrm{C}}\right)^2 + \left(p_3^{\mathrm{C}}\right)^2}} \begin{pmatrix} 0 \\ +p_3^{\mathrm{C}} \\ -p_2^{\mathrm{C}} \end{pmatrix}, \tag{A.43}$$

$$\epsilon_{\vec{p}}^{(2)} = \begin{pmatrix} 1 \\ 0 \\ 0 \end{pmatrix}. \tag{A.44}$$

Let us differ from Kasper and Hebenstreit in one central point: We want the momentum operator to have only real eigenvalues. As mentioned earlier we can use the momentum operator which is defined via the central difference, see eq. (A.7). Using this definition, we need write down

1. the Gauß-law,
2. the Coulomb gauge condition in momentum space,
3. how to construct an ensemble of configurations corresponding to a given spectral distribution
4. and the polarisation vectors.

A.3.2.1 Gauß-Law

The Gauß-law does change only in the formulation of the derivative:

$$-\mathrm{i} D_j^{a,b} E^{b,j}(t,\vec{x}) = \left(\hat{p}_j^{\mathrm{C}} \delta^{a,b} - A_j^a(t,\vec{x}) T^{a,b}\right) E^{b,j}(t,\vec{x}) = 0 \tag{A.45}$$

with a central, covariant difference operator.

A.3.2.2 Coulomb Gauge Condition

The Coulomb gauge condition in real space is

$$-\mathrm{i}\nabla^{\mathrm{C}} \cdot \vec{A}^a(t,\vec{x}) = 0 = -\mathrm{i}\nabla^{\mathrm{C}} \cdot \vec{E}^a(t,\vec{x}). \tag{A.46}$$

In momentum space this reads

$$\hat{\vec{p}}^{\mathrm{C}} \cdot \tilde{\vec{A}}^a(t,\vec{p}) = 0 = \hat{\vec{p}}^{\mathrm{C}} \cdot \tilde{\vec{E}}^a(t,\vec{p}). \tag{A.47}$$

Note the appearance of the eigenvalues of the central momentum operator. The one Fourier momenta themselves appear only as arguments to the fields.

A.3.2.3 Ensemble of Configurations

For a given gluon distribution at time $t = 0$ we can write a mode function decomposition [3, p. 14]

$$\vec{A}^a(0,\vec{p}) = \sqrt{\frac{f(t=0,p)}{|\vec{p}^{\mathrm{C}}|}} \sum_\lambda c_{a,\lambda}(\vec{p})\vec{\epsilon}^{\lambda}(\vec{p}), \tag{A.48}$$

$$\vec{E}^a(0,\vec{p}) = \mathrm{i}\sqrt{|\vec{p}^{\mathrm{C}}| f(t=0,p)} \sum_\lambda c_{a,\lambda}(\vec{p})\vec{\epsilon}^{\lambda}(\vec{p}), \tag{A.49}$$

with complex, gaussian random numbers $c_{a,\lambda}(\vec{p})$ fulfilling

$$\left\langle c^*_{a,\lambda}(\vec{p}) \cdot c_{a',\lambda'}(\vec{p}')\right\rangle_{\mathrm{cl}} = \delta_{\vec{p},\vec{p}'}\delta_{a,a'}\delta_{\lambda,\lambda'}\,. \tag{A.50}$$

When filling $\vec{A}^a(0,\vec{p})$ and $\vec{E}^a(0,\vec{p})$ in momentum space, one has to mirror them such that $\vec{A}^a(0,\vec{p}) = \vec{A}^a(0,-\vec{p})^*$ and $\vec{E}^a(0,\vec{p}) = \vec{E}^a(0,-\vec{p})^*$. Special care is to be taken when $\vec{p} = -\vec{p}$.

Note that the index $-j$ corresponding to the negative Fourier momentum $-p_k$ is given by

$$-j \equiv \big(N_k - (j-1)\big) \bmod N_k\,. \tag{A.51}$$

This is particularly important when summing the contributions of $\vec{p}$ and $-\vec{p}$ to $\vec{A}(0,\vec{p})$ and $\vec{E}(0,\vec{p})$.

Assuming that the polarisation vectors are orthonormal and transveral, i.e.

$$\vec{\epsilon}^{\lambda}(\vec{p}) \cdot \vec{\epsilon}^{\lambda'}(\vec{p}) = \delta_{\lambda,\lambda'}\,, \tag{A.52}$$

$$\vec{p}^{\mathrm{C}} \cdot \vec{\epsilon}^{\lambda}(\vec{p}) = 0 = \vec{p}^{\mathrm{C}} \cdot \vec{\epsilon}^{\lambda}(-\vec{p})\,, \tag{A.53}$$

we can show that an ensemble of initial configurations following eq. (A.48) and eq. (A.49) reproduces the initial spectral distribution $f(t=0,\vec{p})$ defined in eq. (A.27) and that each configuration fulfills the Coulomb gauge condition in eq. (A.47) and the Gauß-law in eq. (A.45).

Let us start with the Coulomb gauge condition in momentum space:

$$\hat{\vec{p}}^{\mathrm{C}} \cdot \vec{A}^a(0,\vec{p}) = \sqrt{\frac{f(t=0,\vec{p})}{|\vec{p}^{\mathrm{C}}|}} \sum_\lambda c_{a,\lambda}(\vec{p}) \underbrace{\vec{p}^{\mathrm{C}} \cdot \vec{\epsilon}^{\lambda}(\vec{p})}_{=0}\,, \tag{A.54}$$

$$\hat{\vec{p}}^{\mathrm{C}} \cdot \vec{E}^a(0,\vec{p}) = \mathrm{i}\sqrt{|\vec{p}^{\mathrm{C}}| f(t=0,p)} \sum_\lambda c_{a,\lambda}(\vec{p}) \underbrace{\vec{p}^{\mathrm{C}} \cdot \vec{\epsilon}^{\lambda}(\vec{p})}_{=0}\,. \tag{A.55}$$

Let us continue with the Gauss-law constraint:

$$\begin{aligned}&\left(-\mathrm{i}\vec{\nabla}^{\mathrm{C}}\delta^{a,b} - \vec{A}^a(0,\vec{x}) \cdot T^{a,b}\right)\vec{E}^b(0,\vec{x})\\ &= \underbrace{-\mathrm{i}\vec{\nabla}^{\mathrm{C}} \cdot \vec{E}^b(0,\vec{x})}_{=0}\,\delta^{a,b} - T^{a,b}\vec{A}^a(0,\vec{x}) \cdot \vec{E}^b(0,\vec{x})\,.\end{aligned} \tag{A.56}$$

The first term vanishes due to the transversality of the polarisation vectors and thus each spectral component:

$$-\mathrm{i}\vec{\nabla}^{\mathrm{C}} \cdot \vec{E}^b(0,\vec{x}) = \sum_{\vec{p}} e^{\mathrm{i}\vec{p}\cdot\vec{x}} \underbrace{\hat{\vec{p}}^{\mathrm{C}} \cdot \vec{E}^b(0,\vec{p})}_{=0} = 0\,. \tag{A.57}$$

The second term is a bit more involved. This was trivial in [3, p. 9] because there only abelian fields were considered:

$$\begin{aligned} T^{a,b}\vec{A}^a(0,\vec{x}) \cdot \vec{E}^b(0,\vec{x}) = \\ T^{a,b}\mathrm{i}\sum_{\vec{p},\vec{p}'} e^{\mathrm{i}(\vec{p}+\vec{p}')\cdot\vec{x}} \sum_{\lambda,\lambda'} \\ c_{a,\lambda}(\vec{p})\vec{\epsilon}^{\lambda}(\vec{p}) \cdot c_{b,\lambda'}(\vec{p}')\vec{\epsilon}^{\lambda'}(\vec{p}') \end{aligned} \tag{A.58}$$

With an additional sum over $\vec{x}$, which refers to the global gauss constraint, the exponential reproduces a Kronecker-delta $\delta_{\vec{p},-\vec{p}'}$. Then the polarisation vectors reproduce $\delta_{\lambda,\lambda'}$. The relative minus-sign lets the overall expression vanish, then, after all. Locally, however, the Gauss constraint is not necessarily fulfilled. For a given configuration we always have to check if it is. If not, the proecudre given by [54] was employed.

In order to show that the ensemble reproduces the spectral distribution function $f(t = 0, p)$ we only need to use the properties of the gaussian random numbers and the orthonormality of the polarisation vectors:

$$\mathcal{O}_{AA}(0,p) = \frac{1}{n_g}\left\langle A_a^j(0,\vec{p}) P_{ij}^T(\vec{p}) \left(A_a^i(0,\vec{p})\right)^* \right\rangle_{\mathrm{cl}} \tag{A.59}$$

$$= \frac{1}{n_g} P_{ij}^T(\vec{p}) \left\langle \frac{f(0,p)}{|\vec{p}^{\mathrm{C}}|} \sum_{\lambda,\lambda'} c_{a,\lambda}(\vec{p})\epsilon_j^{\lambda}(\vec{p}) \cdot c_{a,\lambda'}^*(\vec{p})\epsilon_i^{\lambda'}(\vec{p}) \right\rangle_{\mathrm{cl}} \tag{A.60}$$

$$= \frac{f(0,p)}{|\vec{p}^{\mathrm{C}}| n_g} P_{ij}^T(\vec{p}) \sum_{\lambda,\lambda'} \Big[\underbrace{\left\langle c_{a,\lambda}(\vec{p}) c_{a,\lambda'}^*(\vec{p}) \right\rangle_{\mathrm{cl}}}_{=n_g\delta_{\lambda,\lambda'}} \epsilon_j^{\lambda}(\vec{p})\epsilon_i^{\lambda'}(\vec{p}) \Big] \tag{A.61}$$

$$= \frac{f(0,p)}{|\vec{p}^{\mathrm{C}}|} P_{ij}^T(\vec{p}) \sum_{\lambda} \epsilon_j^{\lambda}(\vec{p})\epsilon_i^{\lambda}(\vec{p}) \tag{A.62}$$

$$= \frac{f(0,p)}{|\vec{p}^{\mathrm{C}}|} \sum_{\lambda,\kappa} \frac{1}{2} \left[\epsilon_i^{\kappa}(\vec{p})\epsilon_j^{\kappa}(\vec{p})\right] \cdot \epsilon_j^{\lambda}(\vec{p})\epsilon_i^{\lambda}(\vec{p}) \tag{A.63}$$

$$= \frac{f(0,p)}{|\vec{p}^{\mathrm{C}}|} \sum_{\lambda,\kappa} \frac{1}{2} \underbrace{\epsilon_i^{\kappa}(\vec{p})\epsilon_i^{\lambda}(\vec{p})}_{=\delta_{\lambda,\kappa}} \underbrace{\epsilon_j^{\kappa}(\vec{p})\epsilon_j^{\lambda}(\vec{p})}_{=\delta_{\lambda,\kappa}} \tag{A.64}$$

$$= \frac{f(0,p)}{2|\vec{p}^{\mathrm{C}}|} \underbrace{\sum_{\lambda} 1}_{=2} \tag{A.65}$$

$$= \frac{f(0,p)}{|\vec{p}^{\mathrm{C}}|} \tag{A.66}$$

$$\mathcal{O}_{EE}(0,p) = \frac{1}{n_g}\left\langle E_a^j(0,\vec{p}) P_{ij}^T(\vec{p}) \left(E_a^i(0,\vec{p})\right)^* \right\rangle_{\mathrm{cl}} = \cdots = |\vec{p}^{\mathrm{C}}| \cdot f(0,p), \tag{A.67}$$

$$\Rightarrow f(0,p) = \sqrt{\mathcal{O}_{EE}(0,p) \cdot \mathcal{O}_{AA}(0,p)}\,. \tag{A.68}$$

Acknowledgements

It is my great pleasure to thank all the people who supported me over the past three years in this project.

First of all, I would like to thank my advisor, Alexander Rothkopf, for giving me the opportunity to work on this topic. I appreciated the support and encouragement he provided through many insightful discussions throghout this work. I would like to thank for numerous opportunities to participate in international conferences and workshops throughout the world, from which I benefited enormously. I would like to especially acknowledge the handling of our joint relocation from Heidelberg to Stavanger and thus giving me the rare and exciting opportunity to continue our work together in Norway and thus getting introduced to the local phyiscal community and the Norwegian society.

I would like to thank the *instituttet for matematikk og fysikk* of the *Universitetet i Stavanger* for their two years long hospitality.

I thank Jan Pawlowski for interesting discussions during my time in Heidelberg and his support as co-advisor during the transition from Heidelberg to Stavanger.

I would like to thank Y. Akamatsu, K. Boguslavski, H. Fujii, M. Kitazawa, Sören Schlichting and Semeon Valgushev for insightful discussions during conferences and workshops. I thank the Nuclear Theory Group at Osaka University for their hospitality.

A special thanks is dedicated to all my present and former colleauges in Heidelberg, Aleksandr Chatrchyan, Michael Heinrich, Aleksias Mazeliauskas, Oscar Garcia Montero, Niklas Müller, Rober Ott, Edoardo Rizzardi, Nils Schlusser, Linda Shen, Jan Torben Schneider, Torsten Zache, Savvas Zafeiropoulos and Felix Ziegler, and in Stavanger, Matthew Terje Aadne, Daniel Auestad, Mark Bogers, Abhijit Bhat Kademane, Georgios Filios, Anna Cecilie Åsland, Gaurang Parkar, Giorgio Pattarini, Marco Rampazzo, Arne Ravndal, Sammy Alaoui Soulimani, for many stimulating discussions and providing a friendly work environment.

This work is supported by the DFG Collaborative Research Centre "SFB 1225 (ISOQUANT)". I am grateful for a generous allocation of computing resources by UNINETT Sigma2 AS, Norway.

Finally, I would like to express my gratitude towards my parents for supporting me during the entire time of my studies.

Bibliography

[1] J. Berges et al. “Universal attractor in a highly occupied non-Abelian plasma”. In: *Phys. Rev. D* 89 (11 June 2014), p. 114007. DOI: 10.1103/PhysRevD.89.114007.

[2] J. Berges et al. “Universality Far from Equilibrium: From Superfluid Bose Gases to Heavy-Ion Collisions”. In: *Phys. Rev. Lett.* 114 (6 Feb. 2015), p. 061601. DOI: 10.1103/PhysRevLett.114.061601.

[3] V. Kasper, F. Hebenstreit, and J. Berges. “Fermion production from real-time lattice gauge theory in the classical-statistical regime”. In: *Phys. Rev.* D90.2 (2014), p. 025016. DOI: 10.1103/PhysRevD.90.025016. arXiv: 1403.4849 [hep-ph].

[4] M. Laine, O. Philipsen, and M. Tassler. “Thermal imaginary part of a real-time static potential from classical lattice gauge theory simulations”. In: *JHEP* 09 (2007), p. 066. DOI: 10.1088/1126-6708/2007/09/066. arXiv: 0707.2458 [hep-lat].

[5] M. Tanabashi et al. “Review of Particle Physics”. In: *Phys. Rev. D* 98 (3 Aug. 2018), p. 030001. DOI: 10.1103/PhysRevD.98.030001.

[6] A. Rothkopf. “Heavy Quarkonium in Extreme Conditions”. In: (Dec. 2019). arXiv: 1912.02253v1 [hep-ph].

[7] K. Yagi, T. Hatsuda, and Y. Miake. *Quark-gluon plasma. From big bang to little bang*. Ed. by T. Ericson and P. V. Landshoff. Vol. 23. Camb. Monogr. Part. Phys. Nucl. Phys. Cosmol. Cambridge University Press, 2005. ISBN: 978-0-521-56108-2.

[8] T. Matsui. “J / psi SUPPRESSION BY PLASMA FORMATION”. In: *Z. Phys.* C38 (1988), p. 245. DOI: 10.1007/BF01574543.

[9] V. Khachatryan et al. “Suppression of Υ(1S), Υ(2S), and Υ(3S) quarkonium states in PbPb collisions at sNN=2.76TeV”. In: *Physics Letters B* 770 (2017), pp. 357–379. ISSN: 0370-2693. DOI: https://doi.org/10.1016/j.physletb.2017.04.031.

[10] T. Matsui and H. Satz. “J/ψ suppression by quark-gluon plasma formation”. In: *Physics Letters B* 178.4 (1986), pp. 416–422. ISSN: 0370-2693. DOI: https://doi.org/10.1016/0370-2693(86)91404-8.

[11] J. Berges, S. Schlichting, and D. Sexty. “Over-populated gauge fields on the lattice”. In: *Phys. Rev.* D86 (2012), p. 074006. DOI: 10.1103/PhysRevD.86.074006. arXiv: 1203.4646 [hep-ph].

[12] J. Berges et al. “Basin of attraction for turbulent thermalization and the range of validity of classical-statistical simulations”. In: *JHEP* 05 (2014), p. 054. DOI: 10.1007/JHEP05(2014)054. arXiv: 1312.5216 [hep-ph].

[13] J. Berges et al. “Turbulent thermalization process in heavy-ion collisions at ultrarelativistic energies”. In: *Physical Review D* 89.7 (Apr. 2014). ISSN: 1550-2368. DOI: 10.1103/physrevd.89.074011.

[14] S. Schlichting. “Non-Equilibrium Dynamics and Thermalization of Weakly Coupled Non-Abelian Plasmas”. PhD thesis. Heidelberg, Germany: Ruprecht-Karls-Universität, May 2013. DOI: 10.11588/heidok.00015314.

[15] K. Boguslavski. “Universality classes far from equilibrium: From heavy-ion collisions to superfluid Bose systems”. PhD thesis. Heidelberg, Germany: Ruprecht-Karls-Universität, Aug. 2016. DOI: 10.11588/heidok.00015314.

[16] K. Boguslavski et al. “Spectral function for overoccupied gluodynamics from real-time lattice simulations”. In: *Phys. Rev. D* 98 (1 July 2018), p. 014006. DOI: 10.1103/PhysRevD.98.014006.

[17] M. Laine et al. “Real-time static potential in hot QCD”. In: *JHEP* 03 (2007), p. 054. DOI: 10.1088/1126-6708/2007/03/054. arXiv: hep-ph/0611300 [hep-ph].

[18] M. Tassler. “Real-Time Techniques for the Yang-Mills Plasma”. PhD thesis. Münster, Germany: Westfälische Wilhelms-Universität, Aug. 2009.

[19] C. N. Yang and R. L. Mills. “Conservation of Isotopic Spin and Isotopic Gauge Invariance”. In: *Phys. Rev.* 96 (1 Oct. 1954), pp. 191–195. DOI: 10.1103/PhysRev.96.191.

[20] F. Mandl and G. Shaw. *Quantum Field Theory*. 2nd ed. Chichester, United Kingdom: John Wiley & Sons, Ltd, Apr. 2010. ISBN: 978-0-471-49684-7.

[21] M. D. Schwartz. *Quantum Field Theory and the Standard Model*. 1st ed. Cambridge University Press, 2014. ISBN: 978-1-107-03473-0. DOI: 10.1063/PT.3.2624.

[22] H. J. Rothe. *Lattice Gauge Theories. An Introduction*. 4th ed. Vol. 82. World Scientific Lect. Notes in Phys. World Scientific Publishing Co. Pte. Ltd., Mar. 2012. ISBN: 978-981-4365-85-7. DOI: 10.1142/8229.

[23] C. Gattringer and C. B. Lang. *Quantum Chromodynamics on the Lattice. An Introductory Presentation*. 1st ed. Vol. 788. Lect. Notes in Phys. Springer, 2010. ISBN: 978-3-642-26095-7. DOI: 10.1007/978-3-642-01850-3.

[24] A. Bazavov, P. Petreczky, and A. Velytsky. “Quarkonium at finite temperature”. In: *Quark-Gluon Plasma 4*. Ed. by R. C. Hwa and X.-N. Wang. 1st ed. Vol. 4. Quark-Gluon Plasma. Singapore: World Scientific Publishing Co. Pte. Ltd., Feb. 2010, pp. 61–110. ISBN: 981-4293-28-8. DOI: 10.1142/9789814293297_0002.

[25] W. E. Caswell and G. P. Lepage. “Effective Lagrangians for Bound State Problems in QED, QCD, and Other Field Theories”. In: *Phys. Lett.* 167B (1986), pp. 437–442. DOI: 10.1016/0370-2693(86)91297-9.

[26] B. Grinstein. “A Modern introduction to quarkonium theory”. In: *Int. J. Mod. Phys.* A15 (2000), pp. 461–496. DOI: 10.1142/S0217751X00000227. arXiv: hep-ph/9811264 [hep-ph].

[27] N. Brambilla et al. “Effective-field theories for heavy quarkonium”. In: *Rev. Mod. Phys.* 77 (4 Dec. 2005), pp. 1423–1496. DOI: 10.1103/RevModPhys.77.1423.

[28] C. Quigg and J. L. Rosner. “Quantum mechanics with applications to quarkonium”. In: *Physics Reports* 56.4 (1979), pp. 167–235. ISSN: 0370-1573. DOI: https://doi.org/10.1016/0370-1573(79)90095-4.

[29] L. L. Foldy and S. A. Wouthuysen. “On the Dirac Theory of Spin 1/2 Particles and Its Non-Relativistic Limit”. In: *Phys. Rev.* 78 (1 Apr. 1950), pp. 29–36. DOI: 10.1103/PhysRev.78.29.

[30] S. Tani. "Connection between Particle Models and Field Theories, I: The Case Spin 1/2". In: *Progress of Theoretical Physics* 6.3 (June 1951), pp. 267–285. ISSN: 0033-068X. DOI: 10.1143/ptp/6.3.267. eprint: https://academic.oup.com/ptp/article-pdf/6/3/267/5239186/6-3-267.pdf.

[31] M. Berwein et al. "Poincaré invariance in NRQCD and potential NRQCD revisited". In: *Phys. Rev.* D99.9 (2019), p. 094008. DOI: 10.1103/PhysRevD.99.094008. arXiv: 1811.05184 [hep-th].

[32] C. Monahan, J. Shigemitsu, and R. Horgan. "Matching lattice and continuum axial-vector and vector currents with nonrelativistic QCD and highly improved staggered quarks". In: *Physical Review D* 87 (Feb. 2013). DOI: 10.1103/PhysRevD.87.034017.

[33] G. T. Bodwin, E. Braaten, and G. P. Lepage. "Rigorous QCD analysis of inclusive annihilation and production of heavy quarkonium". In: *Phys. Rev.* D51 (1995). [Erratum: Phys. Rev.D55,5853(1997)], pp. 1125–1171. DOI: 10.1103/PhysRevD.51.1125. arXiv: hep-ph/9407339 [hep-ph].

[34] G. Aarts et al. "What happens to the Upsilon and η_b in the quark-gluon plasma? Bottomonium spectral functions from lattice QCD". In: *JHEP* 11 (2011), p. 103. DOI: 10.1007/JHEP11(2011)103. arXiv: 1109.4496 [hep-lat].

[35] J. Berges. "Introduction to nonequilibrium quantum field theory". In: *AIP Conf. Proc.* 739.1 (2004), pp. 3–62. DOI: 10.1063/1.1843591. arXiv: hep-ph/0409233 [hep-ph].

[36] J. Schwinger. "Brownian Motion of a Quantum Oscillator". In: *Journal of Mathematical Physics* 2.3 (1961), pp. 407–432. DOI: 10.1063/1.1703727.

[37] L. V. Keldysh. "Diagram technique for nonequilibrium processes". In: *Zh. Eksp. Teor. Fiz.* 47 (1964). [Sov. Phys. JETP20,1018(1965)], pp. 1515–1527.

[38] J. Berges and T. Gasenzer. "Quantum versus classical statistical dynamics of an ultracold Bose gas". In: *Phys. Rev. A* 76 (3 Sept. 2007), p. 033604. DOI: 10.1103/PhysRevA.76.033604.

[39] R. Kubo. "Statistical-Mechanical Theory of Irreversible Processes. I. General Theory and Simple Applications to Magnetic and Conduction Problems". In: *Journal of the Physical Society of Japan* 12.6 (1957), pp. 570–586. DOI: 10.1143/JPSJ.12.570.

[40] P. C. Martin and J. Schwinger. "Theory of Many-Particle Systems. I". In: *Phys. Rev.* 115 (6 Sept. 1959), pp. 1342–1373. DOI: 10.1103/PhysRev.115.1342.

[41] E. Wigner. "On the Quantum Correction For Thermodynamic Equilibrium". In: *Phys. Rev.* 40 (5 June 1932), pp. 749–759. DOI: 10.1103/PhysRev.40.749.

[42] S. Jeon. "Boltzmann equation in classical and quantum field theory". In: *Phys. Rev. C* 72 (1 July 2005), p. 014907. DOI: 10.1103/PhysRevC.72.014907.

[43] A. Krasnitz, Y. Nara, and R. Venugopalan. "Coherent Gluon Production in Very-High-Energy Heavy-Ion Collisions". In: *Phys. Rev. Lett.* 87 (19 Oct. 2001), p. 192302. DOI: 10.1103/PhysRevLett.87.192302.

[44] K. G. Wilson. "Confinement of quarks". In: *Phys. Rev. D* 10 (8 Oct. 1974), pp. 2445–2459. DOI: 10.1103/PhysRevD.10.2445.

[45] J. Smit. "Massive vector particles with Yang-Mills couplings". PhD thesis. Los Angeles, USA: UCLA, 1974.

[46] A. Ipp and D. Müller. “Implicit schemes for real-time lattice gauge theory”. In: *Eur. Phys. J.* C78.11 (2018), p. 884. DOI: 10.1140/epjc/s10052-018-6323-x. arXiv: 1804.01995 [hep-lat].

[47] A. Dougall, C. M. Maynard, and C. McNeile. “The Charm quark mass with dynamical fermions”. In: *Nucl. Phys. Proc. Suppl.* 140 (2005). [,428(2004)], pp. 428–430. DOI: 10.1016/j.nuclphysbps.2004.11.297. arXiv: hep-lat/0409089 [hep-lat].

[48] J. Kogut and L. Susskind. “Hamiltonian formulation of Wilson’s lattice gauge theories”. In: *Phys. Rev. D* 11 (2 Jan. 1975), pp. 395–408. DOI: 10.1103/PhysRevD.11.395.

[49] H. Nielsen and M. Ninomiya. “Absence of neutrinos on a lattice: (I). Proof by homotopy theory”. In: *Nuclear Physics B* 185.1 (1981), pp. 20–40. ISSN: 0550-3213. DOI: https://doi.org/10.1016/0550-3213(81)90361-8.

[50] H. Nielsen and M. Ninomiya. “Absence of neutrinos on a lattice: (II). Intuitive topological proof”. In: *Nuclear Physics B* 193.1 (1981), pp. 173–194. ISSN: 0550-3213. DOI: https://doi.org/10.1016/0550-3213(81)90524-1.

[51] R. Sommer. “A New way to set the energy scale in lattice gauge theories and its applications to the static force and alpha-s in SU(2) Yang-Mills theory”. In: *Nucl. Phys.* B411 (1994), pp. 839–854. DOI: 10.1016/0550-3213(94)90473-1. arXiv: hep-lat/9310022 [hep-lat].

[52] S. Hashimoto and T. Onogi. “Heavy Quarks on the Lattice”. In: *Annual Review of Nuclear and Particle Science* 54.1 (Dec. 2004), pp. 451–486. ISSN: 1545-4134. DOI: 10.1146/annurev.nucl.53.041002.110550.

[53] PETSc. *Portable, Extensible Toolkit for Scientific Computation Toolkit for Advanced Computation*. Sept. 2019. URL: https://www.mcs.anl.gov/petsc/ (visited on 09/30/2019).

[54] R. J. Hudspith. “Fourier Accelerated Conjugate Gradient Lattice Gauge Fixing”. In: *Comput. Phys. Commun.* 187 (2015), pp. 115–119. DOI: 10.1016/j.cpc.2014.10.017. arXiv: 1405.5812 [hep-lat].

[55] G. E. P. Box and M. E. Muller. “A Note on the Generation of Random Normal Deviates”. In: *Ann. Math. Statist.* 29.2 (June 1958), pp. 610–611. ISSN: 0003-4851. DOI: 10.1214/aoms/1177706645.

[56] F. James. “RANLUX: A Fortran implementation of the high-quality pseudorandom number generator of Lüscher”. In: *Computer Physics Communications* 79.1 (1994), pp. 111–114. ISSN: 0010-4655. DOI: https://doi.org/10.1016/0010-4655(94)90233-X.

[57] M. Luscher. “A Portable high quality random number generator for lattice field theory simulations”. In: *Comput. Phys. Commun.* 79 (1994), pp. 100–110. DOI: 10.1016/0010-4655(94)90232-1. arXiv: hep-lat/9309020 [hep-lat].

[58] G. Marsaglia and A. Zaman. “A New Class of Random Number Generators”. In: *Ann. Appl. Probab.* 1.3 (Aug. 1991), pp. 462–480. DOI: 10.1214/aoap/1177005878.

[59] A. Rothkopf, T. Hatsuda, and S. Sasaki. “Complex Heavy-Quark Potential at Finite Temperature from Lattice QCD”. In: *Phys. Rev. Lett.* 108 (16 Apr. 2012), p. 162001. DOI: 10.1103/PhysRevLett.108.162001.

[60] Y. Burnier and A. Rothkopf. "Disentangling the timescales behind the nonperturbative heavy quark potential". In: *Phys. Rev. D* 86 (5 Sept. 2012), p. 051503. DOI: 10.1103/PhysRevD.86.051503. arXiv: 1208.1899 [hep-ph].

[61] I. J. D. Craig, A. M. Thompson, and W. J. Thompson. "Why Laplace Transforms Are Difficult To Invert Numerically". In: *Computers in Physics*. Practical Numerical Algorithms 8.6 (1994), pp. 648–653. DOI: 10.1063/1.4823347.

[62] G. D. Moore. "Motion of Chern-Simons number at high temperatures under a chemical potential". In: *Nucl. Phys.* B480 (1996), pp. 657–688. DOI: 10.1016/S0550-3213(96)00445-2. arXiv: hep-ph/9603384 [hep-ph].

[63] Y. Akamatsu, A. Rothkopf, and N. Yamamoto. "Non-Abelian chiral instabilities at high temperature on the lattice". In: *Journal of High Energy Physics* 2016.3 (Mar. 2016), p. 210. ISSN: 1029-8479. DOI: 10.1007/JHEP03(2016)210.

[64] D. Bödeker, G. D. Moore, and K. Rummukainen. "Chern-Simons number diffusion and hard thermal loops on the lattice". In: *Physical Review D* 61.5 (Feb. 2000). ISSN: 1089-4918. DOI: 10.1103/physrevd.61.056003.

[65] T. Miura et al. "Quantum Brownian motion of a heavy quark pair in the quark-gluon plasma". In: *Physical Review D* 101.3 (Feb. 2020). ISSN: 2470-0029. DOI: 10.1103/physrevd.101.034011.